For Reference

NOT TO BE TAKEN FROM THIS ROOM

Ex libris
Universitatis
Albertaensis

QUAECUMQUE VERA

The University of Alber
Printing Department
Edmonton, Alberta

Digitized by the Internet Archive
in 2020 with funding from
University of Alberta Libraries

https://archive.org/details/Dzidic1970

THE UNIVERSITY OF ALBERTA

MASS SPECTROMETRIC INVESTIGATIONS OF THE HYDRATION OF ALKALI IONS IN THE GAS PHASE

by

© ISMET DZIDIC

A THESIS
SUBMITTED TO THE FACULTY OF GRADUATE STUDIES
IN PARTIAL FULFILMENT OF THE REQUIREMENTS FOR THE DEGREE
of
DOCTOR OF PHILOSOPHY

DEPARTMENT OF CHEMISTRY

EDMONTON, ALBERTA

FALL, 1970

THE UNIVERSITY OF ALBERTA
FACULTY OF GRADUATE STUDIES

The undersigned hereby certify that they have read, and recommend to the Faculty of Graduate Studies for acceptance, a thesis entitled

"MASS SPECTROMETRIC INVESTIGATIONS OF THE
HYDRATION OF ALKALI IONS IN THE
GAS PHASE"

submitted by ISMET DZIDIC, in partial fulfilment of the requirements for the degree of Doctor of Philosophy.

May 18 1973
Date

ABSTRACT

The gas phase hydration of the alkali ions, M^+ (M = Li, Na, Rb, Cs) was studied by means of a specially designed mass spectrometer which was capable of operating at ion source pressures in the torr range. The mass spectrometer was used to analyze the equilibrium concentrations of the gas phase hydrated ions arising from the thermal equilibrium of alkali ions and water vapour in the ion source. The analyses proved the occurrence of the general reaction (1)

$$(1) \qquad M^+(H_2O)_{n-1} + H_2O \rightleftarrows M^+(H_2O)_n \qquad n = 1\text{-}6$$

where notation n-1,n is used to denote specific reactions. Equilibrium constants, $K_{n-1,n}$, for the general reaction (1) were determined over a range of water pressures. Typically the pressure was varied from 0.2 to 3 torr to demonstrate that $K_{n-1,n}$ is pressure independent. By the determination of the equilibrium constants $K_{n-1,n}$ at various temperatures the thermodynamic values $\Delta H^\circ_{n-1,n}$, $\Delta G^\circ_{n-1,n}$ and $\Delta S^\circ_{n-1,n}$ were obtained.

A theoretical calculation of the potential energies of the clusters $M^+(H_2O)_n$ is presented. This calculation was based on the various electrostatic forces between the central ion and the ligand molecules as well as those among the ligand molecules. The potential energies $\Delta E^\circ_{n-1,n}$ were compared with $\Delta H^\circ_{n-1,n}$ obtained experimentally. The

comparison of $\Delta H^{\circ}_{n-1,n}$ with $\Delta E^{\circ}_{n-1,n}$ revealed some important features concerning the nature of hydration of alkali ions in the gas phase, i.e. the type of bonding and the structure of $M^{+}(H_2O)_n$ clusters where n = 1 to 6. The entropy values, $\Delta S_{0,1}$ for reaction (1) calculated from statistical mechanics were found to be in excellent agreement with the experimental values.

From the results of this work and the study of the gas phase hydration of halide negative ions, carried out by other workers in this laboratory, the hydration energies of the positive and negative ions were compared. Our studies indicate that initial hydration steps are more favorable for positive ions. However as more water molecules are added to the clusters, negative ion hydration becomes more favorable.

Another important feature of the present study was the comparison of the gas phase results for the hydration of alkali and halide ions with the individual ion hydration energies in solution. The trend in our data supports the individual ion hydration energies obtained by Randles.

ACKNOWLEDGEMENTS

Sincere appreciation and gratitude to Dr. P. Kebarle, whose patience, originality, and thoroughness have been the guidance and encouragement throughout this research.

The author is deeply indebted to Dr. S. K. Searles who schooled the author in the technique of mass spectrometry.

The author wishes to thank Dr. R. Yamdagni for programming the theoretical calculations and other members of the mass spectrometry group for their valuable suggestions during the course of this study.

Special thanks go to Mrs. Mary Waters. Her care in typing the manuscript was invaluable.

The financial assistance provided by the University of Alberta is gratefully acknowledged.

TABLE OF CONTENTS

Page

Abstract. ii

Acknowledgements iv

List of Figures ix

List of Tables xi

1. INTRODUCTION

1.1 The present study 1

1.2 The nature of solvation 1

A. Solvation of the ions in the solution. 1

B. Solvation of the ions in the gas phase 4

1.3 Principles of the mass spectrometric method for the present gas phase solvation studies 11

1.4 Thermodynamic relations relevant to gas phase solvation reactions 13

1.5 Ion-solvent molecule interaction studies in the present laboratory . . 14

1.6 Purposes of the $M^+(H_2O)_n$ study 16

1.7 Significance of gas phase solvation reactions. 19

2. EXPERIMENTAL

2.1 General. 24

2.2 Instrumental requirements to observe gas phase hydration equilibria and the principles of method 25

2.3 The reaction chamber 30

Page

2.4 The reaction chamber pressure measurement 33

2.5 The reaction chamber temperature control and measurement 33

2.6 Creation of alkali ions and manufacture of a thermionic source 35

2.7 Production and transport of the hydrated ions out of the reaction chamber 37

2.8 Ion acceleration, mass analysis and ion current detection 41

2.9 Relation of the ion current to the ion concentration 42

A. Discrimination in transport through the reaction chamber 42

B. Discrimination due to stripping outside of the reaction chamber 43

C. Discrimination in mass analyzer tube . 44

D. Discrimination in the ion current detection. 45

3. RESULTS OF HYDRATION OF POSITIVE ALKALI IONS M^+ 47

3.1 Introduction and thermodynamic relations 47

3.2 Presentation of the results and general discussion 48

3.3 Equilibrium distribution of $M^+(H_2O)_n$. 83

Page

4. ELECTROSTATIC CALCULATIONS OF THE POTENTIAL ENERGIES OF THE CLUSTERS $M^+(H_2O)_n$ AND COMPARISON WITH EXPERIMENTAL RESULTS 86

4.1 Introduction 86

4.2 Interaction energies 86

A. Ion-permanent dipole forces 86

B. Ion-induced dipole forces 86

C. Dispersion forces 87

D. Dipole-dipole repulsive forces 87

E. Ion-ligand molecule repulsive forces . . 87

4.3 The present model for the electrostatic calculations. 88

A. Ion-permanent dipole interaction (EDIP) . 88

B. Ion-induced dipole interaction (EPOL) . . 91

C. Ion-ligand and ligand-ligand interaction energy due to dispersion forces (EDIS). . 92

D. Dipole-dipole repulsion energy (RDIP) . . 93

E. Ion-ligand molecule repulsive energies (REL) 96

4.4 Evaluation of the numerical value for the constant A in the electronic repulsion term REL = AR^{-12} 97

4.5 Discussion of electrostatic calculations.104

4.6 Comparison of electrostatic potential energies with previous calculations . . .110

4.7 The comparison of calculated $E^{\circ}_{n-1,n}$ with experimental $\Delta H^{\circ}_{n-1,n}$ for $M^+(H_2O)_{n-1}$ + $H_2O \rightleftarrows M^+(H_2O)_n$. 112

Page

4.8 Calculation of the entropy of the $M^+(H_2O)$. 120

5. APPLICATION OF EXPERIMENTAL RESULTS TO PROCESSES IN AQUEOUS SOLUTION 130

5.1 Comparison between the hydration energies of the alkali and halide ions 130

5.1a In solution 130

5.1b In the gas phase 131

5.2 Ion-ligand bond energies and hydration numbers. 140

6. OTHER APPLICATIONS OF HYDRATION MEASUREMENTS IN THE GAS PHASE. 146

6.1 Clustering equilibria and the catalysis of water condensation by ionic charges 146

6.2 Proton affinities of the alkali hydroxides in the gas phase 153

7. SUGGESTION FOR FURTHER RESEARCH 159

7.1 Solvation of alkali and halide ions by polar aprotic solvents. 159

BIBLIOGRAPHY. 161

LIST OF FIGURES

Figure		Page
2.1	Cross-sectional view of mass spectrometer.	26
2.2	Reaction chamber and acceleration plates for hydration reactions of alkali ions.	28
2.3	Cross-section, top and bottom view of reaction chamber	32
3.1 to 3.21	Log $K_{n-1,n}$ for the gas phase hydration of alkali ions, M^+ (M = Li, Na, Rb, Cs), at various temperatures, versus pressure of H_2O	49-69
3.22 to 3.25	Van't Hoff type plots of the equilibrium constants, $K_{n-1,n}$ for gas phase hydration of alkali ions, M^+ (M = Li, Na, Rb, Cs)	70-73
3.26	Enthalpies for clustering reactions $M^+(H_2O)_{n-1} + H_2O \rightleftarrows M^+(H_2O)_n$	79
3.27	Free energies of clustering reactions $M^+(H_2O)_{n-1} + H_2O \rightleftarrows M^+(H_2O)_n$	80
3.28	Plot of $\Delta H^\circ_{o,n}(Cs^+) - \Delta H^\circ_{o,n}(M^+)$ versus n showing that the above differences approach differences of total single ion heats of hydration obtained by Randles (R) and Latimer (L)	81
3.29	Plot of enthalpies for clustering reactions $M^+(H_2O)_{n-1} + H_2O \rightarrow M^+(H_2O)_n$ versus ΔH total single ion heats of hydration obtained by Randles.	82
3.30	Plot of equilibrium distribution of $Na^+(H_2O)_n$ at T = 300°K as a function of water pressure	84
4.1	$M^+(H_2O)$ model used in the theoretical calculations.	90
4.2	Plot of $A^{\frac{1}{2}}$ on logarithmic scale versus the Van der Waals radius of the inert gas atoms.	100

Figure Page

4.3 Comparison between experimental enthalpies $\Delta H_{o,n}$ and potential energies $\Delta E_{o,n}$ obtained on the basis of electrostatic type calculations for sodium hydrates $Na^+(H_2O)_n$ 108

4.4 Comparison between experimental enthalpies $\Delta H_{o,n}$ and potential energies $\Delta E_{o,n}$ for cesium hydrates $Cs^+(H_2O)_n$ 109

4.5 Plot of potential energies evolved for the reactions: $M^+ + H_2O \rightarrow M^+(H_2O)$ 116

4.6 Comparison of experimental $\Delta H^o_{n-1,n}$ and calculated potential energy differences $\Delta E^o_{n-1,n}$ for alkali ion clusters $M^+(H_2O)_n$ 117

4.7 Principal axes of H_2O and $Li^+(H_2O)$ used to calculate the moments of inertia. 123

5.1 Comparison of $\Delta H^o_{n-1,n}$ for hydration of alkali positive and halide negative ions 132

5.2 a,b Comparison of $\Delta H_{o,n}$ hydration of alkali and halide ions with total enthalpies of hydration of Latimer (L) and Randles (R) 137-138

6.1 Comparison of free energy of hydration $\Delta G^o_{n-1,n}$ with free energy of evaporation of 1 mole of water molecules from one mole of water droplets carrying a single ionic charge. 147

6.2 The variation of P_r/P_∞ as a function of droplet radius 151

6.3 Proton affinities of MOH versus ionization potential of M 156

LIST OF TABLES

Table		Page
3.1 to 3.4	Thermodynamic values for the gas phase hydration of the alkali ions	75-78
4.1	Ionization potentials and polarizabilities of alkali ions	94
4.2	Coefficient "A" for repulsion term AR^{-12} between two atoms of the noble gases	99
4.3	Potential energies of clusters $M^+(H_2O)_n$ from electrostatic calculations using repulsion term AR^{-12}	102
4.4	Individual energy contributions to potential energy calculations of cluster $Na^+(H_2O)_n$	106
4.5	Potential energies of clusters $M^+(H_2O)_n$ from electrostatic calculations using repulsion term AR^{-12}	115
4.6	Moments of inertia and M^+—OH_2 equilibrium distances	122
4.7	Force constants, vibrational frequencies and entropy contributions due to stretching vibrations of M^+—OH_2	125
4.8	Potential energy barriers for rotation (ΔP.E.) vibrational frequencies and entropy contributions due to two torsional vibrations of M^+—OH_2	127

Table Page

4.9 Translational, rotational and vibrational contributions to experimentally determined $\Delta S^{\circ}_{298°K}$ for reaction: $M^+ + H_2O \rightarrow M^+(OH_2)$ 128

5.1 Ion-water molecule bond energies in the liquid phase 143

5.2 Hydration numbers "h" for alkali ions 144

6.1 Free energy changes $\Delta G^{\circ}_{(1)}$, $\Delta G^{\circ}_{(2)}$ and ΔG°_{evap} as a function of radius of charged droplet 150

6.2 Proton affinities of alkali hydroxides MOH and thermochemical data used for their evaluation 155

1. INTRODUCTION

1.1 The Present Study

The present work deals with the hydration energies of the alkali ions in the reactions (1.1 to 1.4) occurring in the gas phase where M stands for Li, Na, Rb and Cs.

1.1 $$M^+ + H_2O \rightleftarrows M^+(H_2O) \qquad (0,1)$$

1.2 $$M^+(H_2O) + H_2O \rightleftarrows M^+(H_2O)_2 \qquad (1,2)$$

1.3 $$M^+(H_2O)_2 + H_2O \rightleftarrows M^+(H_2O)_3 \qquad (2,3)$$

1.4 $$M^+(H_2O)_{n-1} + H_2O \rightleftarrows M^+(H_2O)_n \qquad (n-1,n)$$

The present work is a continuation of an earlier investigation which dealt with the hydration of the potassium ion (1). The equilibrium constants for attachment of water molecules to the alkali ions were determined as a function of temperature. The enthalpy, free energy and entropy changes of the hydration reactions were then obtained by Van't Hoff plots. The experimentally determined enthalpy and entropy changes are compared with theoretically calculated values. The enthalpies of hydration (n-1,n) are also compared with the total enthalpies of hydration of ions in aqueous solution.

1.2 The Nature of Solvation

A. Solvation of ions in the solution

Hydration in solution is the result of interactions between the solute (the ions) and the solvent (water). Not

only must the interactions between the ions and the water molecules in their immediate vicinity be considered, but also the interactions with all the rest of the water. Solvation (hydration) in solution may be understood as the sum of all changes caused by the appearance of the ions of the electrolyte in solution (2).

The knowledge of the existence of hydrated ions in solution dates back to the beginning of this century (3). Despite the general acceptance that ions in solution are hydrated, serious disagreement between authors arises as soon as quantitative treatments of hydration are attempted. This difficulty occurs, because the water molecules in the hydration shell are in continuous exchange with the water in the bulk of the solution and it is only on a time average that a hydration shell may be said to exist around most ions (4). In order to account for the large discrepancy between the different methods of measuring hydration in solutions, Bockris (5) has suggested that hydration be divided into two main types, which he called "primary hydration" and "secondary hydration". "Primary" or "close" hydration refers to the water molecules, which are immobilized by the ion and move as one entity with it, while "secondary" or "distant" hydration refers to other ion-water interactions beyond the primary hydration shell.

"Distant" hydration does not depend on specific

molecular interactions between the ion and the solvent molecules and it can usually be dealt with satisfactorily by classical electrostatic theories, such as the Born equation (6), which assumes a continuous solvent. Theories based on continuous solvent models must cope with effects such as dielectric saturation, the true radii of ions in solution and the lack of spherical symmetry near the surface of the ion arising from the finite size of the water molecules (6).

On the other hand, "close" hydration does depend on specific molecular interactions between the ion and the solvent molecules. Molecular interaction models must take into account the coordination number and the orientation of the water molecules, ion-dipole, dipole-dipole interactions etc (6).

For the over-all effect of hydration Bockris used the expression "total hydration".

The separation of the "total hydration" effect into the interactions between ions and water molecules in their immediate vicinity, and the interactions with the rest of the water molecules represents a simplification (6). Since, however, in liquids increasing distance between two given particles is attended by a continuously, but gradually, decreasing regularity some simplification must be made to define a boundary between the water molecules of "close" and "distant" hydration.

It will be shown in the next section that studies of the hydration of ions in the gas phase allow determinations of the thermochemistry and reveal a relative stability of "close" hydrated ions in the absence of the bulk solvent.

B. Solvation of ions in the gas phase

The interactions of ions with solvating molecules in solution have been studied for many years. The corresponding studies of interaction of gaseous ions with "solvent" vapor are relatively recent (7).

Ions composed of clusters or a group of molecules of the type $M^+(H_2O)_n$ where n is a small number, must exist in the gas phase due to the forces of attraction between ions and neutral molecules. An ion of charge e has associated with it an electrical field of strength $F = e/r^2$ at a distance r. This field is of the order of 10^8 volts/cm at $r = 10^{-8}$ cm and 10^4 volts/cm at 10^{-6} cm. In fields of this magnitude all molecules experience a displacement of their electron cloud relative to the nuclei so as to produce an induced electrical dipole moment of $\mu i = el = \alpha F$, where l represents the effective separation of the positive and negative center and α the polarizability of the molecule. In addition a molecule like H_2O will also have an effective part of its permanent dipole moment μp, oriented by the electric field

of the ion. Thus, between the ion and molecule, there is a force of attraction due to ion-permanent dipole and ion-induced dipole forces.

The experimental indications for the existence of clustered ions were obtained by the earliest workers in the field of gaseous electronics. At the beginning of this century Rutherford and Thomson (8) discovered that the mobilities of ions in gases were lower than values predicted by the kinetic theory. They attributed this deviation to the formation of ion-clusters. The formation of ion-clusters was explained on the basis of the attraction forces discussed above.

The rough criterion for the stability of these ion-clusters was set by the earliest workers (10) as follows: $\frac{PE}{KE} = 1$. PE represents the potential energy of a molecule in the cluster and KE stands for the kinetic energy of average ion molecule impact. This comes from the Boltzman factor $e^{-\frac{\Delta E}{RT}}$, where $\Delta E = -PE$ and $RT = KE$. In essence the above expression states that if $PE = KE$ then there are roughly equal numbers of clustered and free ions.

Already in the early 1920's it was recognized that the above criterion was faulty (9). Thermodynamic equilibrium between an ion cluster and its dissociation products essentially depends not only upon the Boltzman factor but also upon entropy factors which weight it heavily in favour of dissociation. This means that the *a priori*

probability of a state must be included as a factor in the ratio of PE/KE in order that the condition for stability be fully represented (9). The ion clusters are a "condensed" state with relatively low entropy, while the dissociated ions and free molecules constitute a "dispersed" state with a higher entropy, or statistical weight. Unless much is known of the specific nature of a given possible cluster and its constituents, the number of molecules etc., it is impossible to evaluate the relative statistical weight factor g for dissociated and condensed states. It is accordingly necessary to set the criterion for cluster stability as $PE/gKE \geq 1$ (9). In this relation, the relative statistical weight g of the dispersed state may be greater than one by a considerable margin.

A second theory, to explain the discrepancy between the theoretical and experimental values of ionic mobility was put forward by Sutherland and Wellisch (9). This theory, which later on became known as "small ion theory", assumes that the increased size of the clustered ions is not the major factor in retarding the motion through the gas, but that the motion is retarded by momentum transfer as a result of the electrical forces between the ions and neutral molecules.

Munson, Tyndall and Hoselitz (10) studied ionic mobility in which the gas phase transport of ions was investigated as a function of F/P; F is the electric field

strength and P is the gas pressure. For example, in the study of the mobility of alkali metal ions in "moist" rare gases, the ion-clusters, $M^+(H_2O)_n$, $n \leq 6$ were used to explain the observed ionic mobilities. Munson et al. observed that the mobility of the clustered ion is not constant, but shows a variation with F/P. At high F/P only the unclustered ions appear and at low F/P only the "fully clustered" ions appear. To explain the anomaly of the appearance of only two mobilities and yet the variation of the mobility with F/P the following hypothesis was made (10). A cluster cannot form readily. It is assumed that until the first molecule is attached to the ion, there will be no attachment for the other molecules. When the first molecule attaches to the alkali ion, it must free itself from the energy of binding. Therefore a third body impact is required to release this energy, otherwise the ion-cluster dissociates. Once the first molecule has attached itself the other molecules can also do so; the excess binding energy can be taken up by the cluster as internal vibrational energy, which can be transferred to surrounding molecules in later collisions. From the initial addition of the first H_2O molecule in a three-body impact, where a noble gas atom serves as third body, the other H_2O molecules in the cluster can attach as rapidly as encountered up to the equilibrium number. The

average number of these molecules in the resulting labile cluster will vary as the energy of the ion varies. Below the highest F/P, possibly only the original ion will remain with one labile-attached molecule. These will be attached and detached in rapid sequence, giving a continuously varying mean mobility of the clustered ions for each F/P value. Therefore, the change of the mobility of clustered ions with F/P according to Munson et al. (10) is due to changing the average size of the cluster formed.

The average size of the ion-cluster varies not only with the polarity of the surrounding molecules but also with the size of the ion and the temperature. This raises the question as to whether only strongly polar molecules can form ion-clusters. Some light was thrown on this matter by the work of Munson and Hoselitz (11), who studied the mobilities of alkali ions at low fields F, in various nonpolar gases. The presence of clustering was observed at low temperatures in some gases and even at room temperatures with Li^+ ions in Xe gas.

Although the existence and the importance of ion clusters in mobility measurements has been recognized for many years, the systematic study of ion-molecule clusters in the gas phase did not start until development of "high pressure" mass spectrometry. In an ordinary mass spectrometer used for analysis (isotope analysis, qualitative

and quantitative analysis of vapours) the pressure in the ion source and mass analysis region is kept low so that the ions can leave the ion source and be mass analyzed without the occurrence of collisions with gas molecules. If the pressure of the ion source is increased, collisions of the ions with gas molecules begin to occur and these can lead to ion molecule reactions which change the nature of the primary ions. The first ion-molecule reaction was observed by J. J. Thomson (12) with the first mass spectrograph. However it was only recognized during the early 1950's that ion-molecule reactions might play a large role in gas phase chemistry. With this in mind V. Talroze (13), D. P. Stevenson (14), W. Hamill (15) and F. H. Field, J. L. Franklin and F. W. Lampe (16) started systematic studies.

For the purposes of the present discussion ion-molecule reactions can be divided into two types: true chemical reactions in which chemical bonds are formed and broken and clustering reactions where association occurs mainly because of the operation of electrostatic forces i.e. ion-dipole and ion-induced dipole attractions. An example of a chemical process is given by the association of an ethylene ion with an ethylene molecule to form a butene ion (reaction 1.5), while reactions 1.6 and 1.7 represent typical clustering reactions

1.5 $C_2H_4^+ + C_2H_4 = C_4H_8^+$

1.6 $Li^+ + nH_2O = Li^+(H_2O)_n$

1.7 $Li^+ + nXe = Li^+(Xe)n$

It is interesting to note that almost all ion-molecule investigations have dealt with reactions of the chemical type.

The clustered ions $H_3O^+(H_2O)_n$ have been detected mass spectrometrically by Beckey (17) who observed clusters $H_3O^+(H_2O)_n$ up to n = 10. Knewstubb and Sugden (18) in a mass spectrometric study of ionization in flames observed the ions $H_3O^+(H_2O)_n$ and $NH_4^+(NH_3)_n$ up to n = 4. Sieck, Abramson and Futrell (19) have studied the mechanisms leading to the formation of $H^+(CH_3OH)_3$ and $H^+(C_2H_5OH)_3$. The ions $H^+(H_2O)_n$, $H^+(CH_3OH)_n$, $H^+(CH_3OCH_3)_n$, $H^+(CH_3NH_2)_n$, $H^+[(CH_3)_2NH]_n$ and $H^+[(CH_3)_3N]_n$ were observed by Munson (20) in the high pressure mass spectra of H_2O, CH_3OH, CH_3OCH_3, CH_3NH_2, $(CH_3)_2NH$ and $(CH_3)_3N$ respectively, where n = 1-2 for each species. Yang and Conway (21) have studied the system O_{2n+2}^+ up to n = 4. The clustered ion $K^+(H_2O)$ was detected by Chupka (22) in a mass spectrometric study of ions emerging from a heated Knudsen cell containing KCl salt. The ion-clusters $M^+(H_2O)$, where M = Li, Na and K were observed in flames by Hayhurst and Sugden (23). They examined the extent to which alkali ions are hydrated under flame conditions (premixed H_2,O_2, N_2) at atmospheric pressure. Aqueous solutions of alkali

metal chlorides were sprayed into the gas mixture to give a concentration of alkali chloride in the flame of 1 part in 10^7. The principal positive ions detected by flame mass spectrometry were $M^+(H_2O)$. From the constancy of the ratio $M^+/M^+(H_2O)$ with distance, over a restricted range of distances, near the reaction zone in which zone the temperature was nearly constant, it was assumed that the equilibrium for the reaction $M^+ + H_2O \rightleftarrows M^+(H_2O)$ was established. On this assumption equilibrium constants, K_{eq} were derived for two temperatures. From the variation of equilibrium constants, $K_{0,1}$ with temperature $\Delta H_{0,1}$ values of 54, 27 and 40 kcal/mole were obtained for M^+ = Li, Na, K respectively. The error in the above values for $\Delta H_{0,1}$ is apparent, since the $\Delta H_{0,1}(K^+) >> \Delta H_{0,1}(Na^+)$. This is opposite to what one would expect, since Na^+ is a smaller ion than K^+ and therefore $Na^+ - H_2O$ interaction energy should be bigger than $K^+ - H_2O$ interaction. This indicates that the author's assumptions about equilibrium conditions and the constancy of the temperature in the reaction zone are somewhat illusory.

1.3 Principles of the Mass Spectrometric Method for the Present Gas Phase Solvation Studies

Mass spectrometric observations of the clustered ions discussed in the previous section were mainly in-

cidental and were not pursued further. The most extensive studies of the ion-cluster or ion solvation reactions in the gas phase occurring under equilibrium conditions were carried out in this laboratory.

In order to measure the gas phase solvation of ions, the instrument required must produce ions, allow them to react and equilibrate at high pressures and finally analyze the reactant and product ions. Because of its ability to satisfy all three requirements a modified mass spectrometer has been used in this study.

The alkali ions were produced by thermionic emission from a heated filament coated with suitable salt containing the desired ion. Since thermionic emission can be obtained only at elevated temperatures, the thermionic source was separated from the reaction chamber whose temperature was controlled independently. In order to attract the ions from the thermionic source to the reaction chamber, a potential difference was applied between thermionic source and reaction chamber. The ions entering the field free reaction chamber gradually lose their excess kinetic energy, through collisions with neutral water molecules. Thermalized ions diffusing to the exit slit and escaping into the vacuum region are captured by electric fields, accelerated, and magnetically mass analyzed. In the present measurements the pressures used in the reaction chamber were in the range of 0.2 - 3 torr. Since

the ion acceleration, mass analysis and collector regions should be maintained at less than 10^{-4} torr for the mass spectrometer to function properly, the present instrument used a high capacity pumping system and reaction chamber with a narrow exit slit (to reduce the gas flow out of the reaction chamber).

1.4 Thermodynamic Relations Relevant to Gas Phase Solvation Reactions

Alkali ions which are ejected by a heated filament drift into the reaction chamber under the influence of an electric field. In the field free reaction chamber the alkali ions lose their excess translational energy and react with water molecules to form hydrated ions. Assuming that equilibrium is achieved, the equilibrium constant $K_{n-1,n}$ for the hydration reaction n-1,n (reaction 1.4) is given by the following relation:

$$K_{n-1,n} = \frac{P_{M^+(H_2O)_n}}{P_{M^+(H_2O)_{n-1}} P_{H_2O}}$$

where $P_{M^+(H_2O)_{n-1}}$ is the pressure of the reacting ion and $P_{M^+(H_2O)_n}$ that of the product. P_{H_2O} is the partial pressure of water in the reaction chamber. The pressure ratio of the ions was assumed to be equal to the ratio of the intensities of the respective ions, recorded by the mass spectrometer. The validity of this assumption is further

discussed in Chapter 2.

The Gibb's free energy of the reactions 1.1 to 1.4 can be calculated by the following equation:

$$(1.1) \qquad \Delta G^{o}_{n-1,n} = -RT \log_e K_{n-1,n}$$

where R is the universal gas constant, T is the absolute temperature and $K_{n-1,n}$ is the equilibrium constant.

Since the values for $K_{n-1,n}$ in the present work were calculated for a standard state of 1 torr, the values for $K_{n-1,n}$ were multiplied by 760 before substitution into the above equation in order to obtain $\Delta G^{o}_{n-1,n}$ in a standard state of 1 atm.

From the measurements of the equilibrium constants at various temperatures, it was possible to determine the enthalpies $\Delta H^{o}_{n-1,n}$ by means of Van't Hoff plots. The entropy values $\Delta S^{o}_{n-1,n}$ were calculated from the well known

$$(1.2) \qquad \Delta G^{o}_{n-1,n} = \Delta H^{o}_{n-1,n} - T\Delta S^{o}_{n-1,n}$$

1.5 Ion-solvent Molecule Interaction Studies Done in the Present Laboratory.

In the past few years the following ion solvation reactions occurring under equilibrium have been investigated in this laboratory:

$H_3O^+(H_2O)_n$

The $H_3O^+(H_2O)_n$ system has been extensively studied in

this laboratory (24) and thermodynamic values for the reactions

$$H_3O^+(H_2O)_{n-1} + H_2O \rightleftarrows H_3O^+(H_2O)_n$$

have been determined up to n=8. More recently the $H_3O^+(H_2O)_n$ system was also invesigated by F. H. Field (25) and his results are in excellent agreement with Kebarle et al (24). A. Good, D. Durden and P. Kebarle (26) have made a kinetic study of hydration of the proton. Employing a quadrupole mass spectrometer they have determined the rate constants for the forward reactions

$$H^+(H_2O)_{n-1} + H_2O \xrightarrow{N_2} H^+(H_2O)_n$$

for n=2 to n=4. With the aid of the equilibrium constants determined previously (24) in this laboratory, they were able also to calculate the rate constant of the reverse reactions.

In addition to the reactions cited above, the competitive solvation of protons by H_2O and CH_3OH was also investigated (27) in this laboratory.

$NH_4{}^+(NH_3)_n$

The solvation of $NH_4{}^+$ ion by NH_3 was studied in this laboratory (28,29) and the thermodynamic values for the reactions:

$$NH_4{}^+(NH_3)_{n-1} + NH_3 \rightleftarrows NH_4{}^+(NH_3)_n$$

have been determined up to n=5. In addition competitive solvation of NH_4^+ by NH_3 and H_2O was also investigated (28).

$X^-(H_2O)_n$

The gas phase hydration of halide negative ions have been studied in this laboratory by M. R. Arshadi, R. Yamdagni and P. Kebarle (30). By determination of the equilibrium constants for the general reaction:

$$X^-(H_2O)_{n-1} + H_2O \rightleftarrows X^-(H_2O)_n$$

at various temperatures the thermodynamic values of $\Delta H^o_{n-1,n}$, $\Delta G^o_{n-1,n}$ and $\Delta S^o_{n-1,n}$ were determined. In addition to the halide negative ions, the gas phase hydration of O_2^-, OH^- and NO_2^- were also studied (31).

1.6 Purposes of the $M^+(H_2O)_n$ Study

One advantage of working in the gas phase is that the hydration of positive and negative ions can be studied separately. Although positive or negative ions have a separate existence in the gas phase, in solution the total number of positive charges is always equal to the total number of negative charges present. This makes it very difficult to assess the properties of individual ions in solution since one is always dealing with both species. The question of the possibility of

producing only positive or only negative ions in the gas phase i.e., the separate existence of the ions in the gas phase is due to very low concentrations at which the work is possible. Thus it can be calculated that the ion concentrations are roughly 10^6 ions/cc, which corresponds to a 10^{-14} molar concentration in solution. At such low concentrations also separate positive ions could be produced in aqueous solution, for example by shooting in Na^+ ions. However, they could not be studied in solution at these low concentrations. The advantage of the technique thus lies in the ability to measure extremely low concentrations of ions in the gas phase with the mass spectrometer.

The excellent review on the methods of assigning individual ion heats, free energies and entropies of hydration in solution, given by Rosseinsky (31) indicates that most methods are either based on dividing by two the thermodynamic functions of selected anion-cation pairs or on using some extrapolation procedure involving the ionic radii. Since water is not a dimensionless and structureless liquid, the hydration of equal-size cations and anions is not necessarily the same. Some authors have attempted to account for the specificity in ionic hydration by adding different increments to the crystal radii of anions and cations (32), by considering the different orientation of water molecules around the ions (33), or

by taking into account the quadrupole moment of the water molecule (34).

The agreement between these different methods is often surprisingly good, especially in the case of individual heats of hydration. However, none of these values should be considered as entirely reliable since they are all based on the assumption that the true ionic radii are known. The only technique that has been developed for the evaluation of absolute hydration energies of single ions, without any assumptions about the dimensions of the ions, is based on the measurement of the volta potential. The volta potential is measured between one electrolyte solution and another surface separated from the solution by a vacuum or an inert gas (35). Randles (35) has applied this method to evaluate individual hydration energies of alkali and halide ions.

In the beginning of this section it was mentioned that one of the advantages of working in the gas phase is that the hydration of positive and negative ions can be studied separately. Thus one of the purposes of the study of the hydration of the positive alkali ions was to compare the results with the hydration energies of negative halide ions. The gas phase hydration of halide ions was carried out in this laboratory (30), simultaneously with the present study. The most important feature of the present study is a comparison of the gas phase results for the

hydration of the alkali and halide ions with the individual ion hydration energies in the solution evaluated as discussed above. This comparison will be discussed in chapter 5.

Another important feature of the present study is a comparison of experimental hydration energies $\Delta H^{\circ}_{n-1,n}$ with classical electrostatic energies $\Delta E^{\circ}_{n-1,n}$, based on ion-dipole interactions. Since the alkali ions are spherical, one might expect that their hydration energies should be most amenable to this type of calculation.

The present results have also allowed us to evaluate the proton affinities of the alkali hydroxides in the gas phase, discussed in chapter 6. Proton affinities of alkali hydroxides have not been previously reported.

The applications of the gas phase cluster studies are not restricted to ionic solutions. There are a number of fields in which ion clusters play an important part. These fields are considered in the next section.

1.7 Significance of Gas Phase Solvation Reactions

Before leaving this chapter, it is appropriate to mention in a few words the importance of ion cluster studies and their application in the other fields of chemistry and physics. The role of clusters in ion mobility and flame chemistry has already been mentioned. Lind (36) has briefly reviewed the role of ionic clusters

in radiation chemistry. According to Lind's theory an ion can attract one or two molecules through polarization and hold them until neutralized by an oppositely charged ion. The heat of neutralization and the close proximity of ions and attached molecules would promote chemical reaction, polymerization, decomposition etc. Later on this theory was over-shadowed by the free radical theory of Eyring, Hirschfelder and Taylor (37). The Eyring theory postulates that the reaction of single ions and free radicals and molecules is more probable than large ion cluster reactions. The product of the neutralization of ions or ion clusters and also the products of dissociation of excited molecules may be free radicals or atoms which can initiate chain reactions and thus improve yield (36).

Early in the 1950's, however, Lind's theory gained additional support when it was shown, by mass spectrometric work that long lived complex ions are formed between ions and neutral molecules (38). Recently in a study of the radiolysis of ethanol vapour, Bansal and Freeman (39) have attributed the decrease of acetaldehyde and hydrogen yields with increasing dose to the scavenging of the electrons by acetaldehyde with ultimate production of $CH_3CHO^-(C_2H_5OH)_n$. The same authors have postulated the formation of $H^+(C_2H_5OH)_n$ and $NH_4^+(C_2H_5OH)_n$.

Formation of ion clusters in the D-region (50 - 85 km

altitude) of the ionosphere has been confirmed by the investigations of Narcisi and Bailey (40). In experiemnts carried out by rocketborne quadrupole mass spectrometers, they have observed that the clusters $H_3O^+(H_2O)_n$ n=0,1,2 appeared to be the dominant positive ions at an altitude of 60 to 80 km. The "D region simulation" flowing afterglow experiment by Ferguson et al (41) have led them to suggest a mechanism for the formation of the clusters $H_3O^+(H_2O)_n$, in the ionosphere with n as large as 6. Recently, Kebarle et al. (27) measured the rate constants for the system $H_3O^+(H_2O)_n$ up to n=4. Utilizing these rate constants, Ferguson et al. (41) calculated concentrations of $H_3O^+(H_2O)_n$ near the concentration maximum at 80 km. They found that calculated values agree well with the observed values of Narcisi and Bailey (40) mentioned above. Thus utilizing Kebarle et al's data the qualitative water cluster ion production scheme proposed earlier has been made nearly quantitative.

Primary negative ions also may form clusters with neutral molecules in the D region. Formation of clusters such as $O_2^-(H_2O)_n$, $NO^-(H_2O)$ and $CO_4^-(H_2O)$ have been postulated (42). Bates and Dalgarno (43) and W. Swider (44) have calculated loss rates for metallic ions for various processes in the ionosphere (90-100 Km altitude). They have postulated that the lifetime of a metallic ion M^+(M^+ = Na, Ca, Mo, K) in the upper atmosphere above 100

km is limited by the radiative association processes,

$$M^+ + O \rightarrow MO^+ + h\nu$$
$$M^+ + O_2 \rightarrow MO_2^+ + h\nu$$

W. Swider (44) suggested that three body reactions probably dominate the loss of metallic ions near 90 km and below.

$$M^+ + O_2 + O_2 \rightarrow MO_2^+ + O_2$$
$$M^+ + O + O_2 \rightarrow MO^+ + O_2$$

The importance of alkali ions in the gas phase chemistry and the applications to the upper atmosphere are evident from the number of papers devoted to it at a recent symposium (45). The chemistry of these alkali ions in the upper atmosphere is not yet established however. In many gas phase situations, including the upper atmosphere the alkali ions are the final ions, since they have the lowest ionization potentials known. Once the charge is transferred to them it is retained. We would suggest that if the gas phase contains traces of water (as in the D-region where $H^+(H_2O)$ and $H^+(H_2O)_2$ account for 35% of the total positive ions), the alkali ions M^+ will probably form $M^+(H_2O)_n$. Like alkali ions, which are the final ions in the ionosphere due to their lowest ionization potential, Ferguson et al (46) postulated that NO_3^- ions are final negative ions in the ionosphere because they are believed to have the highest

electron affinity (46). Recent rocket measurements of negative ions in the ionosphere suggest that $NO_3^-(H_2O)_n$ (n=0-5) may be the dominating negative charge carriers (47). In view of the importance of $NO_3^-(H_2O)_n$ in the ionosphere, a study is currently being conducted in this laboratory (48) to determine the thermodynamics of the reactions

$NO_3^-(H_2O)_{n-1} + H_2O \rightleftarrows NO_3^-(H_2O)_n$

2. EXPERIMENTAL

2.1 General

Measurements were made with a 60°, 15 cm radius mass spectrometer, which had been specially modified for the study of ion hydration in the gas phase. The primary alkali ions were generated by thermal ionization from a platinum filament, coated with a suitable salt containing the desired ion. The ions react with water vapour in the electrically field free high pressure reaction chamber (pressures up to 3 torr). The residence time of the ions is sufficiently long for the achievement of equilibrium with the surrounding water vapour. Some of the ions escape from the reaction chamber by diffusion and mass flow into a high vacuum region containing the accelerating electrodes. High vacuum ($\sim 10^{-4}$ torr) was maintained by the low conductance of the gas out of the reaction chamber and by the high capacity pumping system (pumping speed approximately 350 l/sec outside the chamber).

The ions were accelerated and focussed by a modified Nier type acceleration system. Detection, after magnetic mass analysis was obtained by a 17 stage electron multiplier and a Victoreen femtometer. The mass spectrometer was designed and assembled by G. Collins (49) and the apparatus was modified by S. K. Searles for the study of the gas phase hydration of potassium ions (50). Features of the instrument of particular importance to the gas phase hydration

work are described in the subsequent experimental section.

2.2 Instrumental Requirements to Observe Gas Phase Hydration Equilibria and the Principles of Method.

The instrumentation required for the study of the gas phase hydration of ions, must produce ions, allow them to react and reach equilibrium at high water pressures (in the torr range) and mass analyze the resulting ions. To satisfy these requirements certain modifications had to be made to a conventional mass spectrometer. A diagram of the main mass spectrometer set-up used in the present study is shown in Figure 2.1. A more detailed diagram of the ion source is shown in Figure 2.2 and 2.3. Theory of the mass spectrometer is not new and may be found readily elsewhere (51).

Most of the modifications apply to the reaction chamber (ion source) of the mass spectrometer. In order to assure the achievement of equilibrium, the reaction chamber has to be able to handle pressures in the torr range while maintaining the high vacuum conditions in the analyzing section. Since the primary ions are generated by thermionic emission and the thermionic emission can be obtained only at elevated temperatures, the thermionic source must be separated from the reaction chamber whose temperature is to be controlled independently. See Figure 2.2. It is also necessary that the attachment reactions be carried out in a field free region. Therefore, the

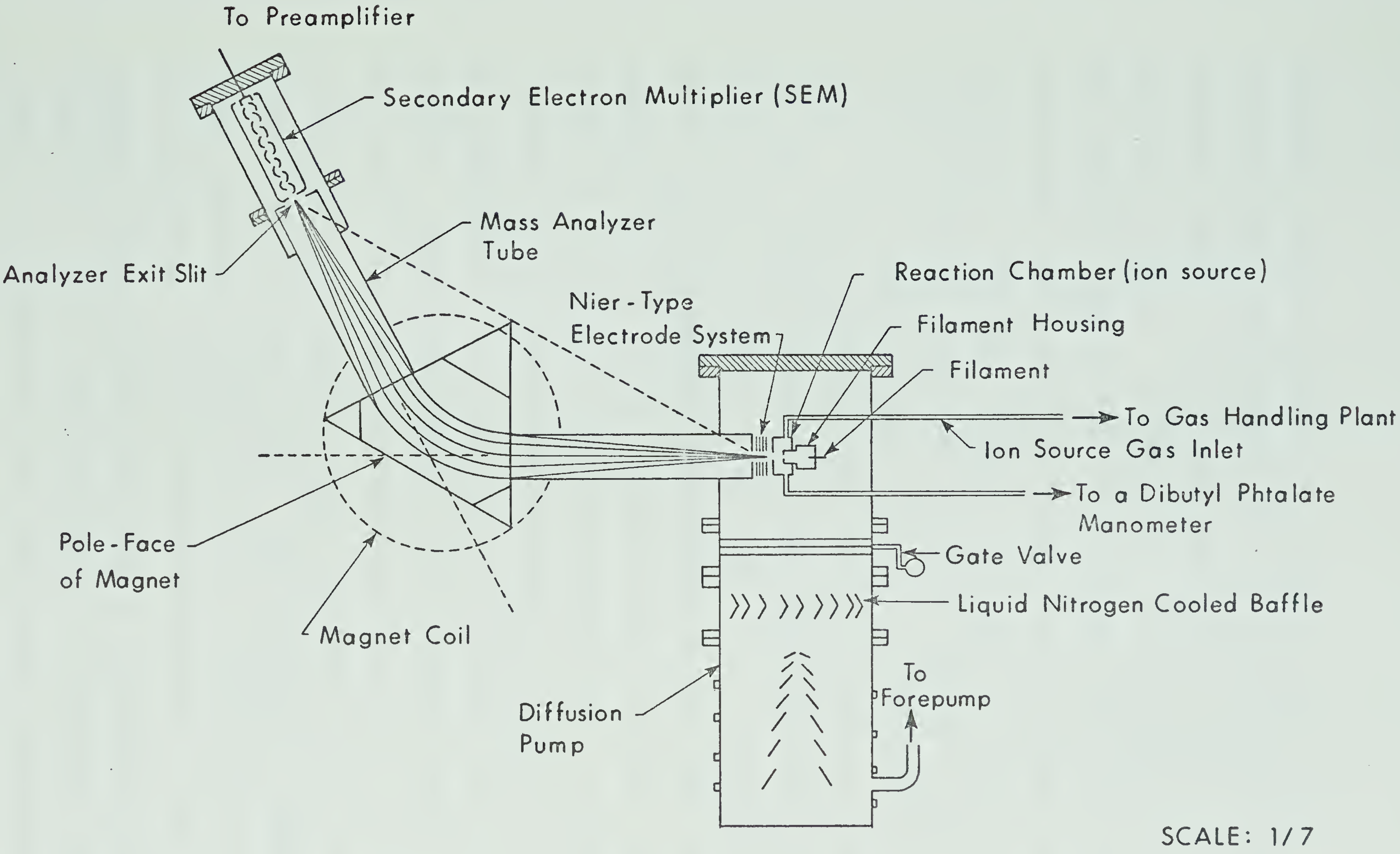
To Preamplifier
Secondary Electron Multiplier (SEM)
Mass Analyzer Tube
Analyzer Exit Slit
Reaction Chamber (ion source)
Nier-Type Electrode System
Filament Housing
Filament
To Gas Handling Plant
Ion Source Gas Inlet
To a Dibutyl Phtalate Manometer
Gate Valve
Pole-Face of Magnet
Liquid Nitrogen Cooled Baffle
Magnet Coil
To Forepump
Diffusion Pump
SCALE: 1/7

FIGURE 2.1 CROSS-SECTIONAL VIEW OF MASS SPECTROMETER

repeller voltage, which is an essential part of the conventional mass spectrometer has to be eliminated from the reaction chamber of the mass spectrometer used in the solvation studies. In order that the high pressure of the reaction chamber does not interfere with the performance of the mass spectrometer, a high capacity pumping speed system is required. The gas was pumped through a six inch liquid nitrogen baffle and six inch gate valve by a 1400 l/sec diffusion pump, backed by a 425 l/minute fore pump. These components were all mounted directly below a six inch diameter tube which surrounded the mass spectrometer reaction chamber. See Figure 2.1. The pumping speed at the reaction chamber was measured as 350 l/sec for ammonia with the liquid nitrogen baffle uncooled (50). The speed was calculated from the pressure drop in the gas handling plant reservoir with respect to time and from the pressure in the vacuum housing (measured by an ion gauge). In this measurement the ion gauge pressure was 2.1×10^{-4} at a reaction chamber pressure of 3 torr. Cooling the baffle with liquid nitrogen decreased the ion gauge pressure to 3.8×10^{-5} torr. This indicates a pumping speed increase to 1900 l/sec due to condensation of ammonia on the baffle. A more detailed description of the high capacity pumping system was given in references (49,50). Figure 2.2 and 2.3 show the design of thermionic source used in the present work and the previous investigation

1. Reaction chamber milled out of solid stainless block
2. Filament
3. Filament housing
4. Nichrome heat reflector
5. Cu heat shield (silver soldered to ion source)
6. Ceramic insulator
7. Chamber lid carrying channels for
    a) vapor supply
    b) pressure measurements
8. Ion exit slit leading to ion accelerating electrodes and mass analysis
9. Thermocouple wells
10. Cu reaction chamber support plate (+ 1850 V)
11. Draw out plate (+ 1500 V)
12. Focus, half plates (+ 100 V, 60 - 180 V)
13. Beam Defining (0.0V)
14. Beam center, half plates (0.0V, 100 V)
15. Entrance to mass analyzer (0.0V).

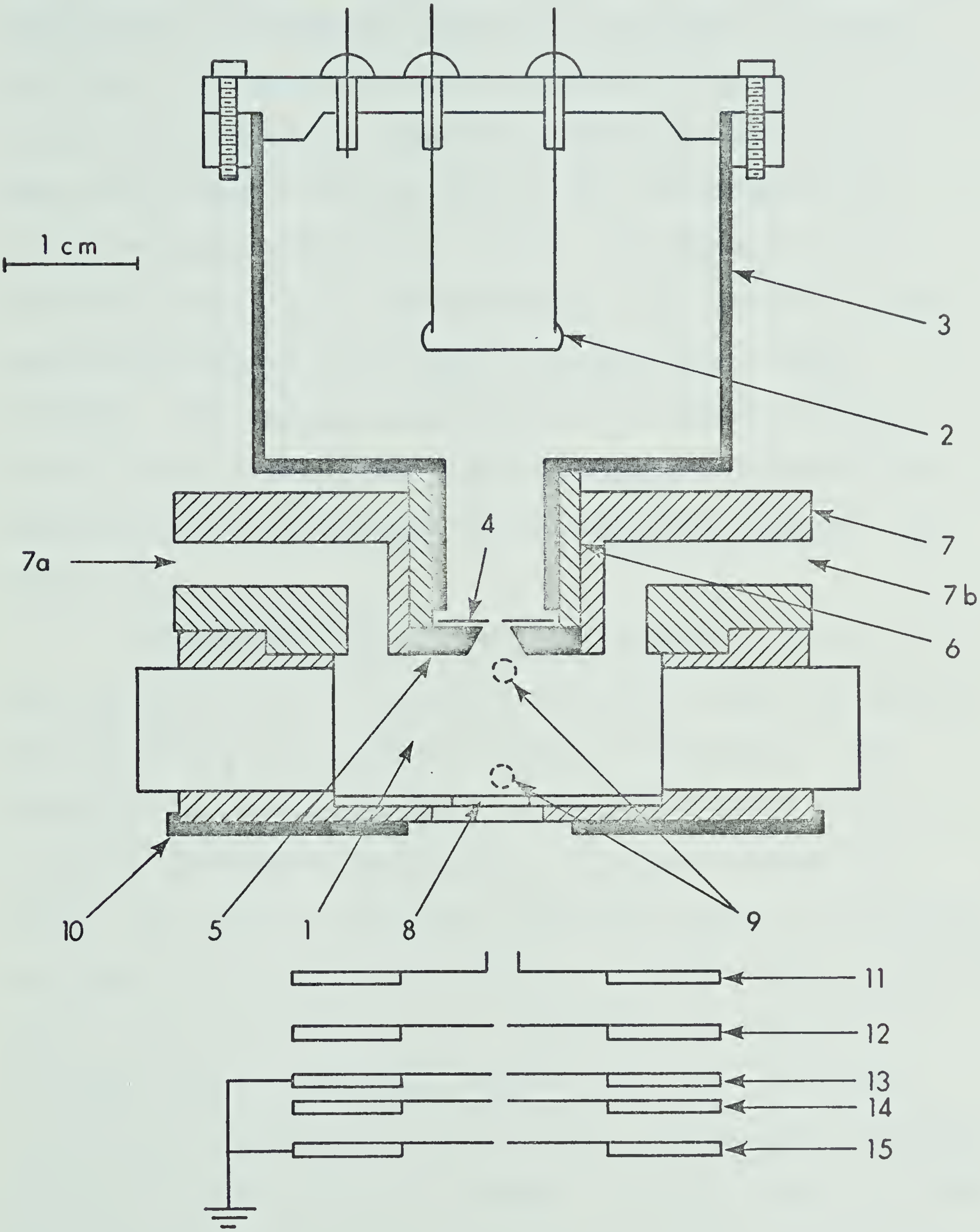
1 cm
3
2
4
7
7a
7b
6
10
5
1
8
9
11
12
13
14
15

FIGURE 2.2 Reaction chamber and acceleration plates for hydration reactions of alkali ions

for hydration of the potassium ion (50). The design of two additional ion sources, which were necessary to prove that the reactions were not in thermal disequilibrium due to the heating of the reaction chamber by the filament and the presence of the drift field are described by S. K Searles in his Ph.D. thesis. The Kunsman source (52), described in the next section, was found to be the most satisfactory source for all alkali ions except lithium. The thermal ionization in the Kunsman source arises from a specially prepared filament located in a housing which was attached to the reaction chamber. See Figure 2.2.

The heater current to the filament in Figure 2.2 was controlled by two variable autotransformers in series and regulated by a constant voltage transformer. The constant voltage transformer received 110 V.A.C. from a 3000 V isolation transformer, which was plugged into mains, 110 V.A.C. The power required to give a sufficient emission of ions from the filament at water vapour pressures up to 1 torr was about 20 W. The distance between the filament and the reaction chamber was 2 cm. A ceramic insulator thermally and electrically isolated the filament housing from the reaction chamber. Thermal radiation from the filament was reflected by a nichrome reflector backed by a copper plate which dissipated heat energy to the reaction chamber. Because the ions which were emitted by

the heated filament diffuse rapidly to the wall, it was necessary to attract the ions to the reaction chamber by potential difference to obtain a detectable ion current after mass analysis. Experimentally, the highest M^+ currents to the reaction chamber occurred with the filament housing, and the filament at the same potential. A potential difference of 225 V between the filament housing and the reaction chamber was necessary to attract a sufficient number of ions into the reaction chamber.

This potential difference gives an electric field strength of about 110 V/cm.

2.3 The Reaction Chamber

Figure 2.2 shows the reaction chamber attached to the filament housing. The purpose of the reaction chamber was to provide a high pressure system where clustering equilibrium conditions could be achieved at uniform temperatures which could be varied over a wide range.

The required reaction chamber pressure for investigation of gas phase solvation reactions can be approximately calculated. To obtain clusters as large as six ligands about the central ion, the ion must undergo six collisions plus additional collisions to remove the excess energy produced by the attachment reaction. For a distance l of 0.5 cm (the distance between the ion entrance and exit slit of the reaction chamber), an ion in a static gas undergoes approximately 150 collisions at 0.1 torr (50).

Since the ion undergoes approximately 150 collisions at 0.1 torr, the ionic clusters are probably in equilibrium. To test the equilibrium assumption it is desirable to be able to vary the pressure in the reaction chamber by about a factor of ten, that is to increase the reaction chamber pressure to 1 torr.

However, the mass spectrometer, ion acceleration and mass analysis region must be maintained at a pressure less than 10^{-4} torr. Above this pressure the ion beam coming out from the reaction chamber is seriously scattered by collisions. Therefore, a pressure differential of about 10^4 must be maintained between the reaction chamber and the ion acceleration region outside. This can be achieved by high capacity pumping discussed in the previous section and by reducing the leakage of gas out of the reaction chamber. In the present instrument the total area of the reaction chamber slots have been reduced by about a factor of 100 and the pumping speed at the reaction chamber increased by about 100 over a conventional mass spectrometer. Because the conductance of a slit increases when the mean free path of the gas is smaller than the slit width it was desired to make the slit width less than 30 μ, the mean free path of water at 1 torr and 273°K (53). The increase in conductance is due to a transition from molecular flow to viscous flow (54). The area of the ion exit slit was 0.012 mm x 3 mm, typically. The ion exit

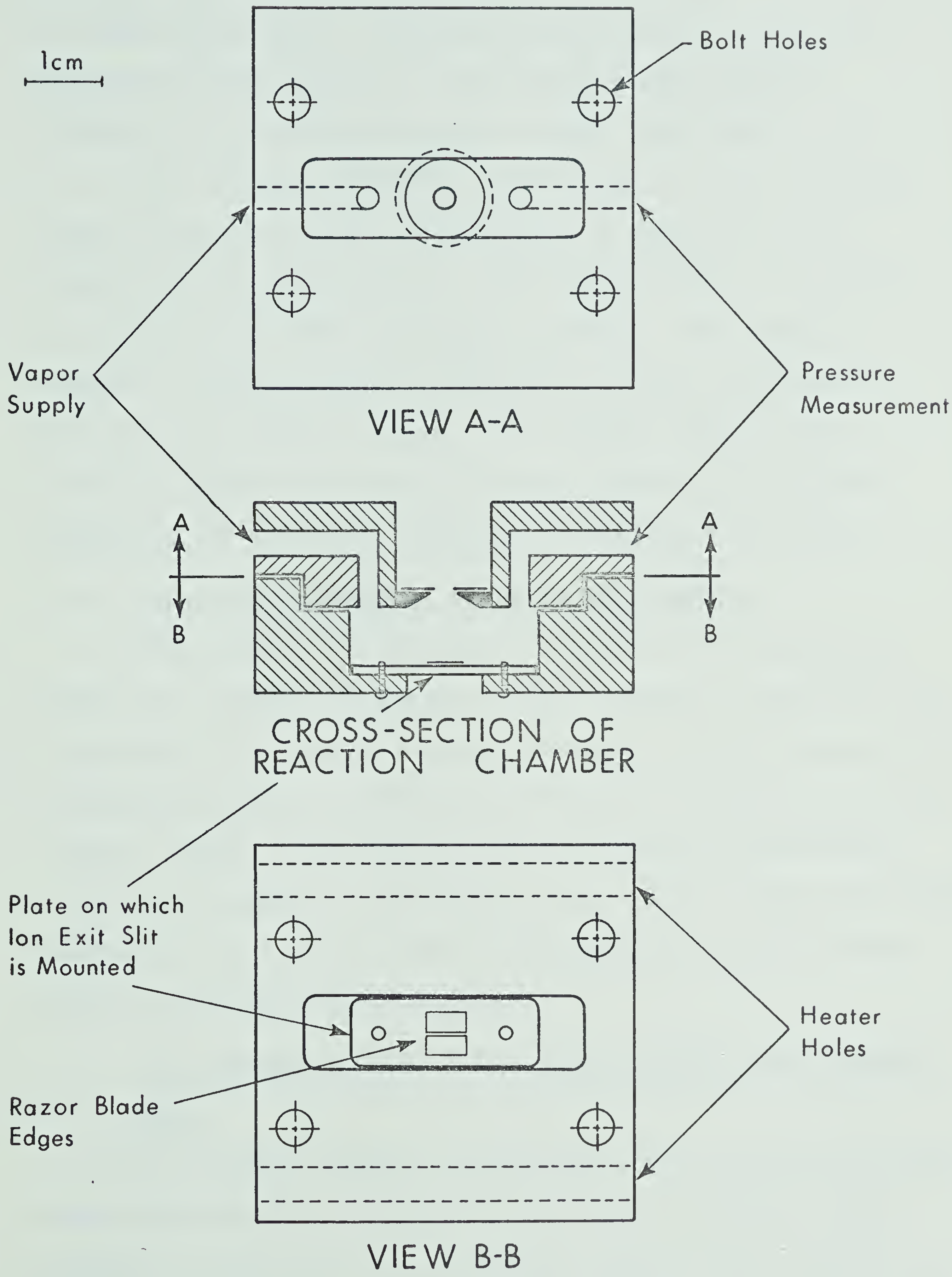
1cm
Bolt Holes
Vapor Supply
Pressure Measurement
VIEW A-A
A
B
A
B
CROSS-SECTION OF REACTION CHAMBER
Plate on which Ion Exit Slit is Mounted
Heater Holes
Razor Blade Edges
VIEW B-B

FIGURE 2.3 Cross-section, top and bottom view of reaction chamber

slit was made by spot welding stainless steel razor blade edges to a plate which was 1.5 mm thick and contained a 1 x 4mm centre slot. A plate on which the ion exit slit was mounted was bolted to the bottom of the reaction chamber by two stainless steel screws. See Figure 2.3.

The reaction chamber (see Figure 2.3) was machined from a single stainless steel block in order to obtain a more uniform temperature. The heater holes were placed 1.5 cm from the reaction chamber cavity. The reaction chamber lid was carefully machined to give a good fit to the reaction chamber bottom. The contact between the reaction chamber top and bottom was improved by securely fastening the two parts together with four heavy bolts.

2.4 The Reaction Chamber Pressure Measurement

The pressure of the reaction chamber was measured by means of a dibutyl phthalate U type manometer connected with a separate line to the reaction chamber. At room temperature the vapor pressure of dibutyl phthalate is almost negligible, (1mm at 148°C). To obtain accurate pressure measurements from the manometer, a cathetometer was used to read the height difference to ± 0.1 mm which corresponds to ± 0.0077 torr error in the ion source pressure.

2.5 The Reaction Chamber Temperature Control and Measurement.

The reaction chamber temperatures above room temperature were achieved by two heaters located in the heater holes drilled in the wall of the reaction chamber (See Figure 2.3).

Each heater was made by winding an 0.010 inch diameter Mo wire around a quartz rod and placing the rod and wire coil inside a 5 mm diameter quartz tube. About 30W was needed to heat the ion source to 400°C. For reaction chamber temperatures less than room temperature, the heaters were removed and the heater holes were used as the cooling channels of a circulatory system. Two Kovar seals were soldered to the two heater holes on the same face of the reaction chamber. Each of these seals were attached to glass tubing which led out of the vacuum housing through "O" ring seals. To complete the reaction chamber circulatory system copper tubing was connected to the remaining open ends of the heater holes. Either water or acetone, depending on the desired final temperature, was circulated through the reaction chamber by a Colora Ultra-Thermostat which regulated the bath temperature to $\pm$ 0.01°C. To achieve temperatures below 0°C, the bath was filled with acetone and cooled with a 2L stainless steel beaker which was filled with dry ice. The greatest depth of beaker immersion in the bath allowed temperatures of the reaction chamber as low as -50°C.

The temperature of the reaction chamber was measured by means of an iron-constantan thermocouple. The thermocouple was placed in a well drilled through to the reaction chamber cavity. The cavity was capped by a piece of 0.005 inch thick nichrome sheet which was spot welded

to the wall.

The thermal emf was measured relative to a 0°C reference thermocouple by a Honeywell potentiometer. The temperature of the thermocouple could be read to within 1°C.

2.6 Creation of Alkali Ions and Manufacture of a Thermionic Source.

It is well known that an abundant supply of alkali ions can be obtained by thermionic emission from a heated filament coated with suitable salt containing the desired ion. The relative probability of emission of positive ions is given by the Langmuir-Saha equation (52)

$$\frac{n_+}{n_o} \propto \exp \frac{\phi - I}{kT}$$

where n_+ is the number of positive ions M^+ and n_o is the number of neutral species M. ϕ is the work function of the filament surface and I is the ionization potential of M. Because $I-\phi >> kT$ at 300°K, thermal ionization sources must be operated at high temperatures. The difficulty in using a high temperature source of ions is that the source has to be sufficiently distant from the reaction chamber so that the reaction chamber is relatively unaffected. (It was desired to study hydration equilibrium at temperatures as low as 260°K). The Kunsman source, described in the following paragraph was found to be the most satisfactory

source for all alkali ions except lithium.

The manufacture of a Kunsman thermionic source is described in a review by Jenkins and Trodden (52). In this laboratory a Kunsman source was first utilized by S. K. Searles who investigated hydration of potassium ion (50). The procedure followed in the present experiment was as follows. A mixture of 98% Fe_2O_3, 1% Al_2O_3 and 1% MNO_3, where MNO_3 represents the corresponding alkali nitrate (M = Na, K, Rb, Cs) was fused in a crucible. In the fused product the Fe_2O_3 becomes oxidized to Fe_3O_4. The product was then ground to a powder. A Pt filament was made from a strip of Pt 1 mm wide and 2 cm long, which was cut from a 0.001 inch thick Pt foil. The Pt strip was spot welded to two nichrome studs which were spaced about 1 cm apart. Then the ground powder was fused onto the filament. This required special care because the melting point of the powder was close to the melting point of Pt. A thin layer of powder, approximately 1 mm high was first spread uniformly along the length of the filament. A torch provided with a 3/4 mm hole tip was adjusted to give a fine intense flame. The powder was heated until it just began to melt and flow. Cycles of melting and cooling were used to obtain a uniform fused layer and prevent the Pt from melting. If the coating is not uniform over the filament surface, the surface temperature and ion emission will be uneven. The reduction of the surface was the next step. The

chamber was evacuated and filled with 3-10 torr H_2. An electric current was passed through the filament until a dull red light was just visible. The necessary wattage was 15-30 W depending on the H_2 pressure. The emitted ion current was collected on a plate with a negative bias. Increasing the wattage until the filament became dull red yielded a positive current of 1-2 μA. If the filament temperature was increased to a bright red, a maximum of 10 μA could be obtained. This high current however lasted only about 20 minutes after which the current dropped well below 1 μA. The surface of the filament was sufficiently reduced in about 30 minutes. A longer reduction period did not improve the filament emission. A satisfactory Li^+ source could not be prepared by the above procedure. Therefore a literature search for suitable thermal ionization source of Li^+ ions was made. It was decided to use β-eucryptite ($1Li_2O.\ 1Al_2O_3.\ 2SiO_2$) as suggested by Blewett and Jones (55). β-eucryptite was made by melting Li_2CO_3, $Al(NO_3)_3\ 9H_2O$ and pure powdered quartz together at about 1400°C. The melts were then powdered and remelted twice. The compound was finally powdered and mounted as a thin layer on a 1 cm x 0.3 cm filament made of platinum gauze.

2.7 Production and Transport of the Hydrated Ions Out of the Reaction Chamber.

The alkali ions are created in the filament chamber

which is at the same pressure as the reaction chamber. After having been ejected from the heated filament, the alkali ions drifted to the reaction chamber under the influence of electric field of approximately 100 V/cm. Lower fields gave insufficient intensity. Upon entering the field free reaction chamber the alkali ions have excess energy due to the drift field. In the previous work on hydration of potassium ions it has been calculated that K^+ ions entering the reaction chamber possess approximately 0.74 eV translational energy. Since the filament housing is at the same pressure as the reaction chamber the alkali ions are already partly hydrated when they enter the reaction chamber. Thus in spite of relatively high potential difference between the filament and the reaction chamber the ions entering the reaction chamber possess relatively low (~ 0.74 eV) translational energy. In the reaction chamber the ions are further thermalized by losing the excess translational energy through collisions with solvating molecules. After the primary ions lose their excess energy, the ions react with neutral molecules as they diffuse toward the wall. During this time the ions should form equilibrium ionic clusters. On their way towards the walls of the reaction chamber, where they are discharged, the primary ions collide with the solvating molecules. Some of these collisions may result in the attachment of the ion to the neutral molecules thus forming ion-clusters. The

ion-clusters stabilize themselves by giving up their excess energy through collisions with other molecules (third body collisions). In order that equilibrium conditions prevail, this stabilization of ion clusters should be achieved, before the ion clusters diffuse out of the reaction chamber.

The time, t, necessary for the ions to travel the distance d can be estimated by the approximate equation (I) given below, which establishes a relationship between the time, t, required by a particle to diffuse the distance, d (56), and the diffusion coefficient, D.

$$\text{(I)} \qquad t \approx \frac{d^2}{2D}$$

In the present case d is the distance between the ion entrance and exit slit of the reaction chamber and is equal to 1.2 cm, D is the diffusion coefficient of the ions through the gas and is taken as 500 cm^2/sec (56) for an ion source pressure of 0.1 torr and temperature 300°K. Thus, the diffusion time t is calculated to be 2.9 milli-sec. This time is an estimate of the ion residence time in the reaction chamber. This estimate is approximate since space charge effects due to presence of the charged particles may alter the diffusion coefficient.

The half-life of the attachment reaction

$$2.1 \qquad M^+ + 2H_2O \rightarrow M^+(H_2O) + H_2O$$

can be calculated if we assume a value for the rate constant k. The reaction

$$2.2 \quad Cl^- + 2H_2O \rightarrow Cl^-(H_2O) + H_2O$$

has been studied by Payzant and Kebarle (57) and Lineberger and Puckett (58). They found the third order rate constants to be $k \approx 10^{-29}$ cc^2/molecule^{2}sec. As an approximation the same value can be assumed for the rate constant for the reaction 2.1, because the ion M^+ is monoatomic and reaction 2.1 bears resemblance to reaction 2.2. The half-life $t_{\frac{1}{2}}$ is then given by

$$\text{II} \qquad t_{\frac{1}{2}} = \frac{1}{10^{-29}[H_2O]^2}$$

where $[H_2O]$ is the concentration of water in the reaction chamber in molecules/cc. At a reaction chamber pressure of 0.1 torr and temperature 300°K, the water concentration is equal to 0.3×10^{16} molecules/cc. Introducing this value into equation (II), the half-life is found to be ~1 milli-sec. This is roughly a factor of three smaller than the ion residence time calculated from equation (I). Thus the reaction time (the ion residence time $t \approx \frac{d^2}{2D}$) would appear to be sufficiently long even at 0.1 torr for the reaction 2.1 to reach an equilibrium. However in the present studies the lowest reaction chamber pressures used were 0.3 torr.

In addition to the diffusion process, the ions can be removed from the ion source by mass flow. It has been shown (50), however, that the mass flow does not become

significant until about 1 mm from the exit slit. Thus starting from the entrance to the reaction chamber, the ions are transported for the first 3 to 4 mm by diffusion and in the last 1 mm by mass flow.

2.8 Ion Acceleration, Mass Analysis and Ion Current Detection.

Ions diffusing out of the ion exit slit of the reaction chamber were accelerated from the reaction chamber potential, + 1850 V, to earth potential. Figure 2.2 shows the electrode system, which was a modified Nier design. The first electrode spacing to the reaction chamber was increased from 1 mm to 10 mm. As discussed in detail in reference (50), the electrode when present with the shorter distance presented a pumping obstacle to the gas escaping from the ion exit slit. The resulting high pressure caused the ionic clusters to undergo collisions outside the reaction chamber, which led to non-equilibrium effects. After acceleration the ions entered the magnetic analysis tube and were deflected by 60°. The resolution calculated from the magnetic analyzer entrance and exit slit widths (49) was 200. The observed resolution was slightly less.

After the ions passed through the analyzer exit slit, they entered the 17 stage secondary electron multiplier (SEM). In the SEM a positive ion is further accelerated

by the potential of the first dynode. On striking the dynode, secondary electrons are ejected and accelerated to the second dynode where each electron ejects more electrons etc. The current amplification of this device is a function of the voltage across its dynodes. Normally there is a uniform potential drop between each dynode, the last dynode (collector) being at ground potential. The ratio of the electron current from the 17th dynode of the SEM to the positive ion current collected from the first dynode is the absolute gain of the SEM. The currents were measured by a Victoreen Femtometer with a 10^{10} ohm input resistor. In the case of the $M^+(H_2O)_n$ series the ion currents were too small to be measured on the first dynode, therefore the absolute gain for $M^+(H_2O)_n$ series could not be determined.

2.9 Relation of the Ion Current to the Ion Concentration

From the time of their formation in the reaction chamber to the time of their recording by the detection system the ion-clusters are engaged in a number of processes. A few of these processes may discriminate against one or the other type of ions. Some of these discriminatory processes will be discussed below.

A. Discrimination in transport through the reaction chamber

The diffusion coefficient of an ion is inversely proportional to the square root of the mass of the ion (56).

Therefore one expects that the lighter ions would travel through the reaction chamber faster and would reach the ion exit slit in a shorter time than the heavier ions. Thus, the actual concentration of the ions with smaller mass would be less than what is represented by the recorded signal. However, since the average half-life of the clustering reaction is short in comparison to the residence time of the ion and thus a cluster $M^+(H_2O)_n$ gains and loses water molecules at a fast rate; all the clusters would have the same average molecular weight and their diffusion coefficient would be equal. However at the moment when the ions effuse through the leak (ion exit slit), discrimination might be expected to occur since effusion rate through the leak is proportional to the average thermal velocity, $v \propto \sqrt{\frac{T}{M}}$. The $\sqrt{\frac{T}{M}}$ difference is highest and equal to 1.88 for Li^+ and Li^+H_2O ratio. However this reaction was not measured. The difference in $\sqrt{\frac{T}{M}}$ for the Na^+ and Na^+H_2O is equal to 1.33. Thus $K_{0,1}$ for the reaction: $Na^+ + H_2O \rightarrow Na^+(H_2O)$ might be out by a factor of 1.33. This correction is small and has been neglected.

B. Discrimination due to stripping outside of the reaction chamber.

If the pressure in the region just outside of the ion exit slit is high, some ion molecule collisions may take place in the vacuum region between the reaction chamber exit slit and the first accelerating electrode. This

problem was encountered by Collins (49) in a preliminary study of the equilibrium reaction

$$H^+(H_2O)_{n-1} + H_2O \rightleftarrows H^+(H_2O)_n$$

Collins found that the ion cluster size began to decrease after a pressure of about 0.3 torr due to ion cluster-water molecule collisions outside the reaction chamber. Due to the presence of the ion accelerating field, these collisions occur with kinetic energies much higher than thermal. As a result of these collisions, the ion-clusters may dissociate. Since a larger cluster has weaker ion-ligand bond strengths and may have larger collision cross section, the larger clusters were preferentially dissociated. The extraneous collisions were eliminated by increasing the pumping speed at the ion exit slit by increasing the distance between the reaction chamber and the first electrode.

As shown in Chapter 3, the calculated equilibrium constants did not change with pressure up to some maximum pressure P after which the equilibrium constant began to decrease. Evidently at higher pressures nonequilibrium collisions again became significant.

C. Discrimination in Mass Analyzer Tube

In general, in a magnetic mass analyzer tube such as the one used in this work any loss of ions due to elastic scattering, collisions with the wall etc., will be the

same for all ions. Consequently, we can assume that the effect of mass discrimination in the analyzer tube was negligible.

D. Discrimination in the ion current detection system

Discrimination may also occur in the secondary electron multiplier. The number of electrons ejected from the first dynode of SEM, is dependent on the velocity of the ions as well as their chemical composition (59). Thus, the gain of the multiplier would not be the same even for two isobaric ions such as N^+ and CH_2^+ (60). The reason for this difference is that, the multi-atom ions may break up when they strike the surface of the SEM dynode and act as a group of particles instead of just one ion. To measure the SEM discrimination the relative gain of the SEM for the series of solvated ions should be measured. However, in the case of the $M^+(H_2O)_n$ series the relative gain of the SEM could not be measured, since the ion currents on the first dynode were too small to be measured directly.

From the work of S. K. Searles (50) the relative gains for $H^+(H_2O)$, $H^+(H_2O)_2$, $H^+(H_2O)_3$ and $H^+(H_2O)_4$ were 1.0, 1.1, 0.8, 0.8 respectively. For $NH_4^+(NH_3)$, $NH_4^+(NH_3)_2$ and $NH_4^+(NH_3)_3$ the relative gains were 1.0, 0.95, 0.95 respectively. Therefore, it appears that the SEM introduces a maximum discrimination of 20% in the measurement of ionic clusters. This error is considered small since the ΔG°

depend on the log $K_{n-1,n}$ and are thus little affected by a 20% error. The $\Delta H_{n-1,n}$ are completely unaffected since they do not change by the presence of a constant factor.

3. RESULTS OF HYDRATION OF POSITIVE ALKALI IONS M^+

3.1 Introduction and Thermodynamic Relations

Alkali ions which are ejected by a heated filament drift into the ion source under the influence of an electric field. In the field free ion source, the alkali ions lose their excess translational energy and react with water molecules as follows:

$$M^+ + H_2O \rightleftarrows M^+H_2O$$

$$M^+(H_2O) + H_2O \rightleftarrows M^+(H_2O)_2$$

$$\cdot$$

$$\cdot$$

$$\cdot$$

$$M^+(H_2O)_{n-1} + H_2O \rightleftarrows M^+(H_2O)_n$$

Provided that the equilibrium is achieved in the ion source the equilibrium constant can be calculated from

$$K_{n-1,n} = \frac{P_{M^+(H_2O)_n}}{P_{M^+(H_2O)_{n-1}} \; P_{H_2O}}$$

where the corresponding equilibrium concentrations of $M^+(H_2O)_n$ and $M^+(H_2O)_{n-1}$ are assumed to be proportional to the mass analyzed ion currents. Determination of $K_{n-1,n}$ at different temperatures is used to obtain $\Delta H^\circ_{n-1,n}$, $\Delta S^\circ_{n-1,n}$ and $\Delta G^\circ_{n-1,n}$.

3.2 Presentation of the Results and General Discussion

The equilibrium constants obtained for the gas phase hydration of the lithium, sodium, rubidium and cesium ions are presented in Figures 3.1 to 3.21. It can be seen that at any one temperature the values of $K_{n-1,n}$ remain relatively constant over the pressure range covered. This independency of $K_{n-1,n}$ of water pressure indicates that equilibrium conditions in the ion source were achieved and no significant amounts of collisions occurred outside of the ion source.

Van't Hoff type plots of the equilibrium constants are shown in Figures 3.22 to 3.25. The equilibrium constants presented in these Figures are $K_{1,2}$ to $K_{5,6}$ for lithium, $K_{0,1}$ to $K_{5,6}$ for sodium, $K_{0,1}$ to $K_{4,5}$ for rubidium and $K_{0,1}$ to $K_{3,4}$ for cesium ion clusters. The $K_{0,1}$ values for lithium ions were not measured since the high temperatures (T > 900°K) were required to observe the equilibrium constant $K_{0,1}$. The reaction chamber used in the present study could be operated at the maximum temperature of 600°K while the $K_{0,1}$ equilibrium for the lithium ion could probably be measured with some refinements of the heating system of the reaction chamber. The additional effort involved was not considered necessary for the present time since a fairly accurate value for $\Delta H^{\circ}_{0,1}$ and $\Delta G^{\circ}_{0,1}$ could be obtained by extrapolation from the other $\Delta H^{\circ}_{n-1,n}$ and $\Delta G^{\circ}_{n-1,n}$ of this ion.

The values for $\Delta H^{\circ}_{n-1,n}$ were determined from the

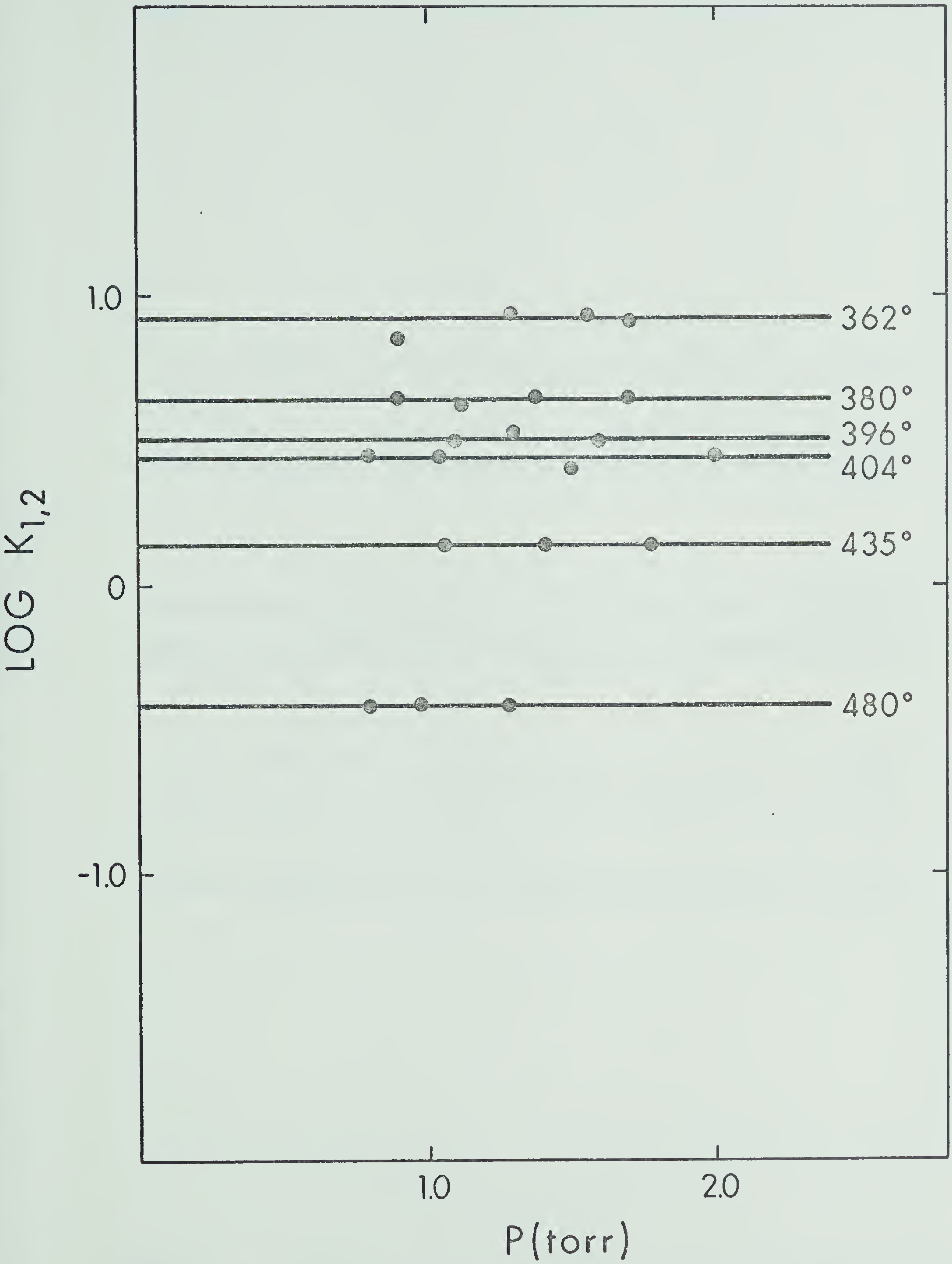

FIGURE 3.1 Plots of Log $K_{1,2}$ for the Gas Phase Hydration of Li^+, at Various Temperatures, Versus Pressure of H_2O.

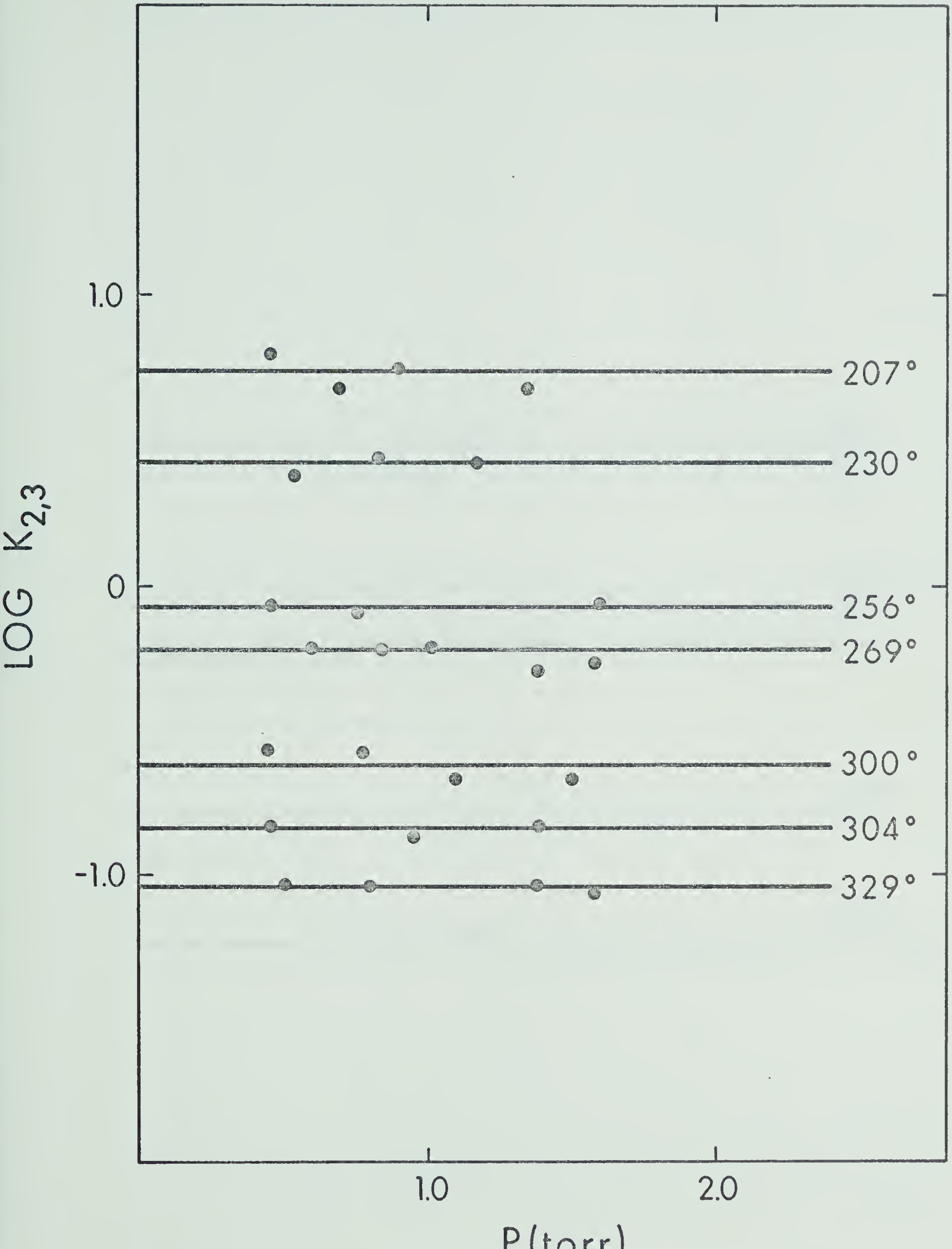

FIGURE 3.2 Plots of Log $K_{2,3}$ for the Gas Phase Hydration of Li^+, at Various Temperatures, Versus Pressure of H_2O.

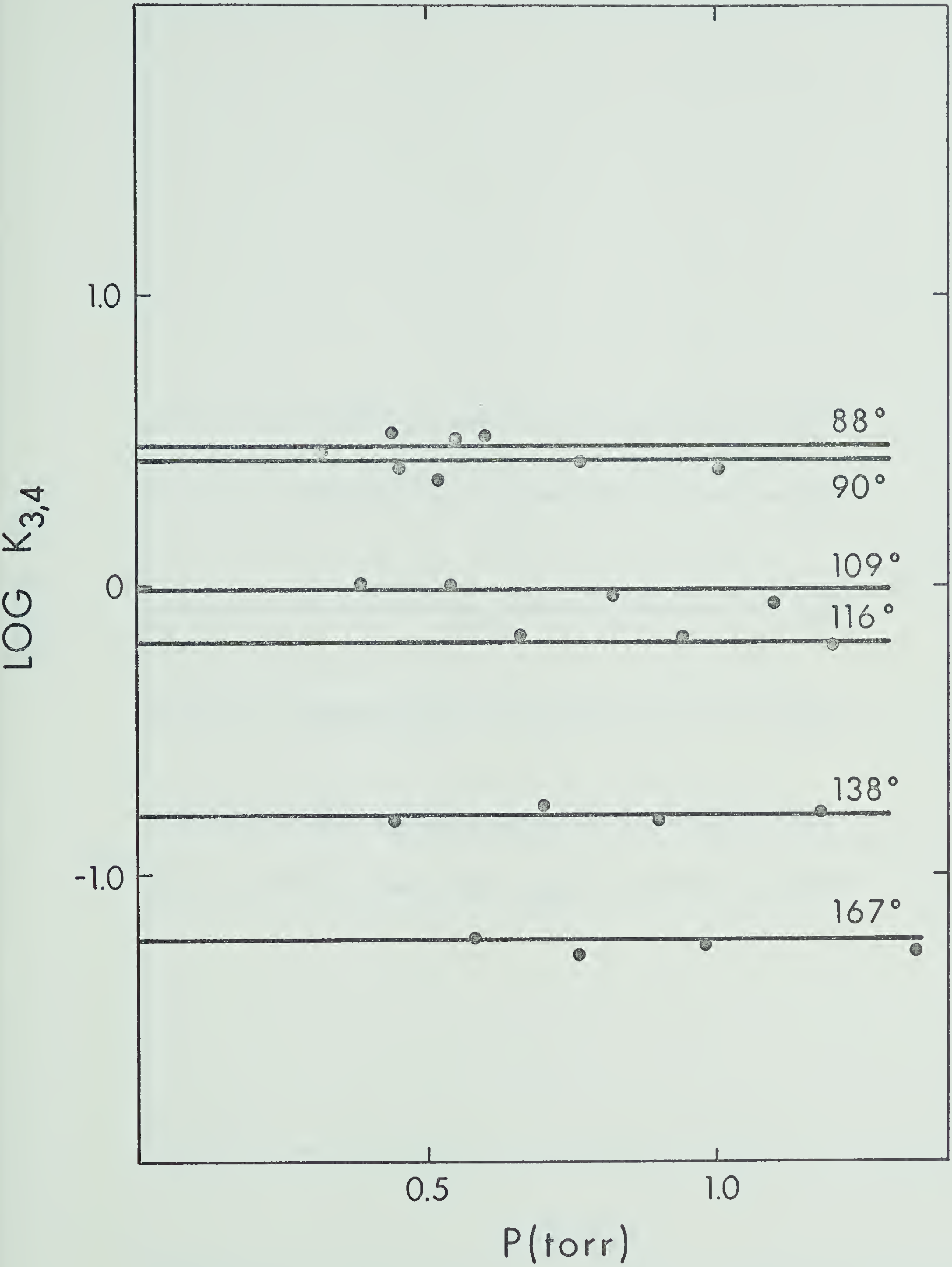

FIGURE 3.3 Plots of Log $K_{3,4}$ for the Gas Phase Hydration of Li^+, at Various Temperatures, Versus Pressure of H_2O.

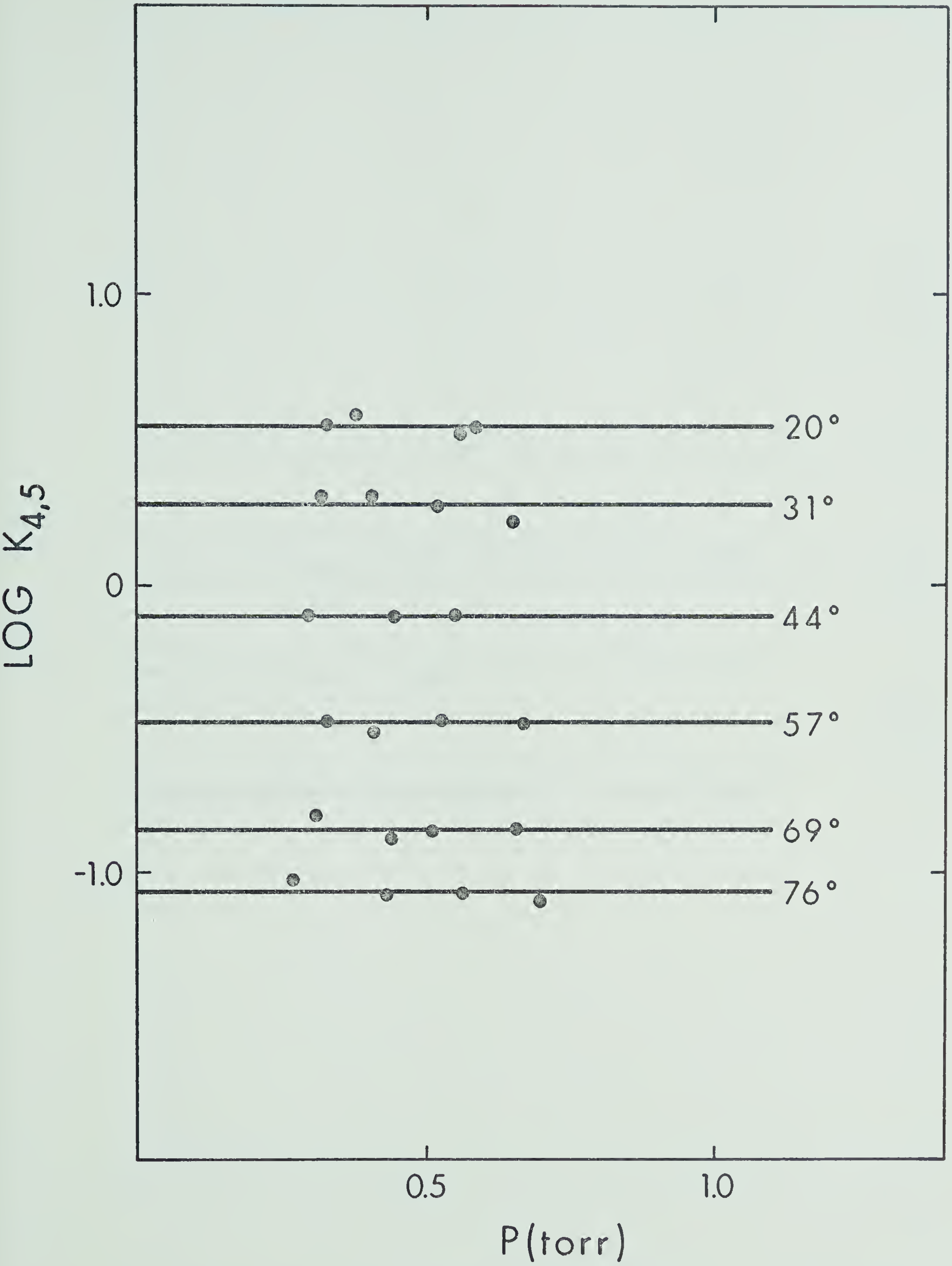

FIGURE 3.4 Plots of Log $K_{4,5}$ for the Gas Phase Hydration of Li^+, at Various Temperatures, Versus Pressure of H_2O.

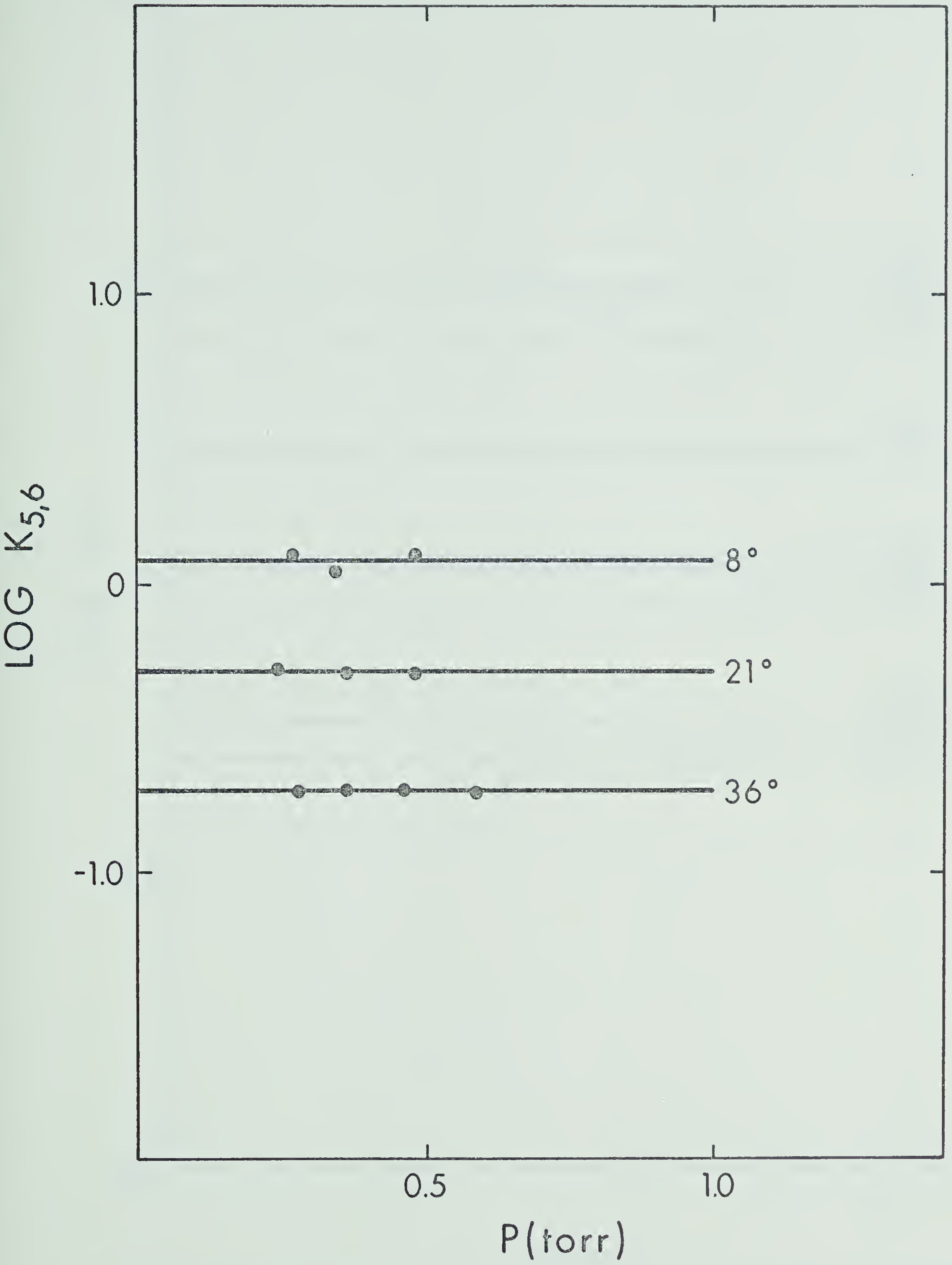

FIGURE 3.5 Plots of Log $K_{5,6}$ for the Gas Phase Hydration of Li^+, at Various Temperatures, Versus Pressure of H_2O.

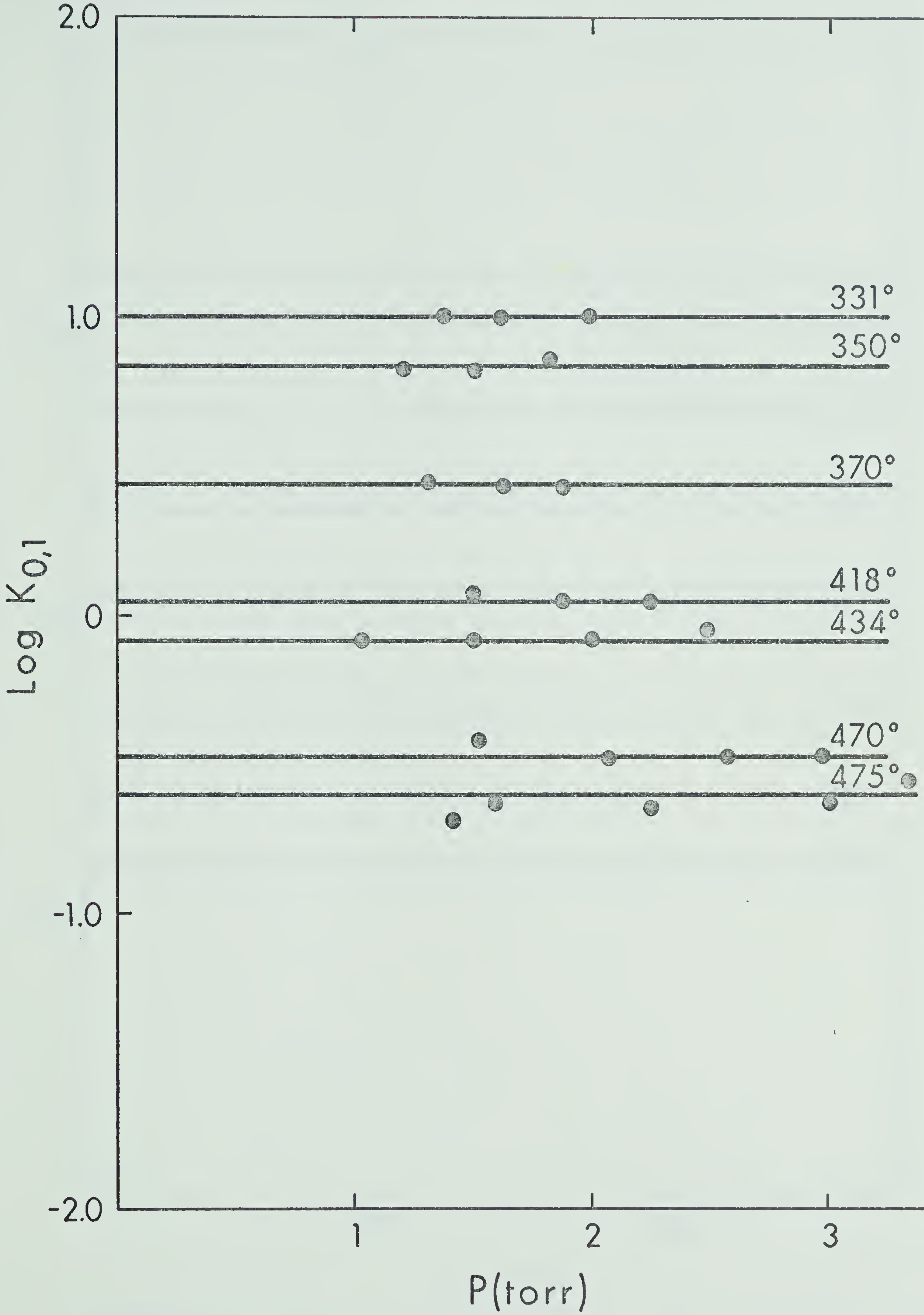

FIGURE 3.6 Plots of Log $K_{0,1}$ for the Gas Phase Hydration of Na^+, at Various Temperatures, Versus Pressure of H_2O.

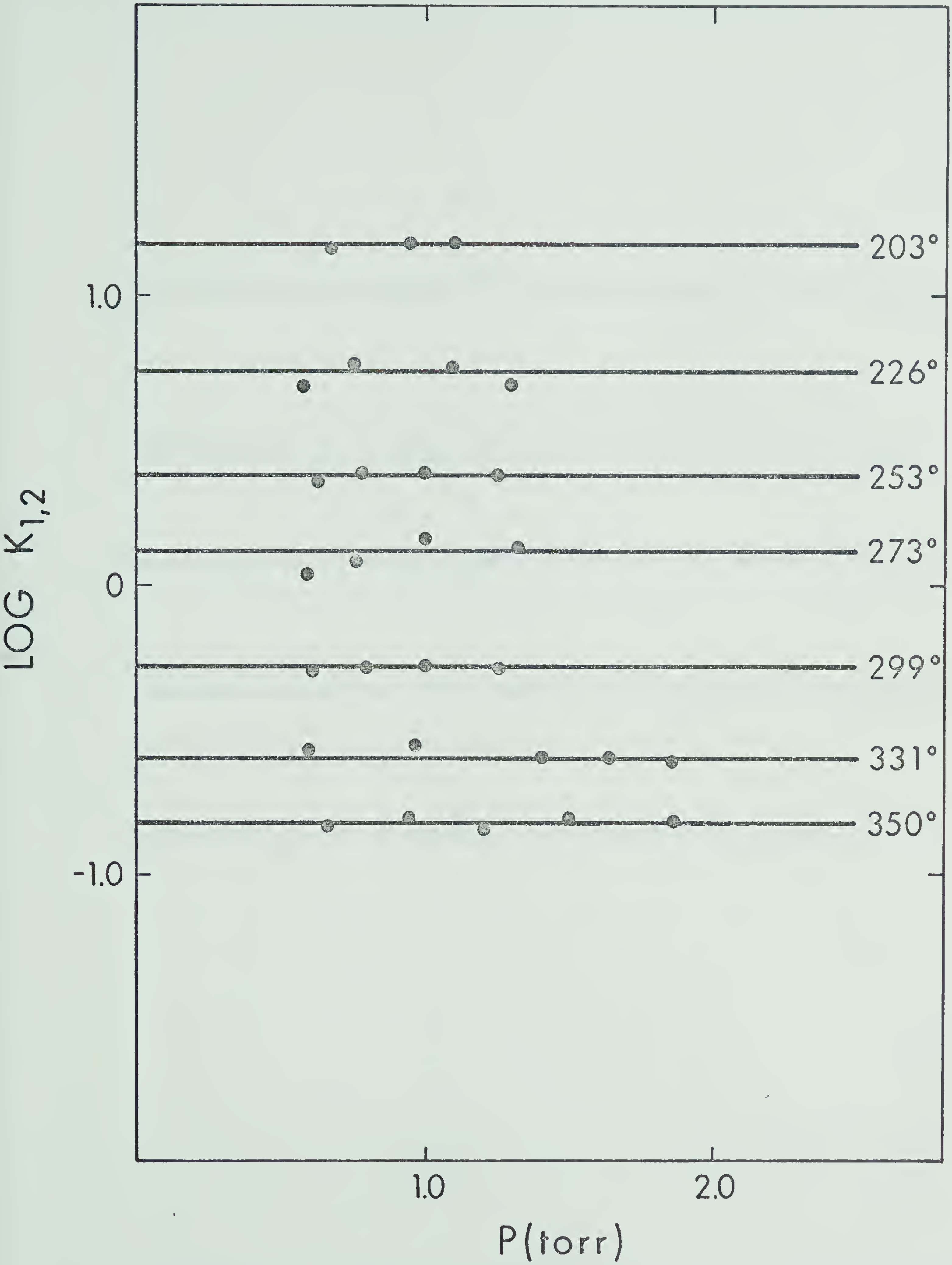

FIGURE 3.7 Plots of Log $K_{1,2}$ for the Gas Phase Hydration of Na^+, at Various Temperatures, Versus Pressure of H_2O.

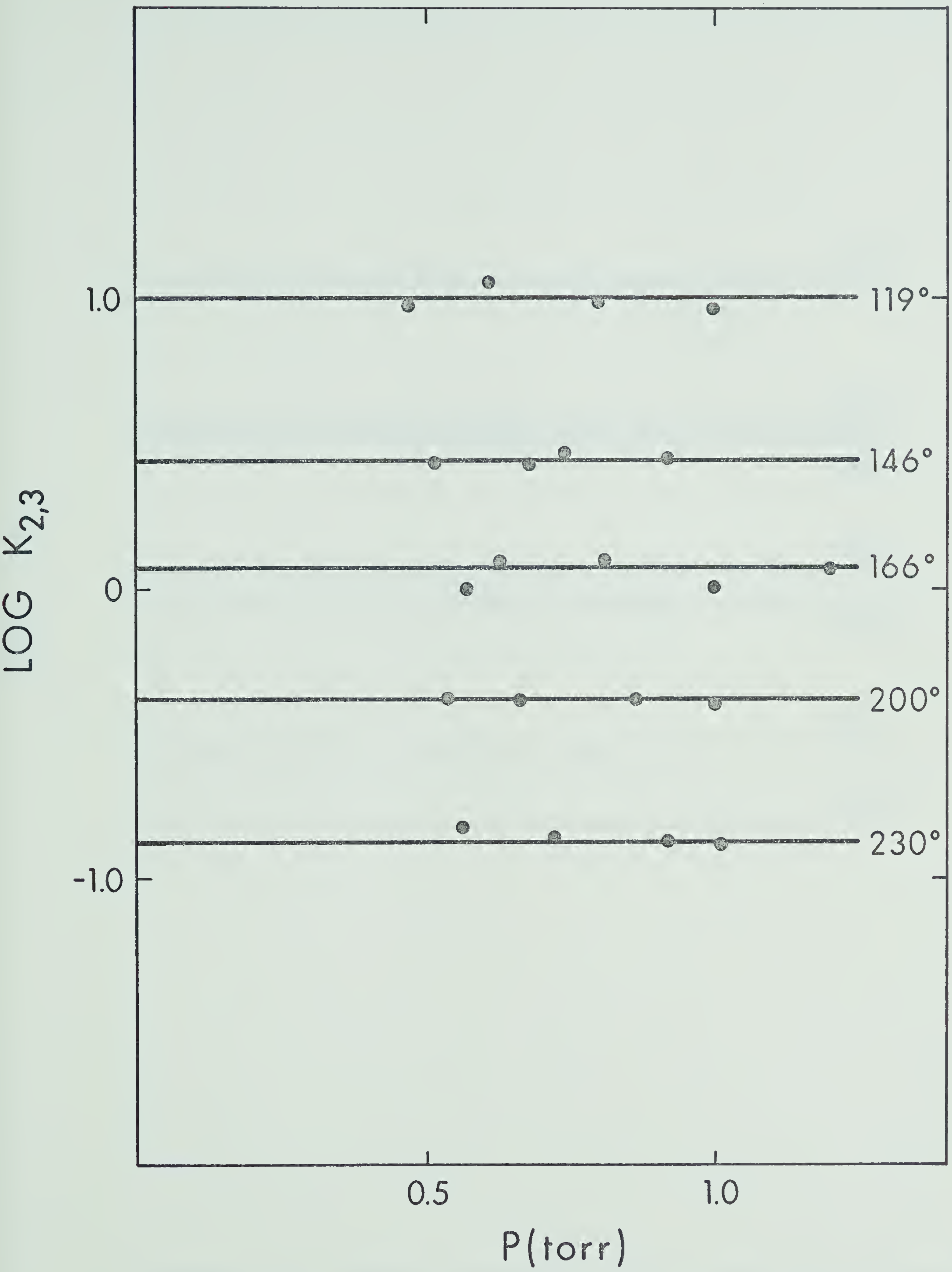

FIGURE 3.8 Plots of Log $K_{2,3}$ for the Gas Phase Hydration of Na^+, at Various Temperatures, Versus Pressure of H_2O.

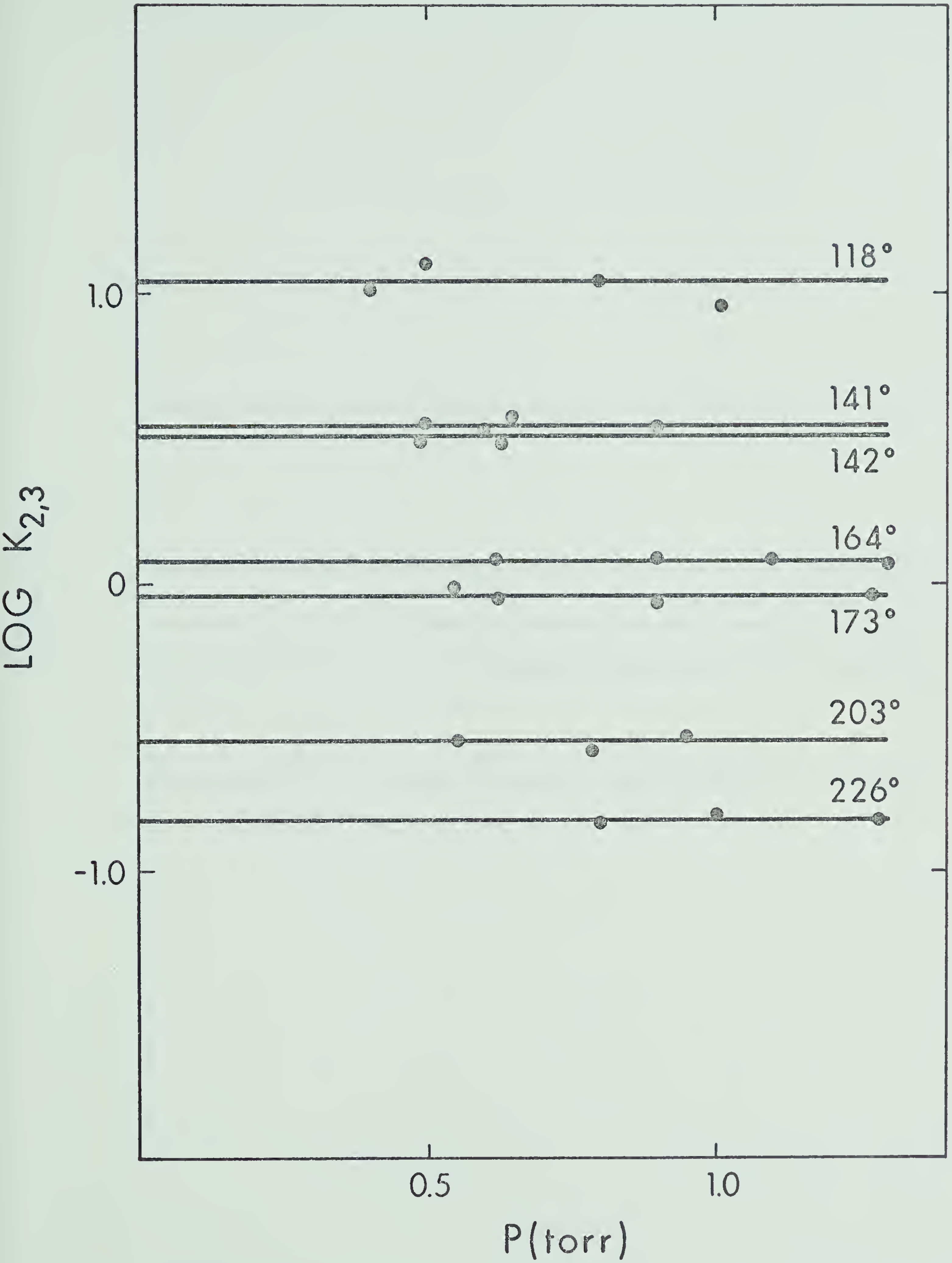

FIGURE 3.9 Plots of Log $K_{2,3}$ for the Gas Phase Hydration of Na^+, at Various Temperatures, Versus Pressure of H_2O

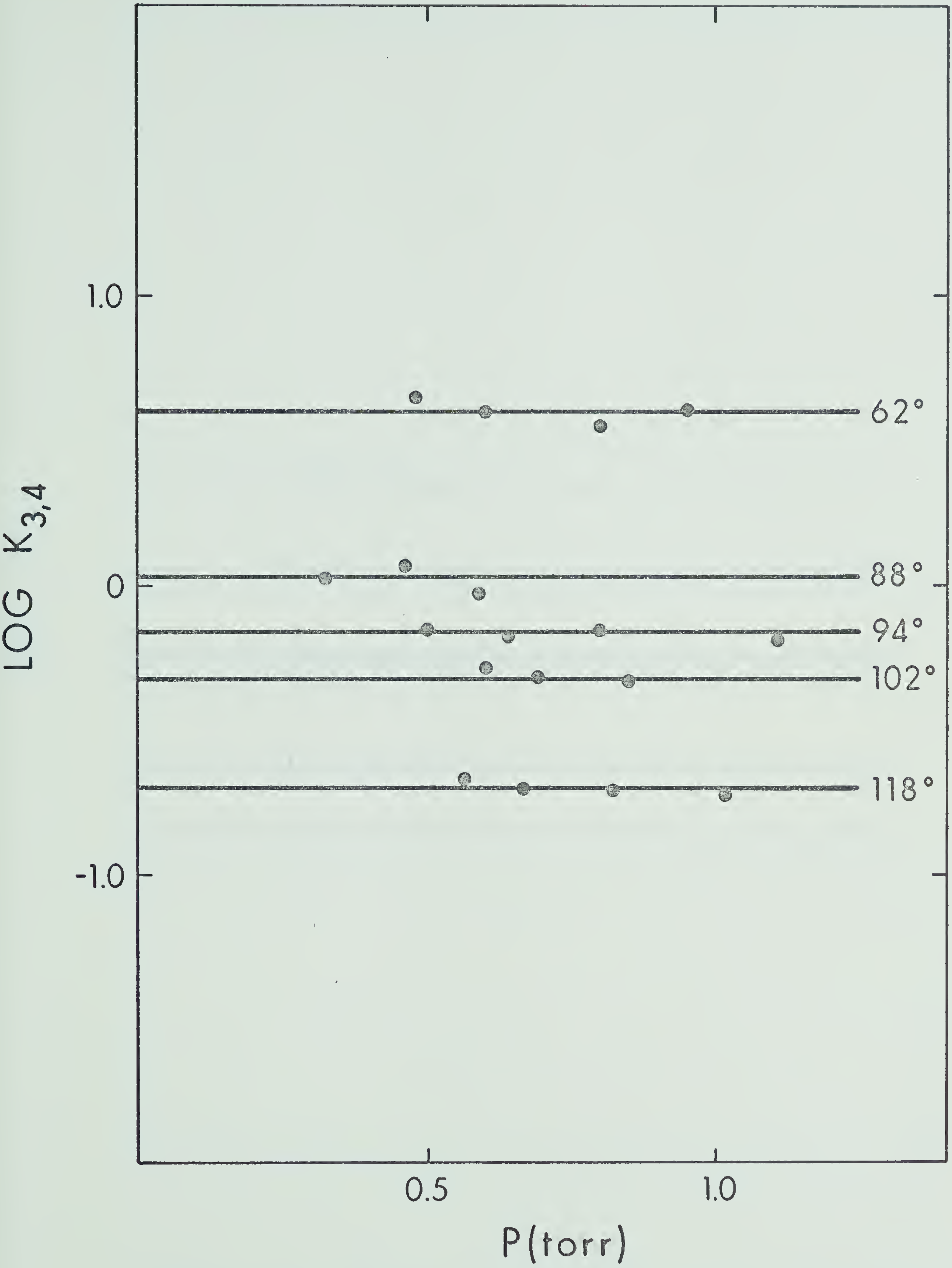

FIGURE 3.10 Plots of Log $K_{3,4}$ for the Gas Phase Hydration of Na^+, at Various Temperatures, Versus Pressure of H_2O

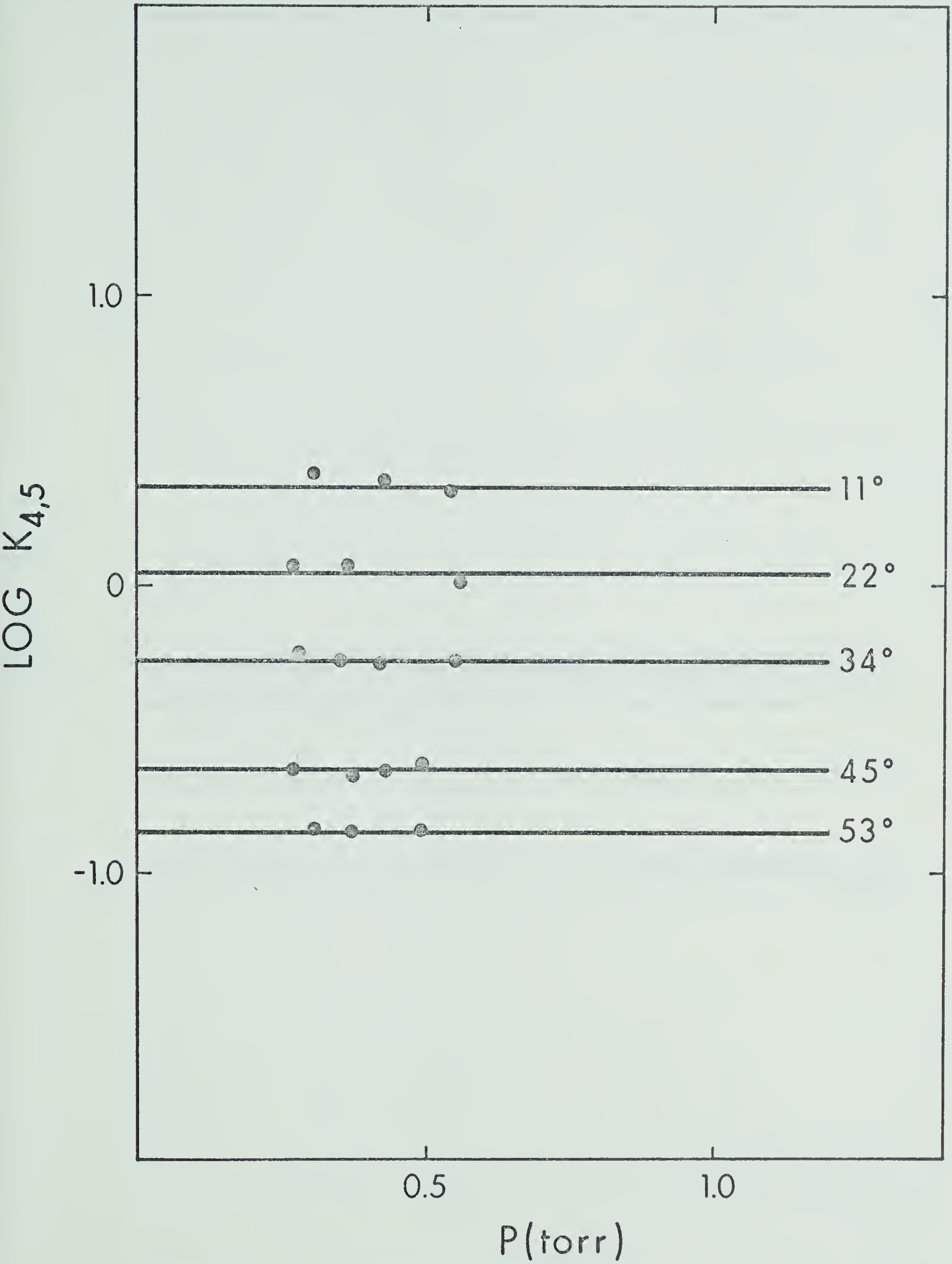

FIGURE 3.11 Plots of Log $K_{4,5}$ for the Gas Phase Hydration of Na^+, at Various Temperatures, Versus Pressure of H_2O

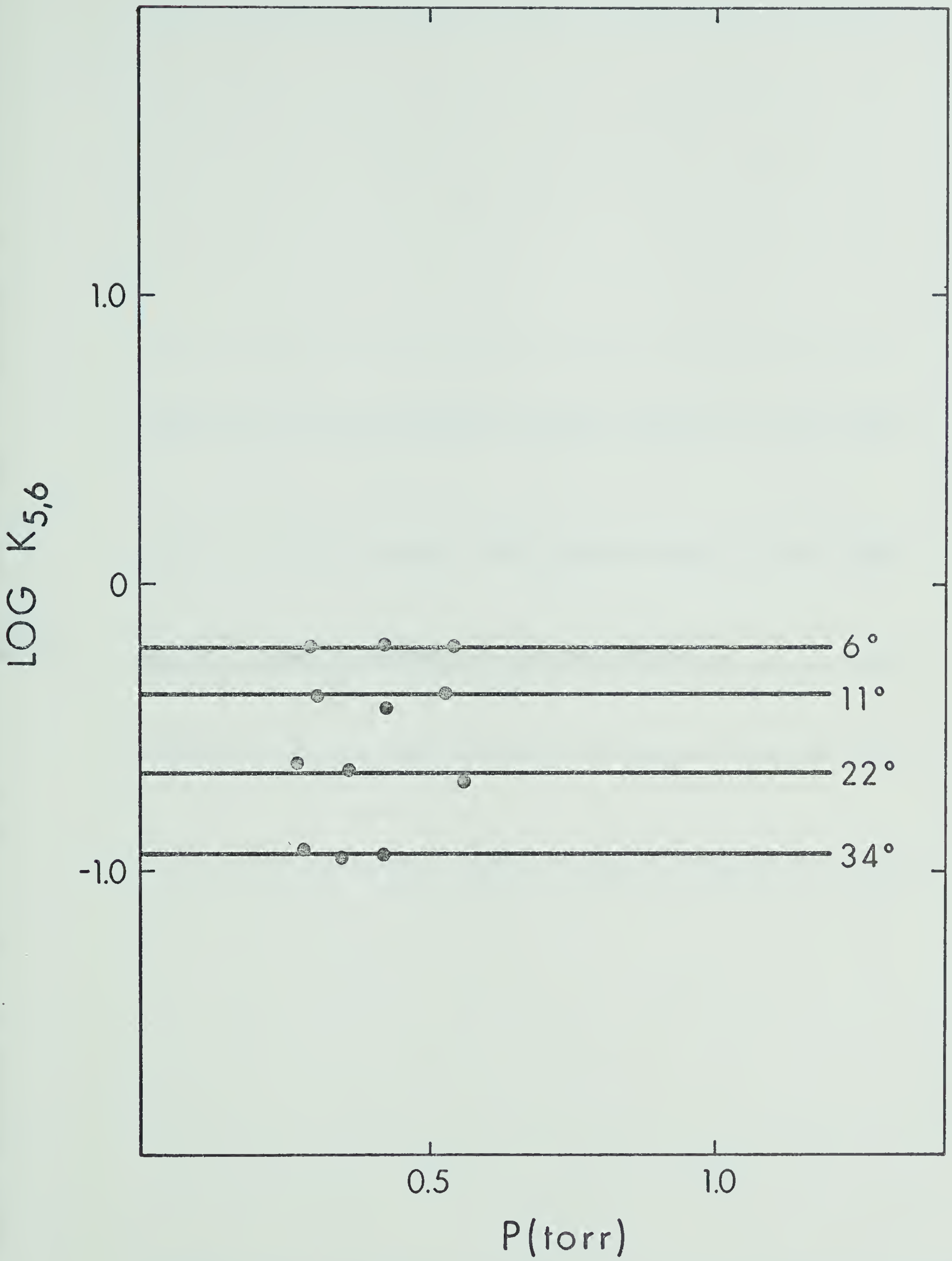

FIGURE 3.12 Plots of Log $K_{5,6}$ for the Gas Phase Hydration of Na^+, at Various Temperatures, Versus Pressure of H_2O

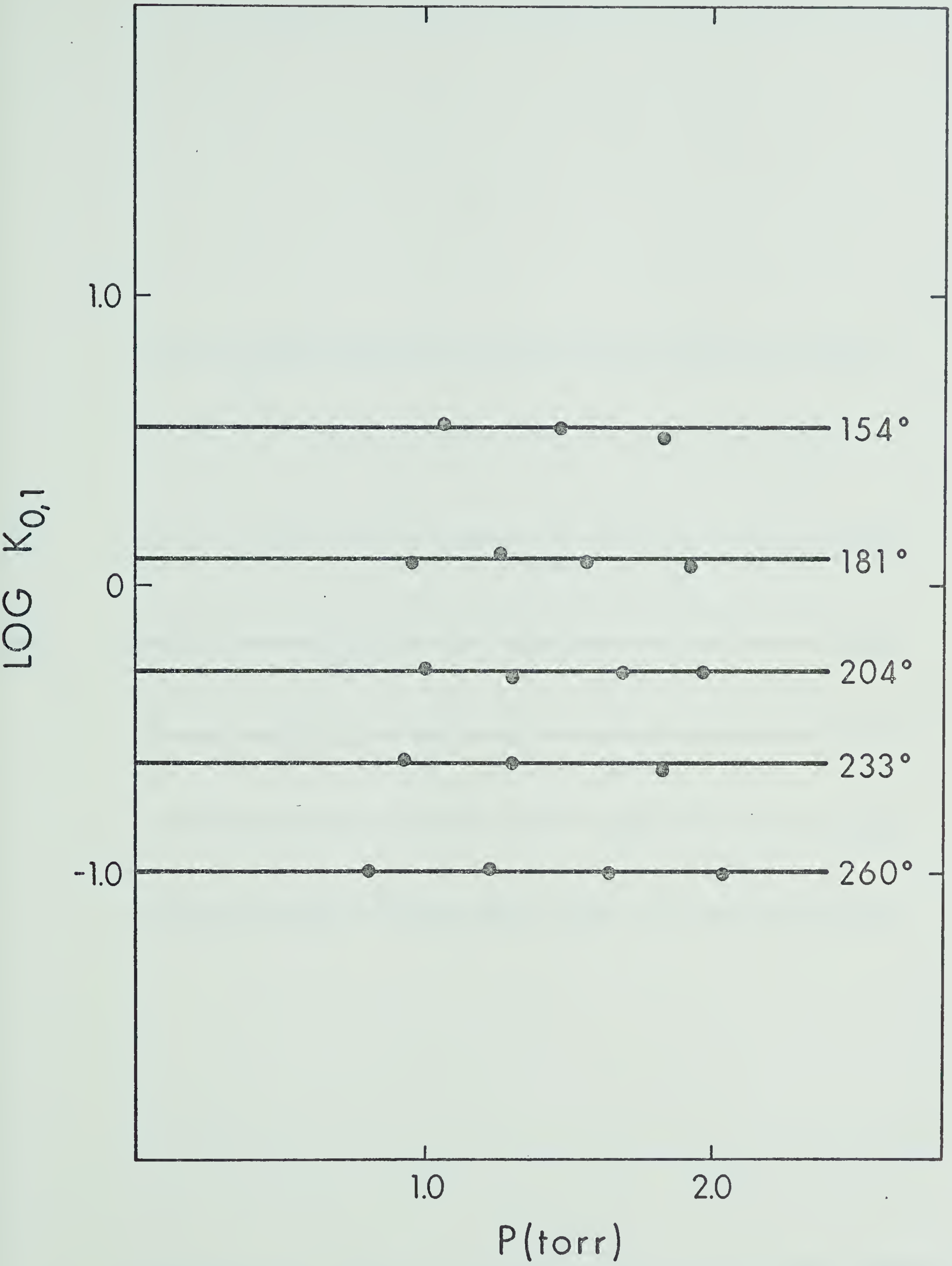

FIGURE 3.13 Plots of Log $K_{0,1}$ for the Gas Phase Hydration of Rb^+, at Various Temperatures, Versus Pressure of H_2O

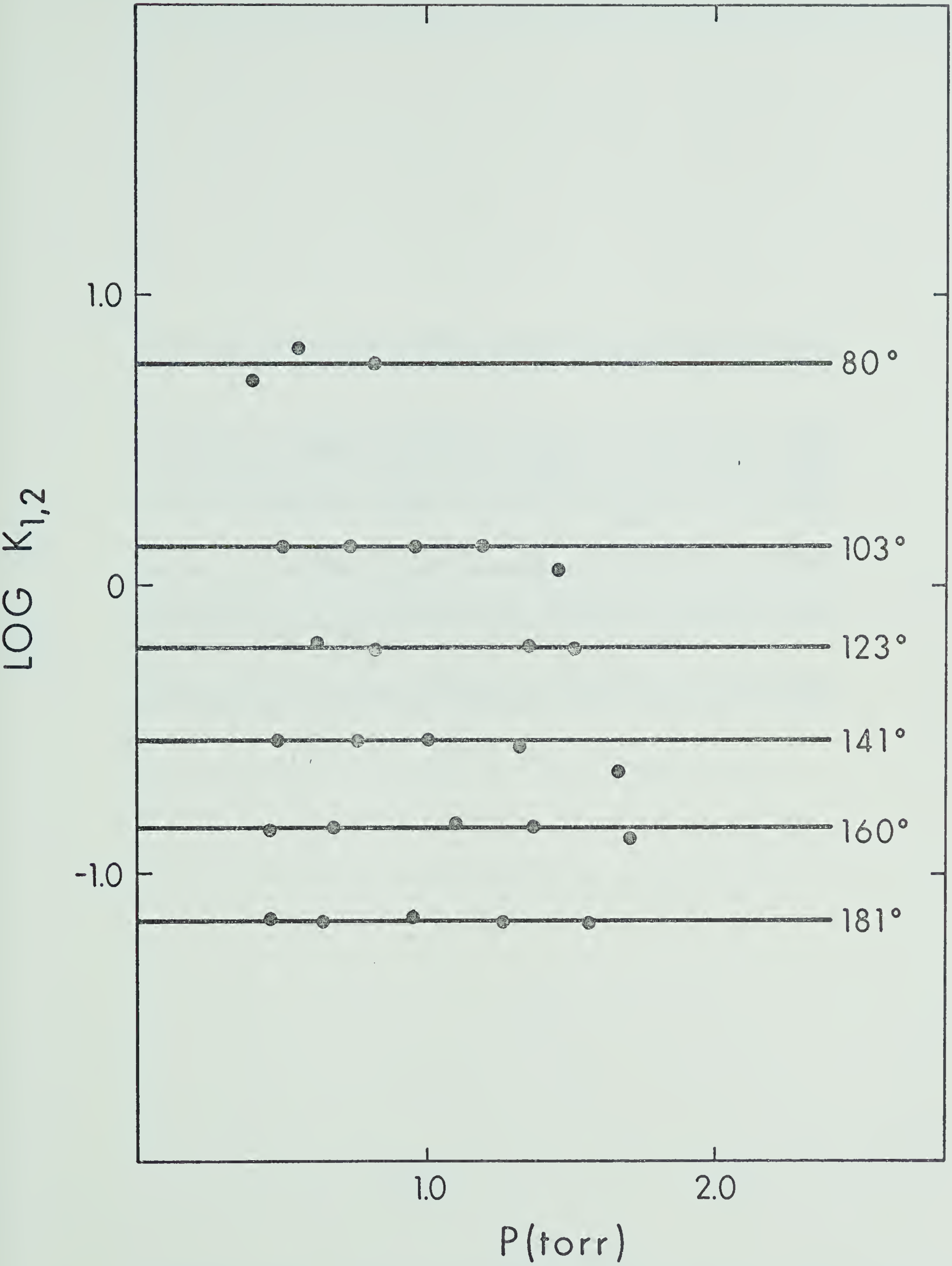

FIGURE 3.14 Plots of Log $K_{1,2}$ for the Gas Phase Hydration of Rb^+, at Various Temperatures, Versus Pressure of H_2O

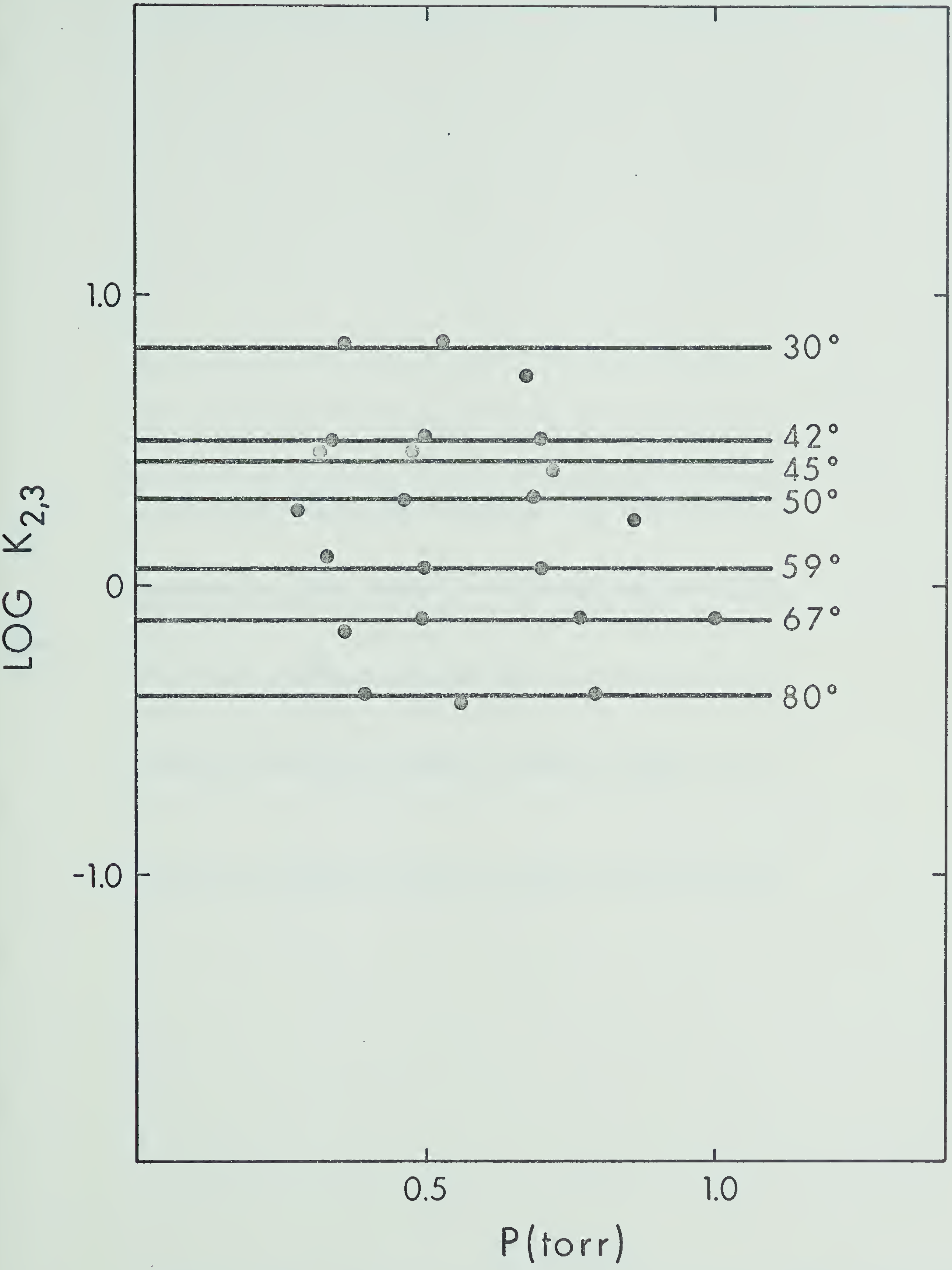

FIGURE 3.15 Plots of Log $K_{2,3}$ for the Gas Phase Hydration of Rb^+, at Various Temperatures, Versus Pressure of H_2O

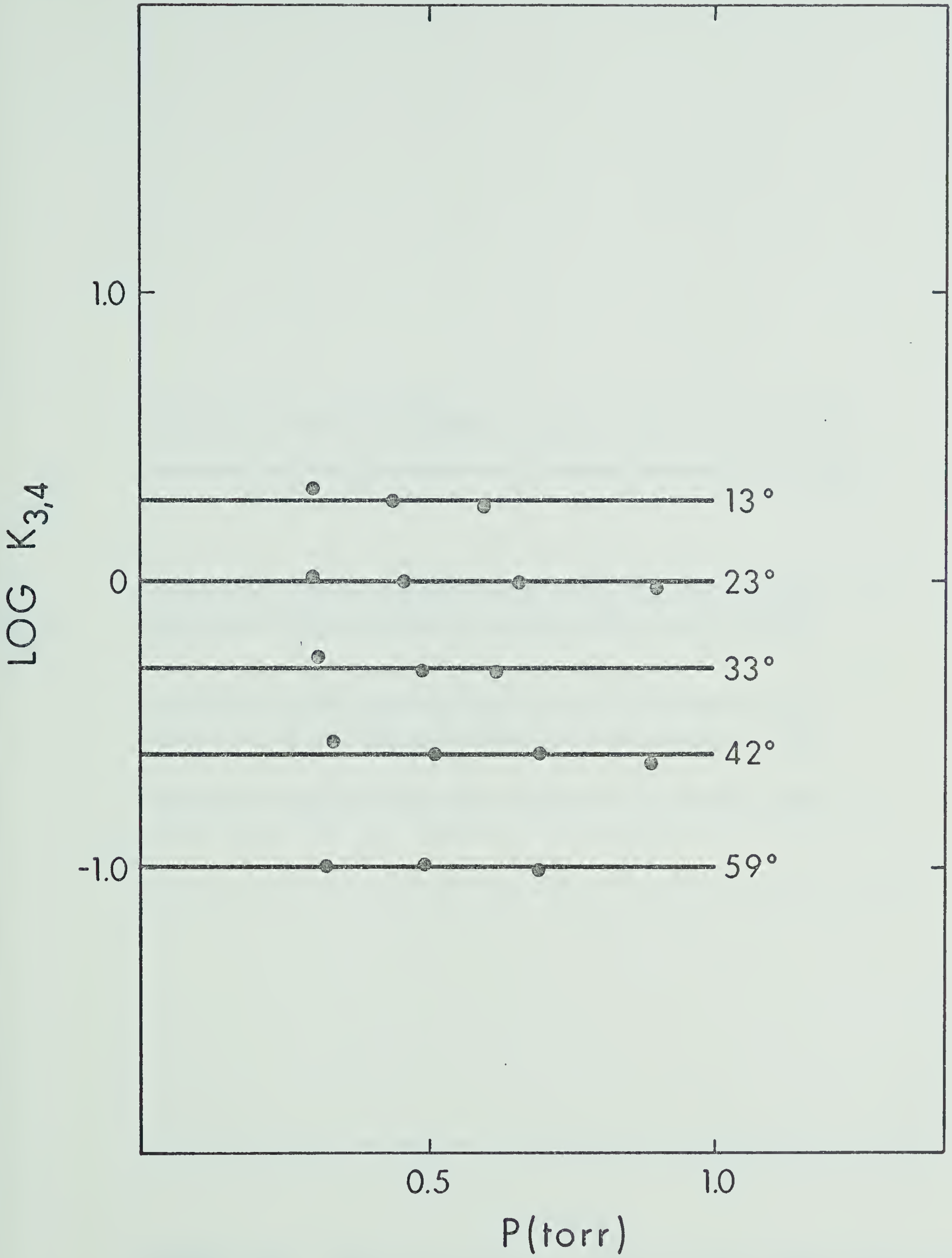

FIGURE 3.16 Plots of Log $K_{3,4}$ for the Gas Phase Hydration of Rb^+, at Various Temperatures, Versus Pressure of H_2O

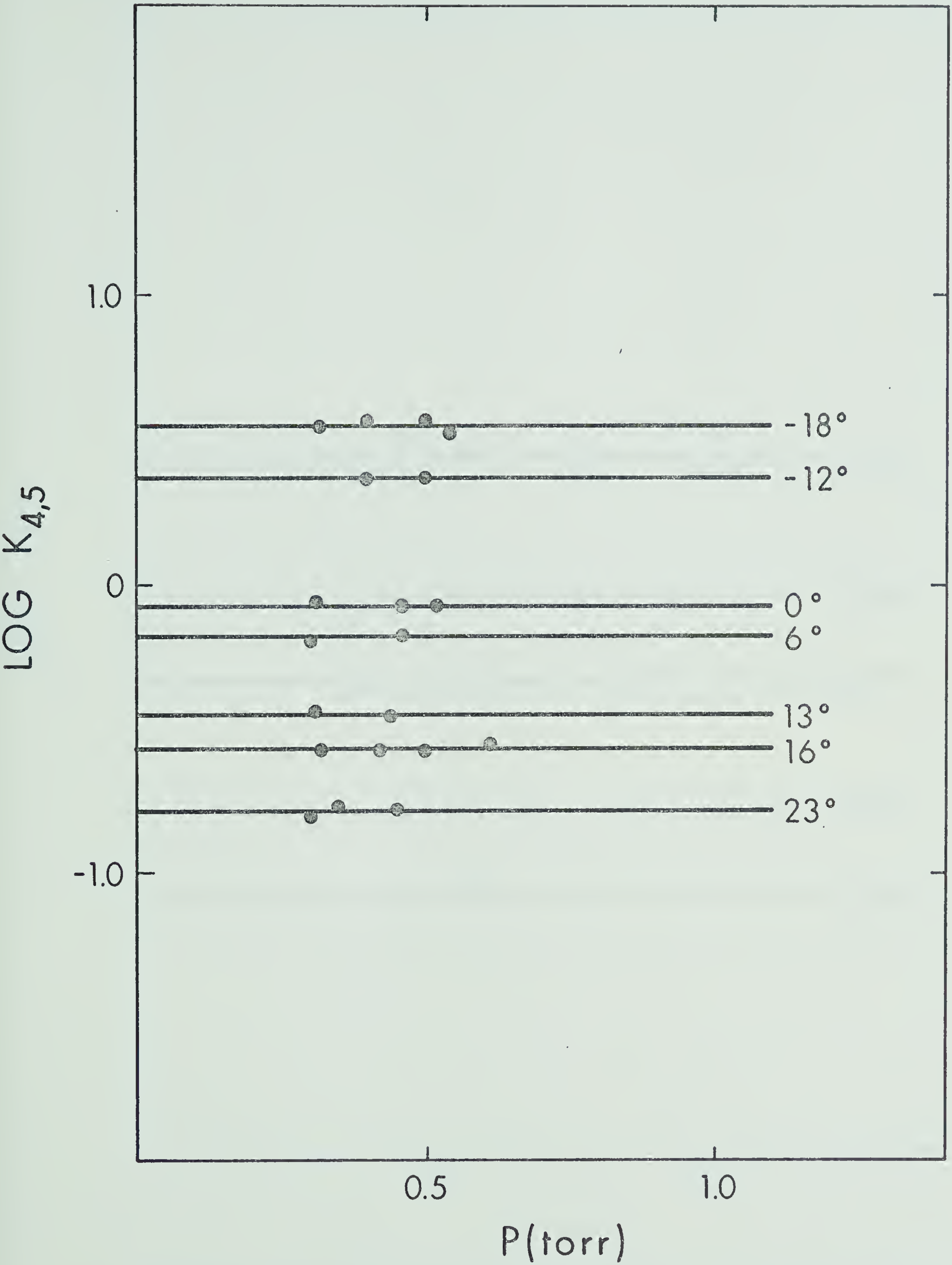

FIGURE 3.17 Plots of Log $K_{4,5}$ for the Gas Phase Hydration of Rb^+, at Various Temperatures, Versus Pressure of H_2O

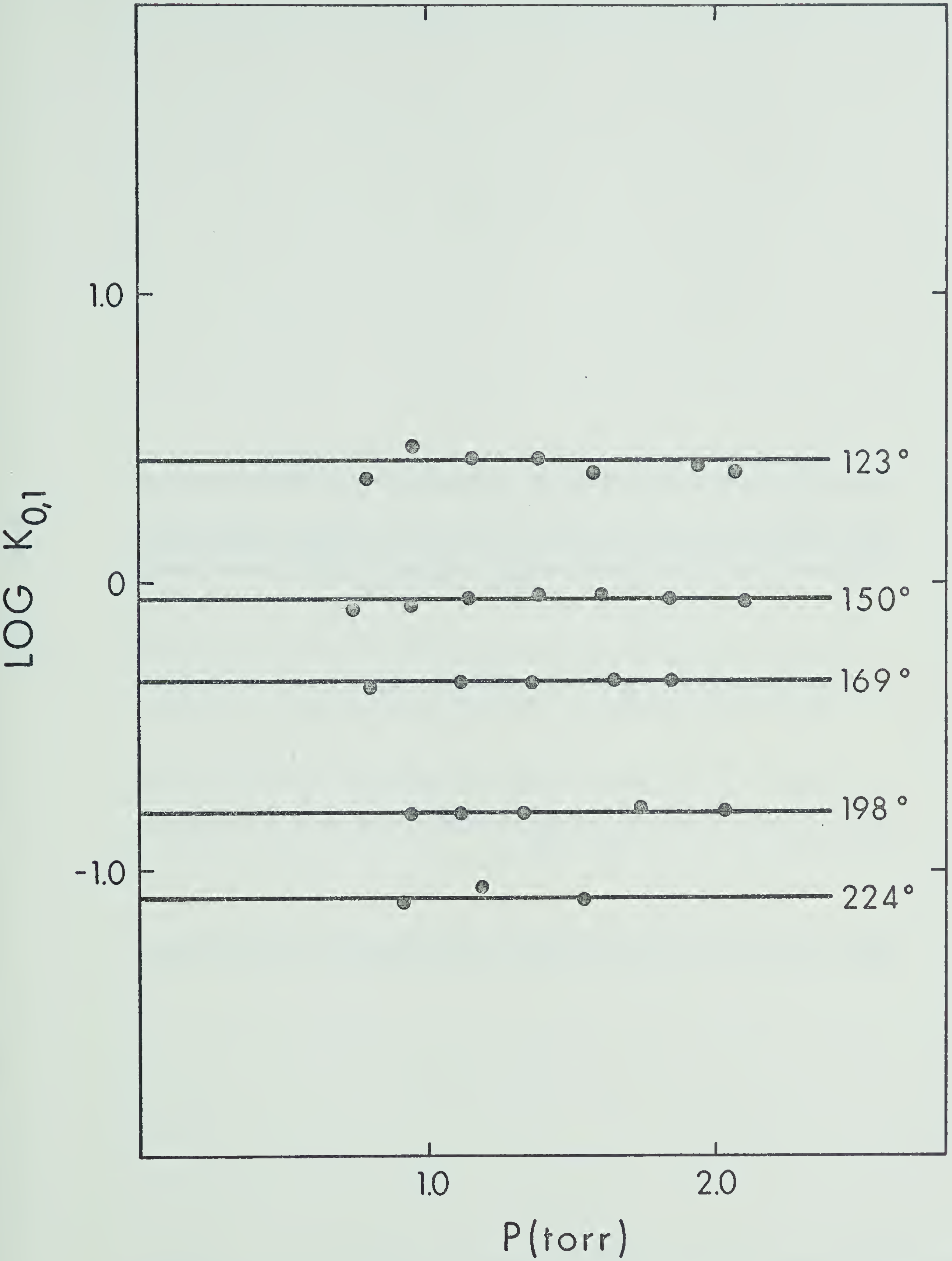

FIGURE 3.18 Plots Of Log $K_{0,1}$ for the Gas Phase Hydration of Cs^+, at Various Temperatures, Versus Pressure of H_2O

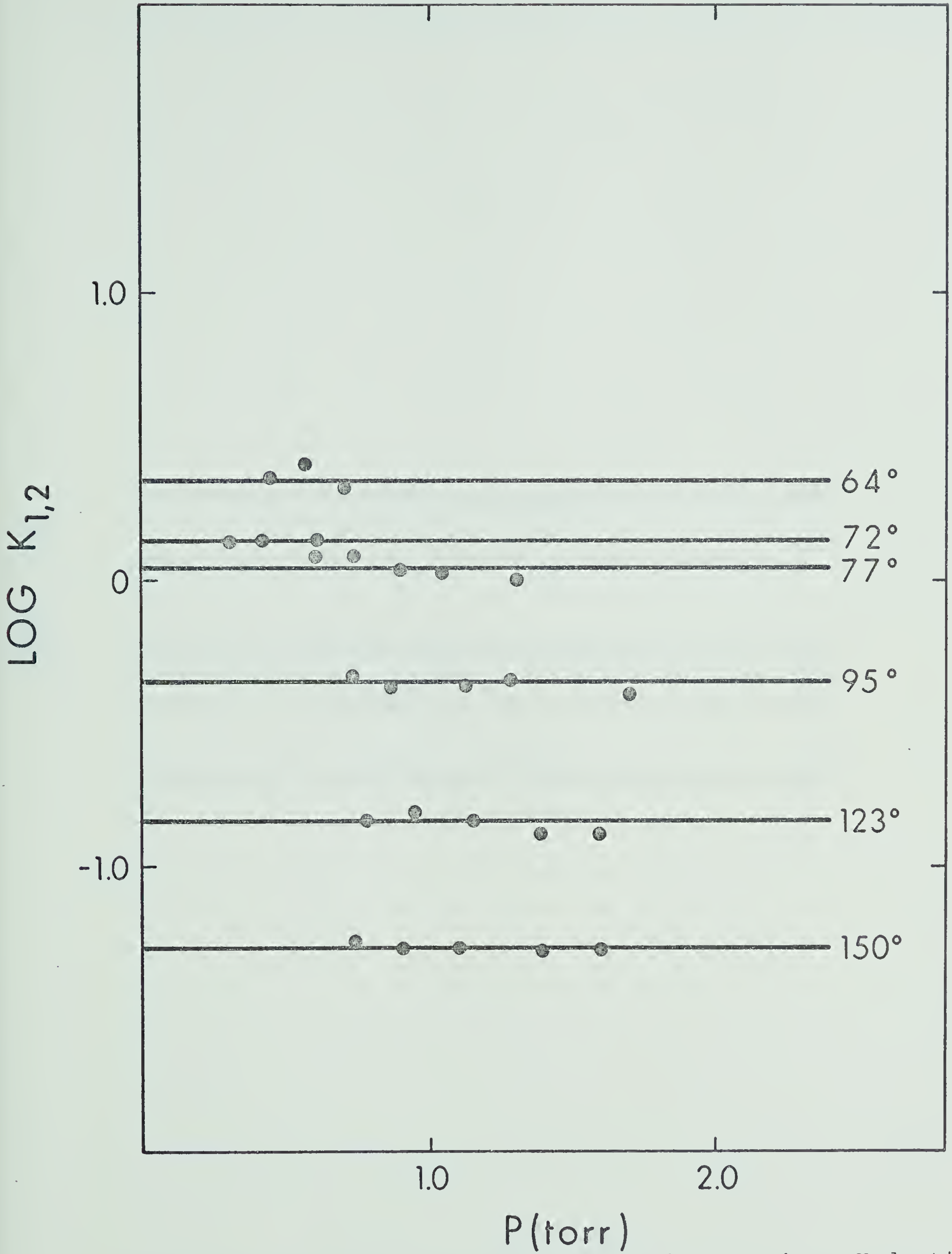

FIGURE 3.19 Plots of Log $K_{1,2}$ for the Gas Phase Hydration of Cs^+, at Various Temperatures, Versus Pressure of H_2O

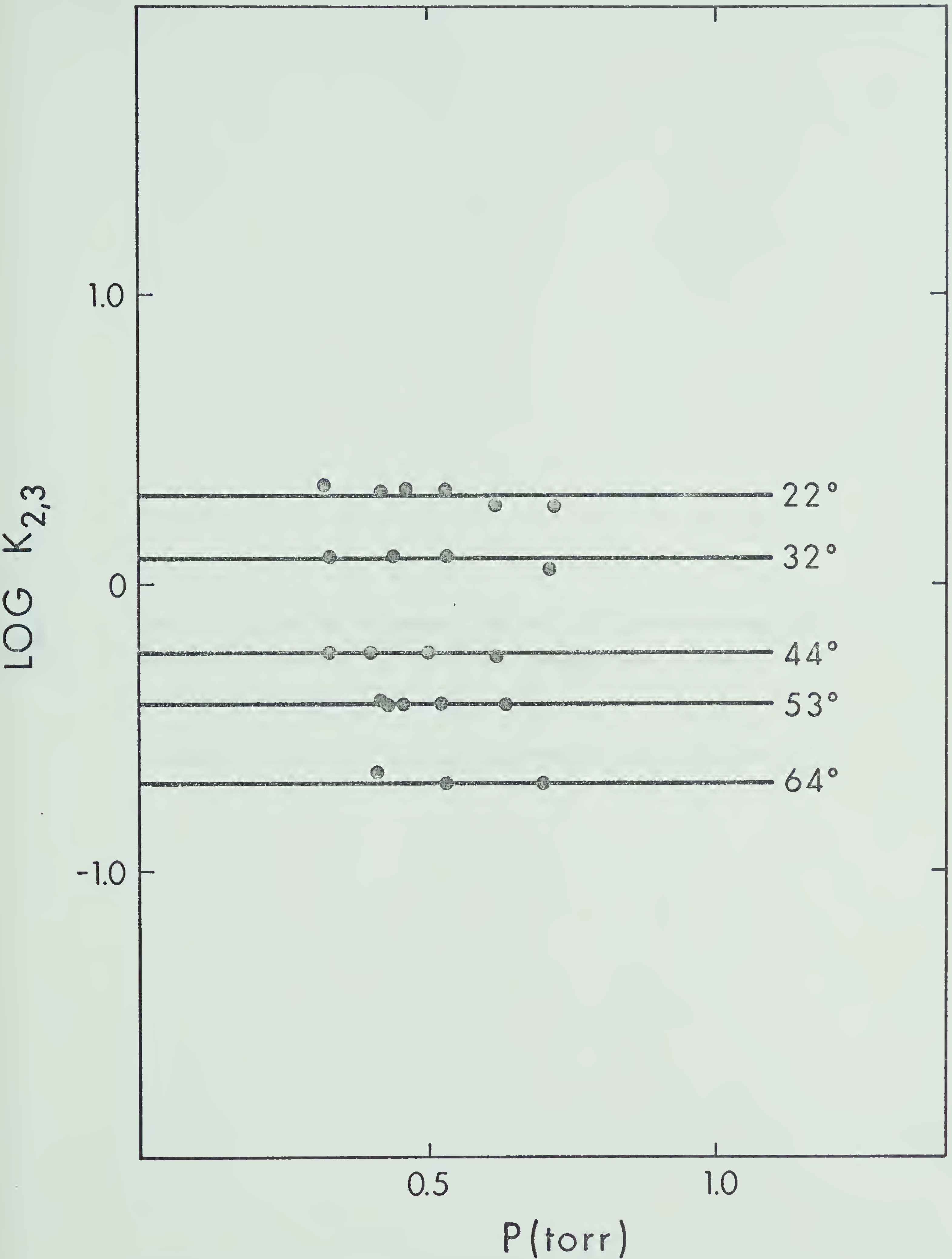

FIGURE 3.20 Plots of Log $K_{2,3}$ for the Gas Phase Hydration of Cs^+, at Various Temperatures, Versus Pressure of H_2O

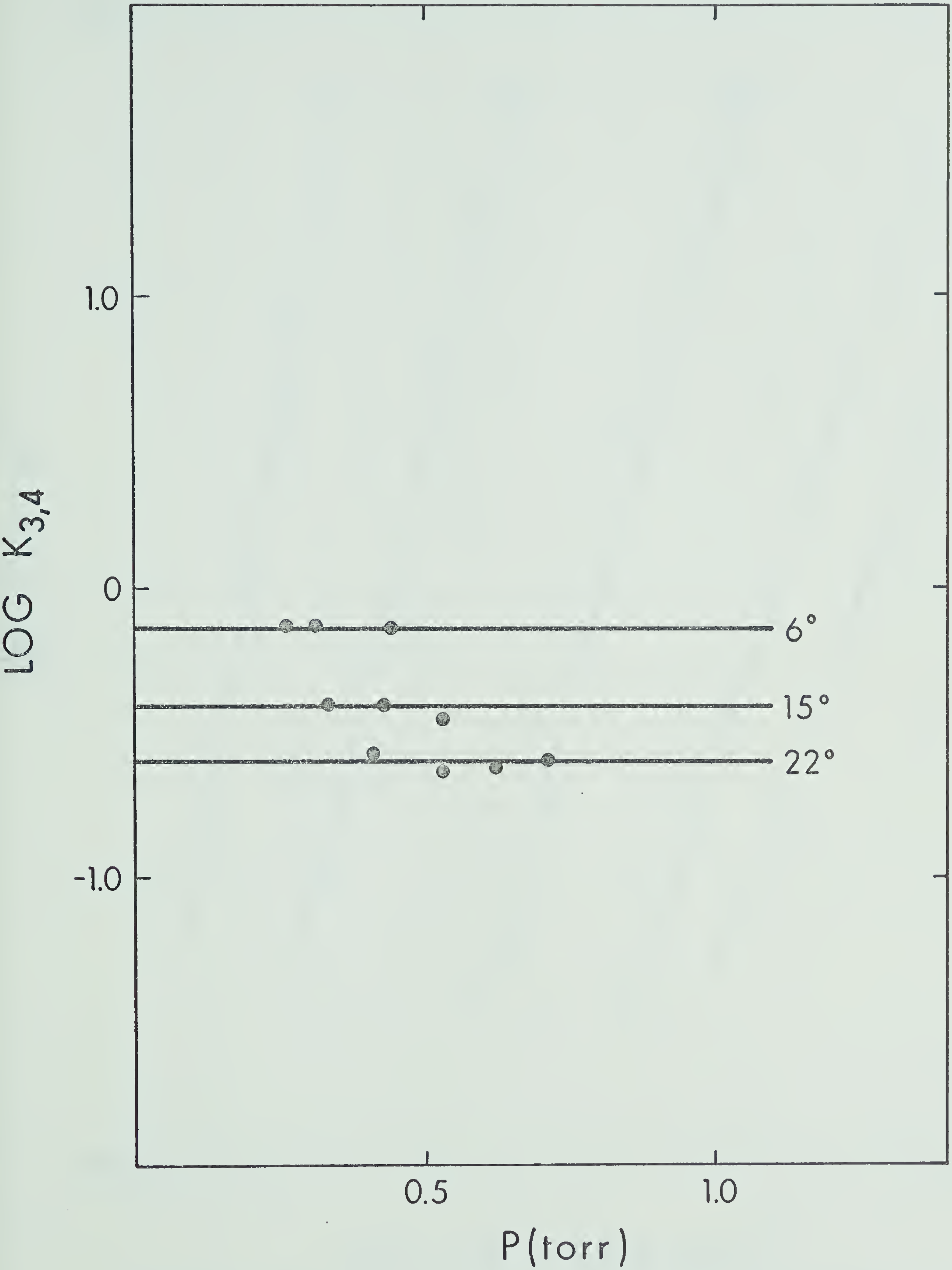

FIGURE 3.21 Plots of Log $K_{3,4}$ for the Gas Phase Hydration of Cs^+, at Various Temperatures, Versus Pressure of H_2O

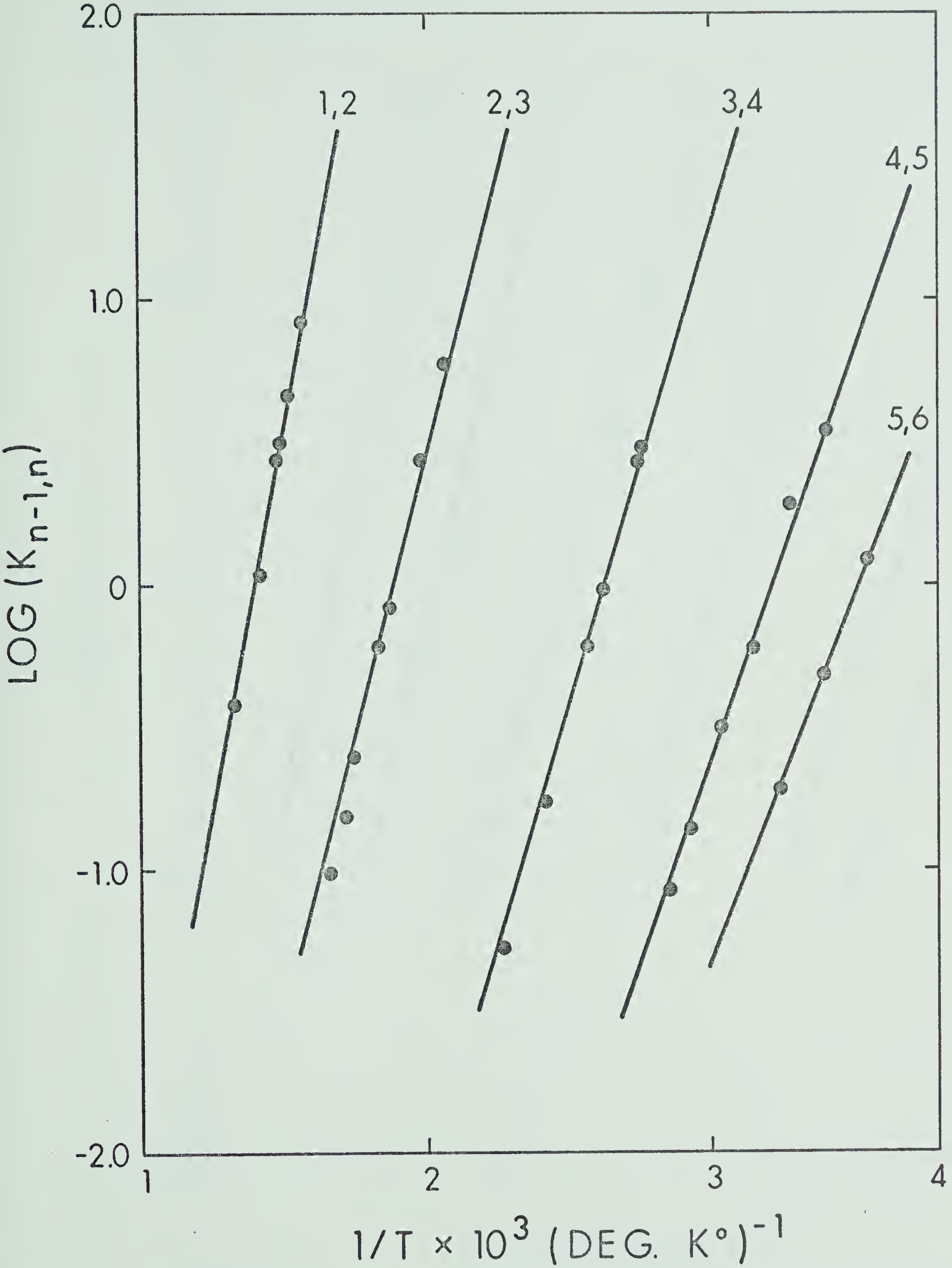

FIGURE 3.22 Van't Hoff Type Plots of the Equilibrium Constants for the Gas Phase Hydration of Li^+

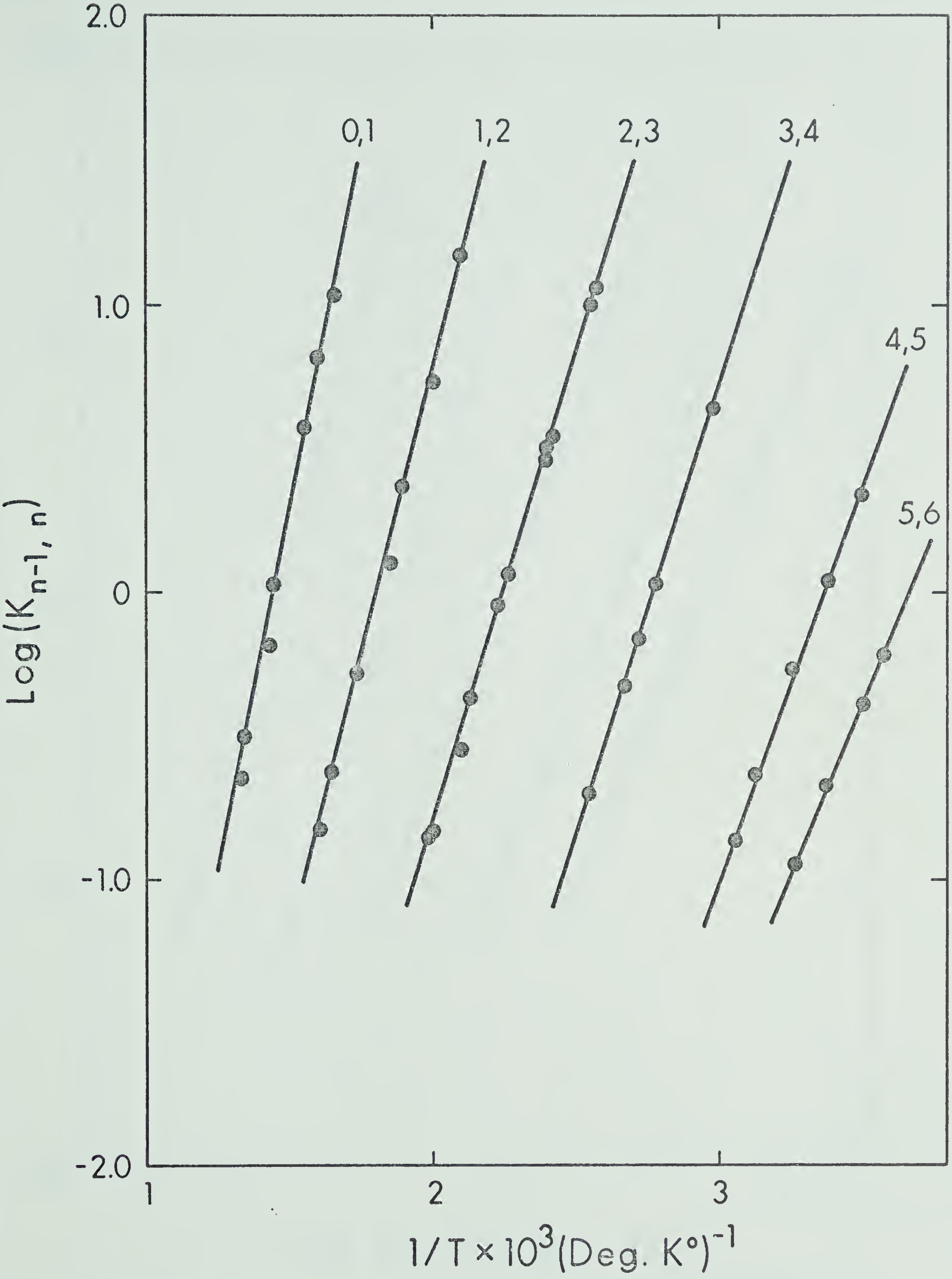

FIGURE 3.23 Van't Hoff Type Plots of the Equilibrium Constants for the Gas Phase Hydration of Na^+

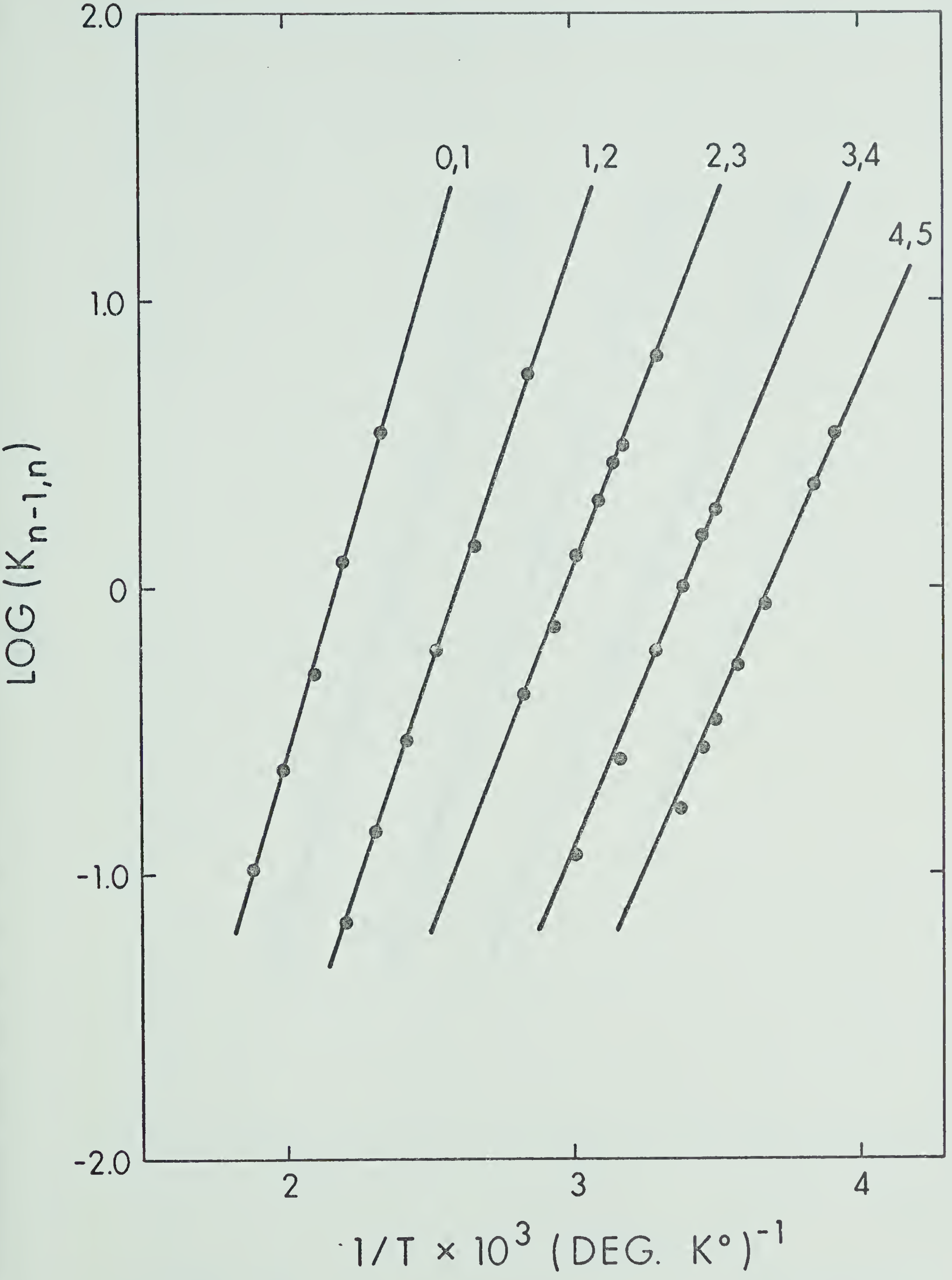

FIGURE 3.24 Van't Hoff Type Plots of the Equilibrium Constants for the Gas Phase Hydration of Rb^+

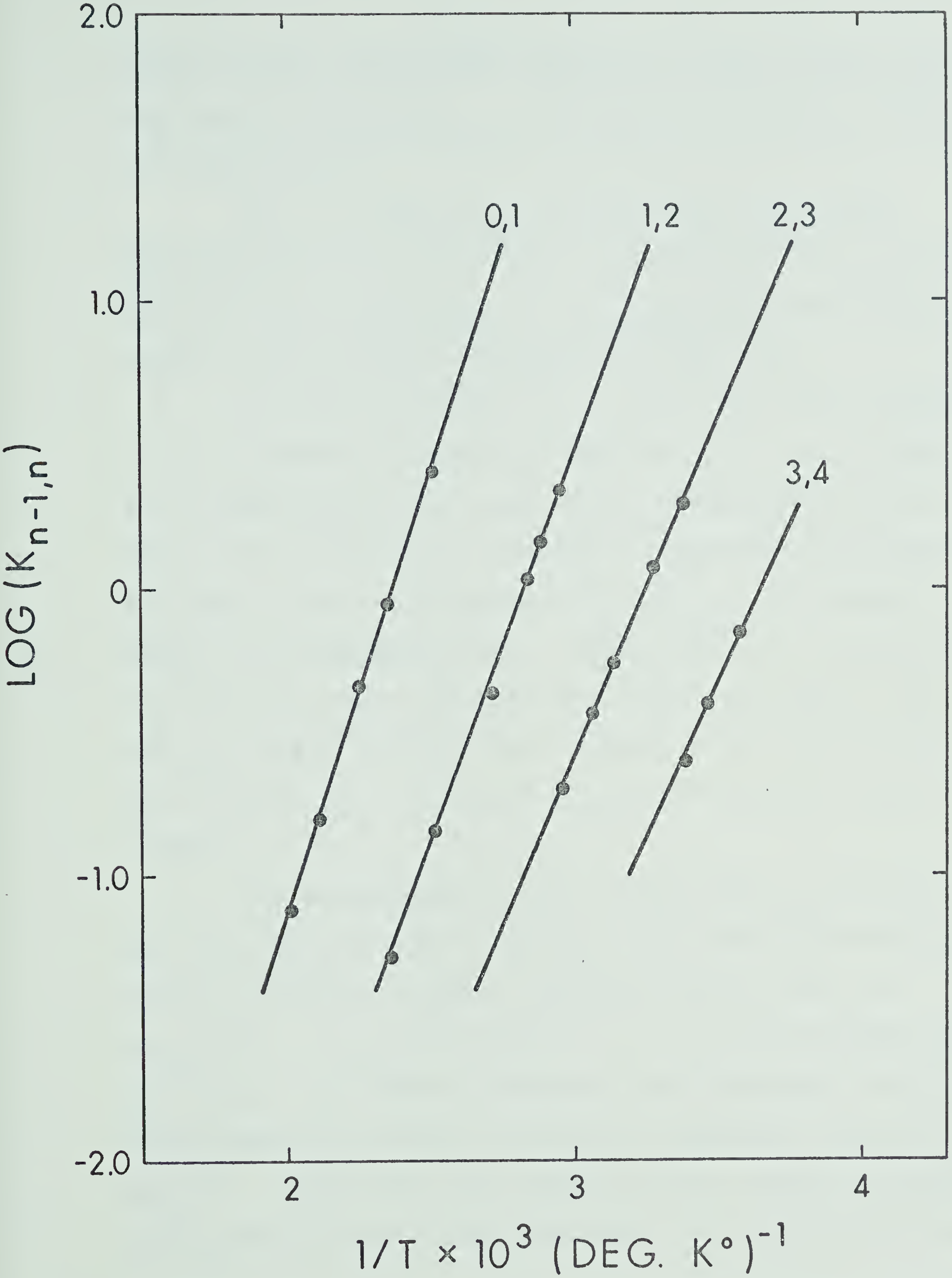

FIGURE 3.25 Van't Hoff Type Plots of the Equilibrium Constants for the Gas Phase Hydration of Cs^+

slopes of Van't Hoff plots, by means of least square treatment using values of $K_{n-1,n}$, measured at various pressures and temperatures.

$\Delta G^\circ_{n-1,n}$ and $\Delta S^\circ_{n-1,n}$ at 298° were calculated from equation (1.1) and (1.2). The values of $\Delta H^\circ_{n-1,n}$ as well as values of $\Delta G^\circ_{n-1,n}$ and $\Delta S^\circ_{n-1,n}$ are presented in Tables 3.1 to 3.4 and in Figures 3.26 and 3.27.

In Figure 3.26 the $\Delta H^\circ_{n-1,n}$ for the ions are shown for the different clustering steps (n-1,n). It is found for a given alkali ion, that $-\Delta H^\circ_{n-1,n}$ decreases as the size of the cluster (n) increases. Comparing the different alkali ions one finds that the $\Delta H^\circ_{n-1,n}$ are largest for Li^+ and smallest for Cs^+. Both results are reasonable and agree with what one would have expected namely, that $\Delta H^\circ_{n-1,n}$ would decrease with increase of the size of the ion. The $\Delta G^\circ_{n-1,n}$ values in Figure 3.27 exhibit similar trends.

The consistency of the relative $\Delta H^\circ_{n-1,n}$ values for the different alkali ions with available thermodynamic data is checked in Figure 3.28 which gives a plot of: $\Delta H_{o,n}(Cs^+) - \Delta H_{o,n}(M^+)$ versus n. It is to be expected that for large n the above difference should approach the difference between the simple ion heats of hydration: $\Delta H_h(Cs^+) - \Delta H_h(M^+)$. Indicated on the figure are the values for these differences obtained from the simple ion hydration enthalpies

TABLE 3.1

Experimental Thermodynamic Values for the Gas Phase Reactions:

$$Li^+(H_2O)_{n-1} + H_2O \rightleftarrows Li^+(H_2O)_n \qquad (n-1,n)$$

Reaction $n-1,n$	$-\Delta H^\circ_{n-1,n}$ (kcal/mole)	$-\Delta G^\circ_{n-1,n}$[a] (kcal/mole)	$-\Delta S^\circ_{n-1,n}$[a] (e.u.)
0,1	34.0[b]	25.5[b]	23.0[b]
1,2	25.8	18.9	23.1
2,3	20.7	13.3	24.9
3,4	16.4	7.5	29.9
4,5	13.9	4.5	31.4
5,6	12.1	2.5	32.0

[a] Standard state 1 atm and 298°K.

[b] Extrapolated values from plots in Figures 3.26 and 3.27

TABLE 3.2

Experimental Thermodynamic Values for the Gas Phase Reactions:

$$Na^+(H_2O)_{n-1} + H_2O \rightleftarrows Na^+(H_2O)_n \qquad (n-1,n)$$

Reaction n-1,n	$-\Delta H^\circ_{n-1,n}$ (kcal/mole)	$-\Delta G^\circ_{n-1,n}$ [a] (kcal/mole)	$-\Delta S^\circ_{n-1,n}$ [a] (e.u.)
0,1	24.0	17.6	21.5
1,2	19.8	13.2	22.2
2,3	15.8	9.3	21.9
3,4	13.8	6.3	25.0
4,5	12.3	3.9	28.1
5,6	10.7	2.9	26.0

[a] Standard state 1 atm and 298°K.

TABLE 3.3

Experimental Thermodynamic Values for the Gas Phase Reactions:

$$Rb^+(H_2O)_{n-1} + H_2O \rightleftarrows Rb^+(H_2O)_n \qquad (n-1,n)$$

Reaction $n-1,n$	$-\Delta H^\circ_{n-1,n}$ (kcal/mole)	$-\Delta G^\circ_{n-1,n}$ [a] (kcal/mole)	$-\Delta S^\circ_{n-1,n}$ [a] (e.u.)
0,1	15.9	9.6	21.2
1,2	13.6	7.0	22.2
2,3	12.2	5.0	24.0
3,4	11.2	3.8	24.8
4,5	10.5	2.8	25.7

[a] Standard state 1 atm and 298°K.

TABLE 3.4

Experimental Thermodynamic Values for the Gas Phase Reactions:

$$Cs^+(H_2O)_{n-1} + H_2O \rightleftarrows Cs^+(H_2O)_n \qquad (n-1,n)$$

Reaction n-1,n	$-\Delta H^\circ_{n-1,n}$ (kcal/mole)	$-\Delta G^\circ_{n-1,n}$ [a] (kcal/mole)	$-\Delta S^\circ_{n-1,n}$ [a] (e.u.)
0,1	13.7	7.9	19.4
1,2	12.5	5.9	22.2
2,3	11.2	4.2	23.7
3,4	10.6	3.0	25.4

[a] Standard state 1 atm and 298°K.

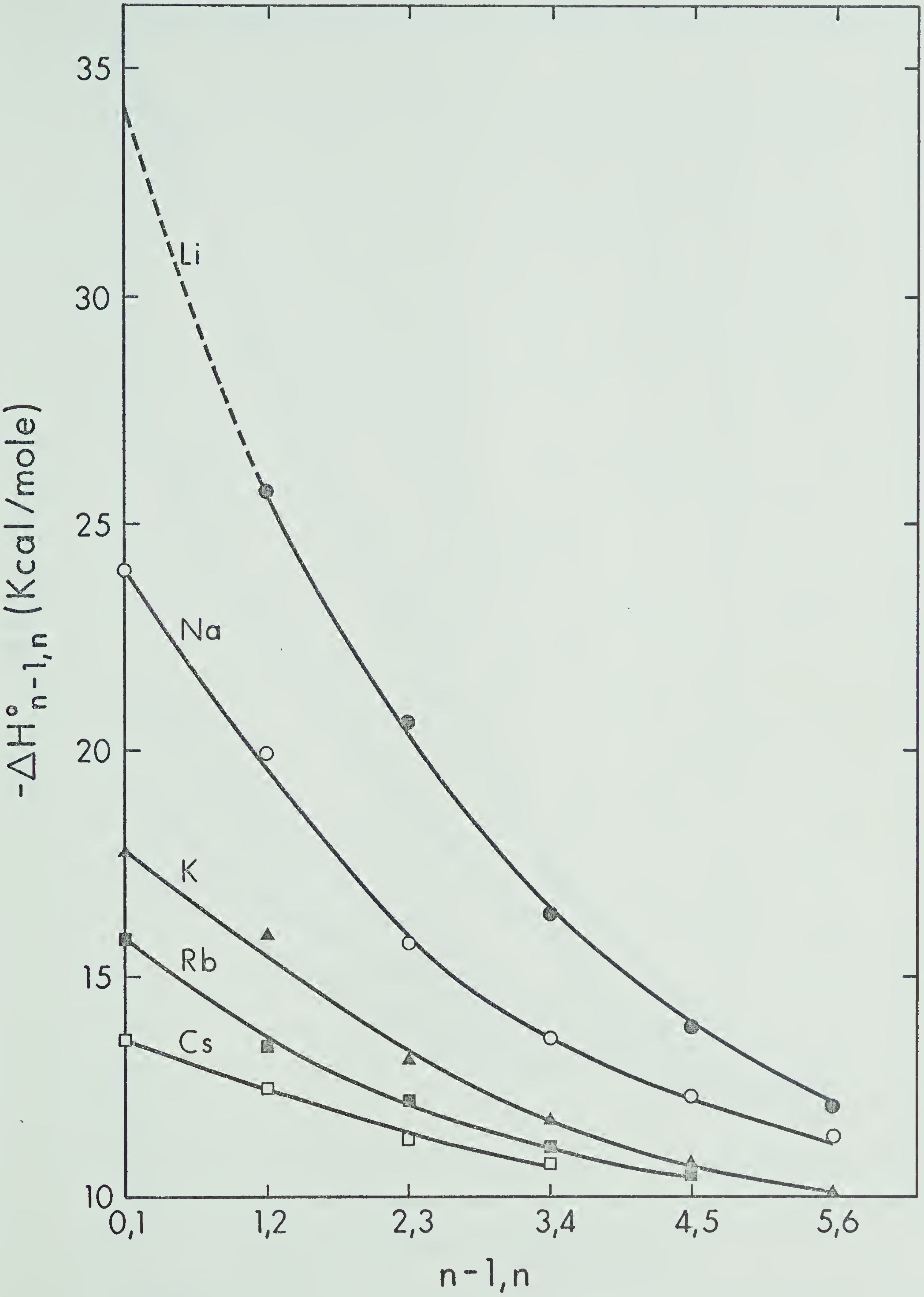

FIGURE 3.26 Enthalpies for Clustering Reactions

$M^+(H_2O)_{n-1} + H_2O \rightarrow M^+(H_2O)_n$

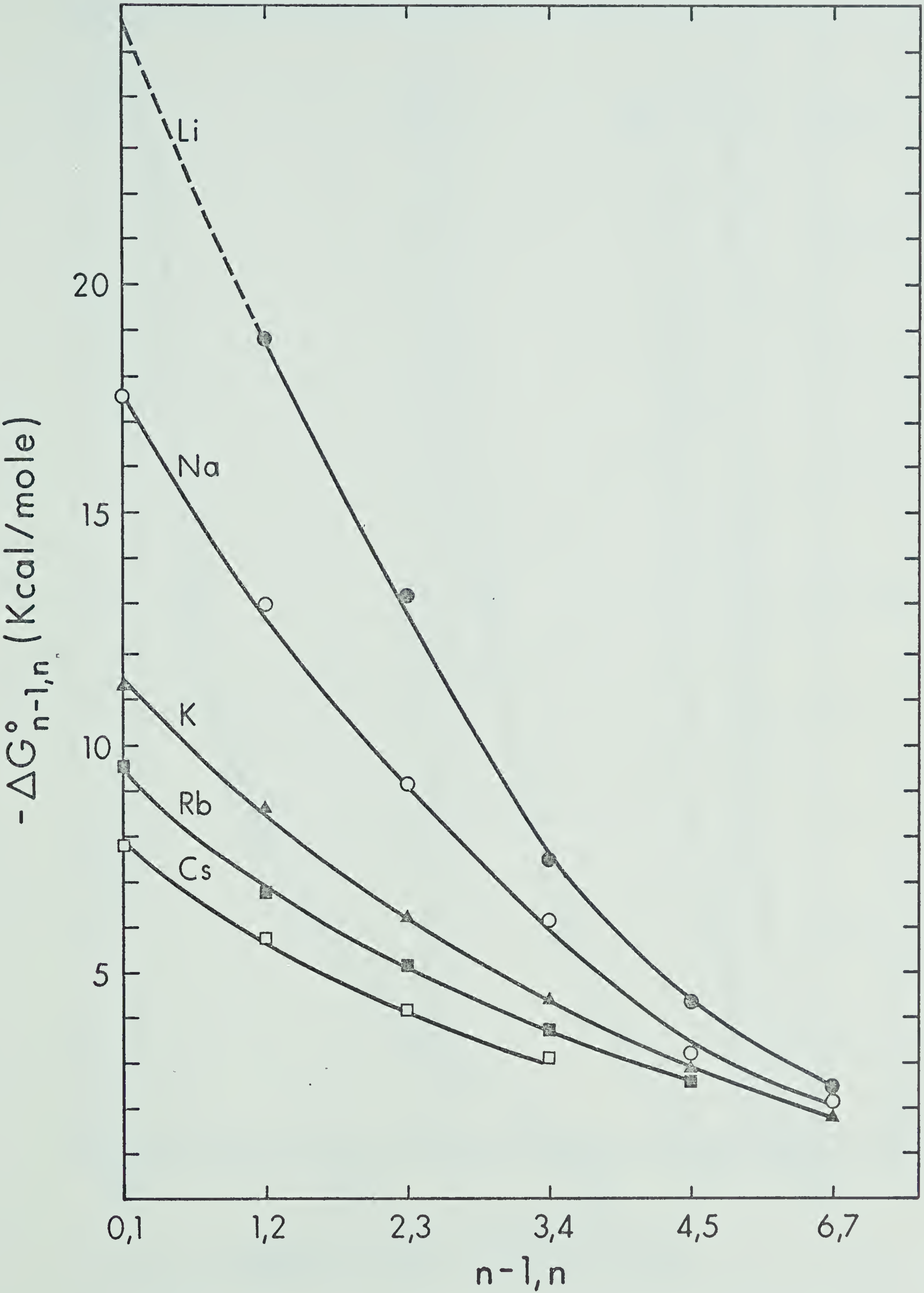

FIGURE 3.27 Free Energies of Clustering Reactions: $M^+(H_2O)_{n-1} + H_2O \rightarrow M^+(H_2O)_n$

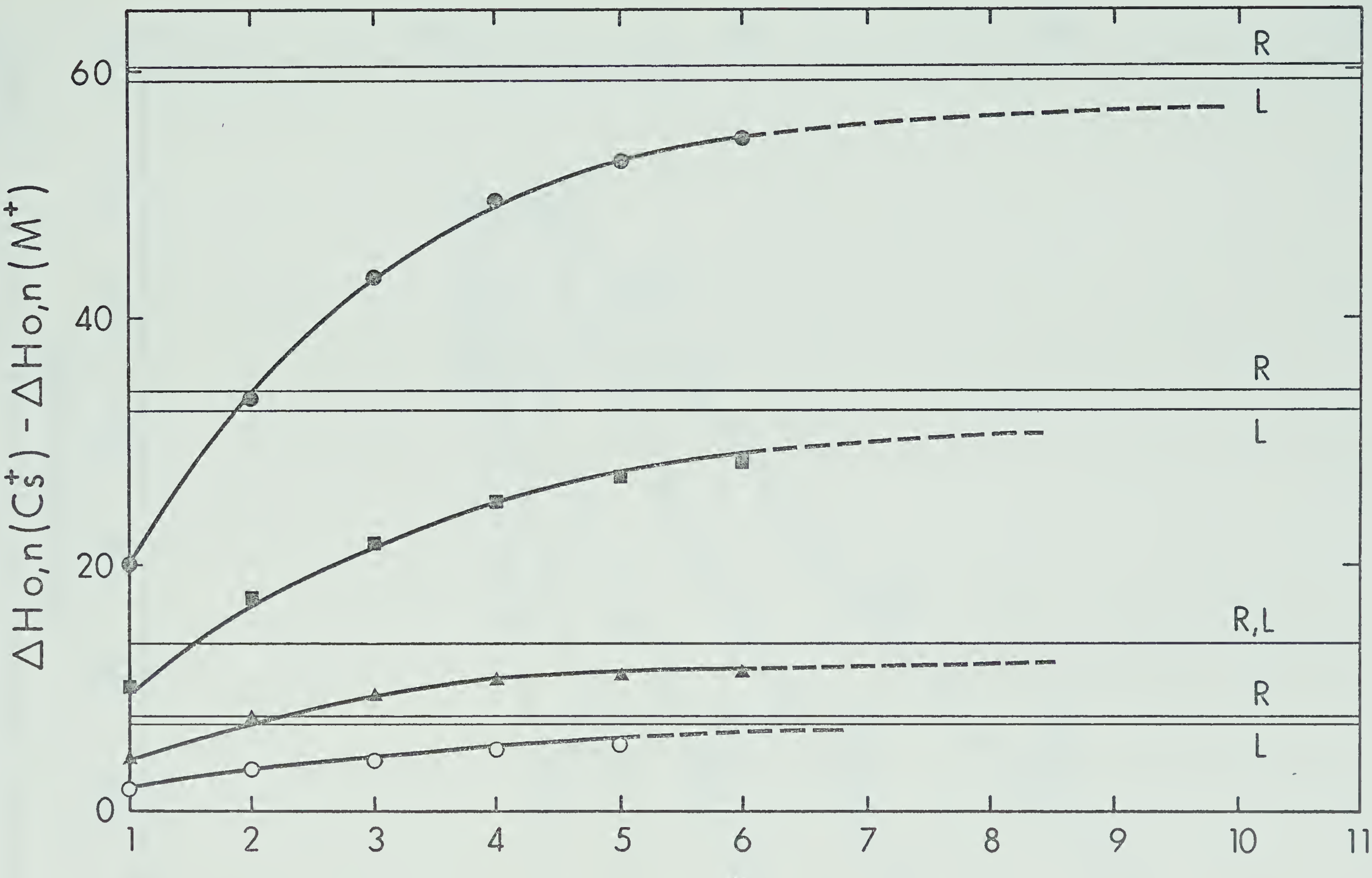

FIGURE 3.28 Plot of $\Delta H^{\circ}_{o,n}(Cs^+) - \Delta H^{\circ}_{o,n}(M^+)$ versus n showing that the above differences approach differences of total single ion heats of hydration obtained by Randles (R) and Latimer (L).

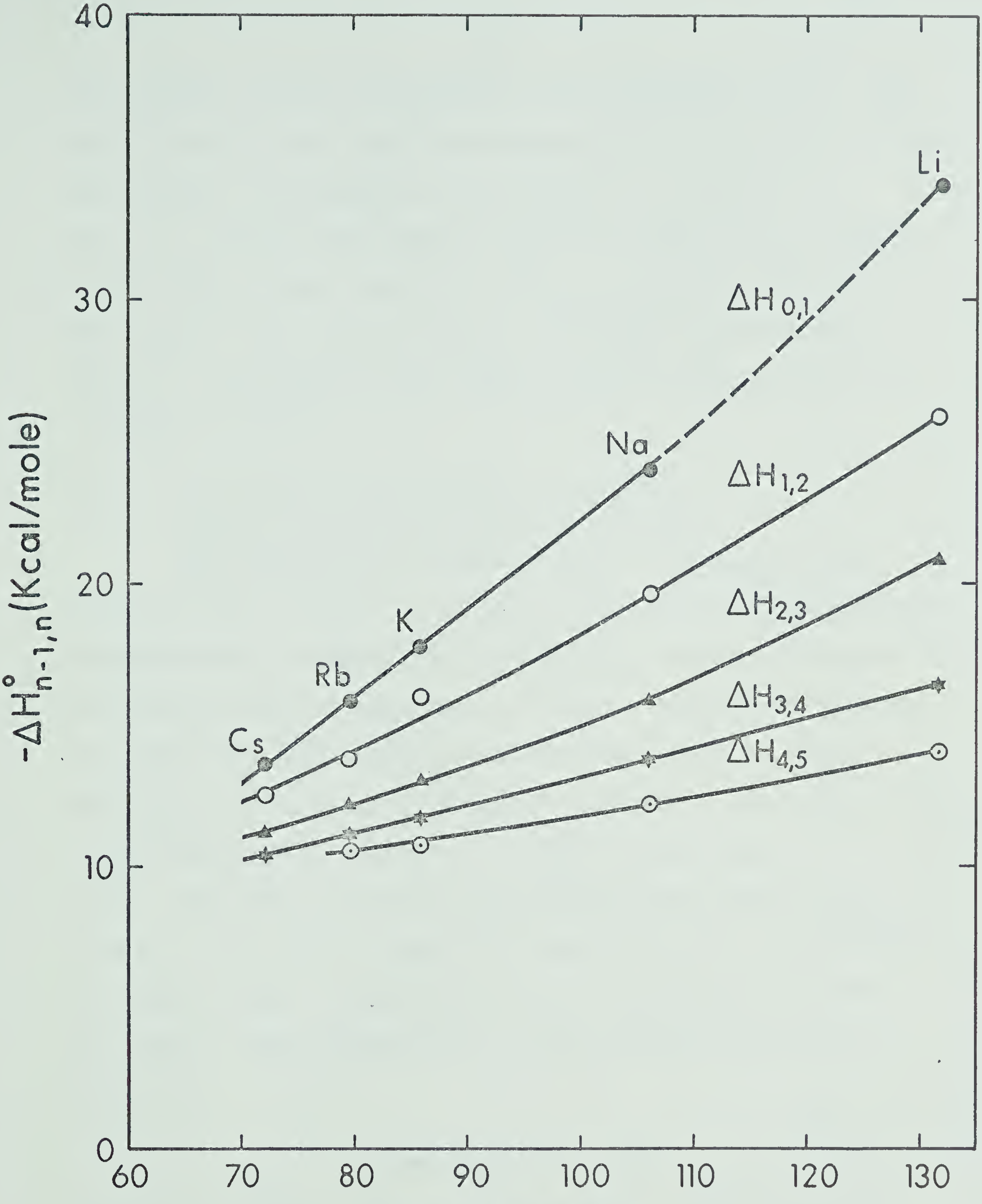

FIGURE 3.29 Plot of enthalpies for clustering reactions $M^+(H_2O)_{n-1} + H_2O \rightarrow M^+(H_2O)_n$ versus ΔH total single ion heats of hydration obtained by Randles.

of Latimer, Pitzer and Slanski (32) and Randles (35). The plot clearly shows that the present data are consistent with the simple ion hydration differences. In Figure 3.29 $\Delta H^{\circ}_{n-1,n}$ values were plotted versus ΔH hydration of Randles (35). This Figure shows that $\Delta H^{\circ}_{n-1,n}$ for Li^+, Na^+, K^+, Rb^+ and Cs^+ ion clusters fall on the same curve and that $\Delta H^{\circ}_{n-1,n}$ decreases as the size of the ion and size of the cluster increases.

3.3 Equilibrium Distribution of $M^+(H_2O)_n$

The equilibrium constant values, obtained in this work can be utilized to calculate the relative equilibrium concentrations of the cluster $M^+(H_2O)_n$ at various temperatures and partial pressures of water. As an illustration, the relative equilibrium concentrations of the clusters $Na^+(H_2O)_n$ are presented in Figure 3.30 for a temperature of 300°K and partial pressures of water ranging from 10^{-5} to 10^{0} torr. For this calculation the equilibrium constants $K_{n-1,n}$ for n = 1 to 6 were taken from Figure 3.22 at a temperature of 300°K. The concentration of Na^+ was arbitrarily set to unity. The concentration of the cluster $Na^+(H_2O)_n$ is given by

$$[Na^+(H_2O)] = K_{o,n}P^n$$

where $K_{o,n}$ is the product of the equilibrium constants from $K_{0,1}$ to $K_{n-1,n}$, and P is the partial pressure of

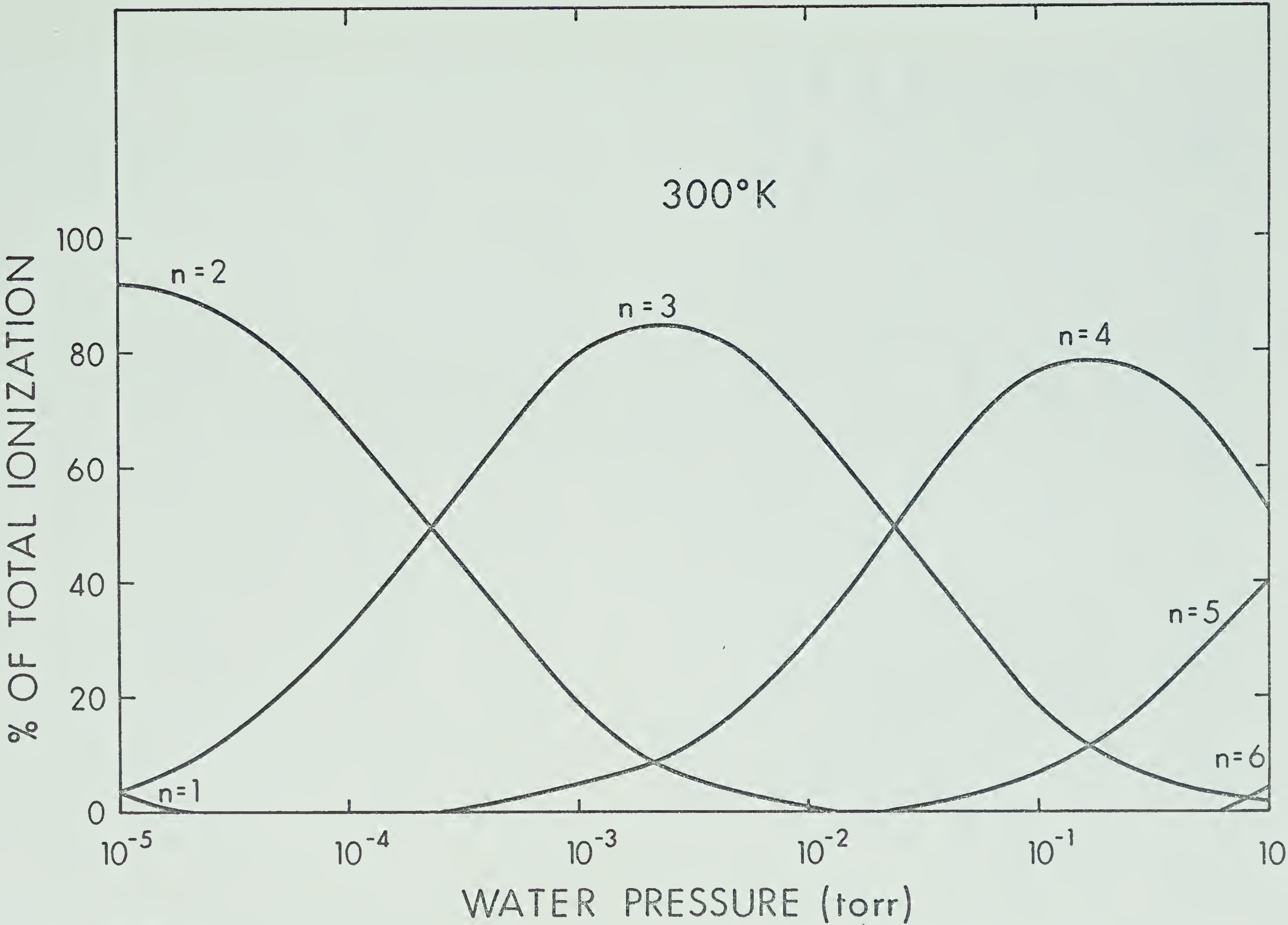

FIGURE 3.30 Plot of equilibrium distribution of Na$^+$(H$_2$O) at T = 300°K, as a function of water pressure.

of water. By setting the sum of the clusters Na^+ to $Na^+(H_2O)_n$ to 100, the relative concentration of each cluster is obtained. The plots in Figure 3.30 show that at low pressures the lower hydrates are present, the difference between the stability (free energy) of the hydrates is large and the concentrations of one or two hydrated species are dominant. At higher pressures where the higher hydrates become stable, differences between the free energies of the hydrates are small and a number of hydrated species are present simultaneously.

4. ELECTROSTATIC CALCULATIONS OF THE POTENTIAL ENERGIES OF THE CLUSTERS $M^+(H_2O)_n$ AND COMPARISON WITH EXPERIMENTAL ENTHALPY CHANGES

In this section, the interaction energy between an ion and its neighbouring water molecules is discussed. The energy of interaction between a spherical ion and neutral water molecule is expressed as a sum of energy terms. The energy terms represent various forces which are known to act between the ion and the surrounding water molecules. The calculated potential energy changes, ($\Delta E_{o,n}$) which occur when the water molecules bond to the ion, will then be compared to the experimental enthalpies of hydration $\Delta H_{o,n}$ of the ions at 298°K.

4.1 Interaction Energies

The energy of interaction between an inert-gas like ion and a water molecule is assumed to be the sum of the following contributions.

A. Ion-permanent dipole forces: The attractive energy between the ion and the permanent dipole of a water molecule is $ze\mu\cos\theta/R^2$, where μ is the dipole moment, ze the charge and θ the angle between the dipole and the line of centers. This attractive energy term has a directional character, the maximum value being $ze\mu/R^2$ (61).

B. Ion-induced dipole forces: The ion induces a dipole in the polarizable water molecule and an attraction results. The energy being $z^2e^2\alpha/2r^4$, where α is the

polarizability (61).

C. Dispersion forces: Even when species have no dipole moments there is an attraction between them due to mutual polarization. The interaction energy corresponding to these dispersion forces leads to a potential energy (61).

$$E = 3/2 \frac{\alpha_1 \alpha_2}{R^6_{i,j}} \frac{I_1 I_2}{I_1 + I_2}$$

The I's represent the ionization energies of the ion and molecule, the α's are their polarizabilities and $R_{i,j}$ is the internuclear separation between the ion and the ligand molecule and between the ligand molecules themselves.

D. Dipole-dipole repulsive forces: These are directional, the maximum interaction energy being $2\mu A \mu B/R^3$ when the dipoles are in line with each other. The μ's are dipole moments of molecules and R is the distance between them.

E. Ion-ligand molecule repulsive forces: The ion-molecule repulsive energies are interpreted by using a term of the form AR^{-n}, A and n are the constants and R is the internuclear separation between the ion and the ligand molecule. A value of 12 for n is assumed in the well-known Lennard-Jones potential.

4.2 The Present Model for the Electrostatic Calculations

The potential energy E_n of a cluster $M^+(H_2O)_n$ relative to that of the alkali ion and n water molecules at infinity can be written as

$$4.1 \quad E_n = EDIP + EPOL + EDIS + RDIP + REL$$

where EDIP represents the attraction energy between the central ion and the permanent dipole of the ligand molecule, EPOL represents the attraction energy due to the polarization of the ligand molecules by the central ion, EDIS represents the dispersion energy between the central ion and the ligands as well as the dispersion energy between the various ligands, RDIP represents the dipole-dipole repulsion energy between the ligand molecules and finally, REL represents the ion ligand repulsion energy. The electronic repulsions between the ligand molecules themselves were neglected. The models and equations used in the present work were designed to give a good approximation to the sum of the electrostatic energies, given by equation 4.1. Each term in equation 4.1 will be discussed separately.

A. Ion-permanent dipole interaction (EDIP)

It is well known that an asymmetric molecule, H_2O for example, possesses a permanent electrical dipole. The permanent dipole of a water molecule is due to a permanent charge shift of the electron cloud in the water molecule.

At large distances between the ion and the water molecule, the point dipole approximation for the water molecule is completely satisfactory. However, as the distance to the dipole molecule is decreased the point dipole approximation becomes unsatisfactory. An approximation that is somewhat better (at close distances between the ion and dipole) is to represent the permanent dipole by a few point charges (62). The placement of the positive and negative point charges should be such as to reproduce the point dipole (at large distances). For this calculation it is reasonable to place the negative charge on the oxygen nucleus and positive charges on the hydrogen nuclei of a water molecule. For a given charge separation the size of the charges is determined from the permanent dipole of water 1.85 Debye and the bond angle of 105°. The O-H bond distance was taken as 0.97 Å (63).

To determine the energy of interaction of an ion and the permanent dipole, one simply adds the coulombic terms due to the interaction of the ion with the three point charges of the water molecule. The point charge model used in the present calculation is shown in Figure 4.1 and equation 4.2. The same model has been used by Doyne and Caldwell (62) who considered the $H_3O^+(H_2O)_n$ system.

$$4.2 \qquad \mathrm{EDIP} = \sum_{j=1}^{n} \sum_{i=1}^{p} \frac{(334)(Q_{ion})(Q_{i,j})}{R_{i,j}}$$

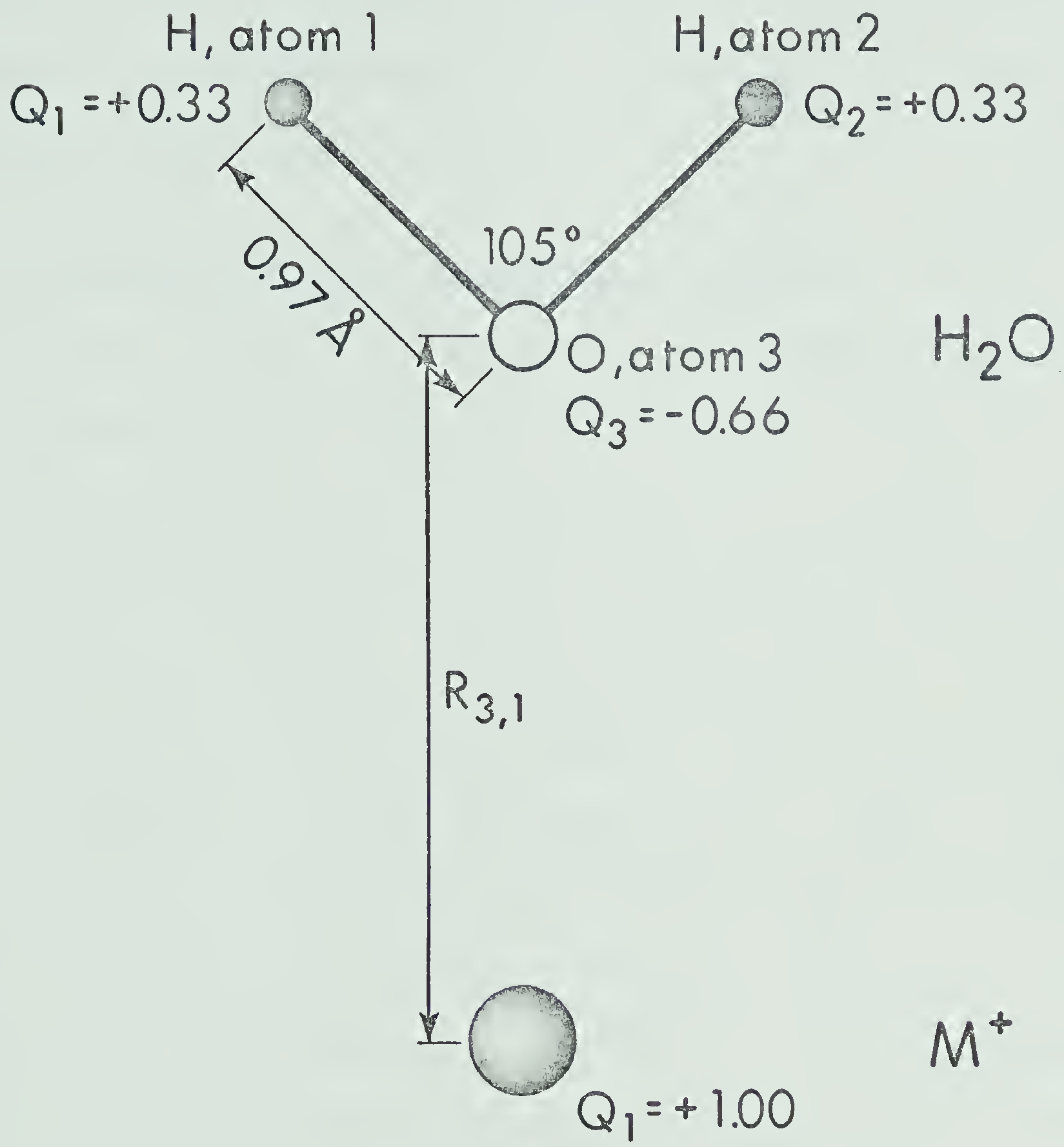
H, atom 1
Q_1 = +0.33
H, atom 2
Q_2 = +0.33
0.97 Å
105°
O, atom 3
Q_3 = -0.66
H_2O
$R_{3,1}$
M^+
Q_1 = + 1.00

FIGURE 4.1 $M^+(H_2O)$ model used in the theoretical calculations.

Q_{ion} is the ionic charge, $Q_{i,j}$ is the charge on i^{th} atom of the j^{th} molecule with p atoms per molecule and n molecules per cluster. $R_{i,j}$ is the ion-atom distance.

The numerical factor (334) in the above equation is adjusted to give the energy in kcal/mole, for values of Q in atomic units and R in Å.

B. Ion-induced dipole interaction (EPOL)

The ion, carrying a charge Q, produces an electric field of magnitude $E = \frac{Q}{R^2}$ at a distance R from its center. If a water molecule of polarizability α is placed at R it will be polarized, assuming an induced dipole moment of magnitude $\mu = \alpha E = \frac{\alpha Q}{R^2}$. There will thus be an attractive force between the positively charged ion and the induced dipole of moment μ, which is equal to: $F = \mu\frac{dE}{dR} = 2\mu\frac{Q}{R^3} = \frac{2\alpha Q^2}{R^5}$. The potential energy describing this attraction is related to the force F by Pot. Energy $= -\int F dR$ and is therefore equal to: Pot. Energy $= -\alpha Q^2/2R^4$. In the present calculation of the above potential energy which we call EPOL is expressed by equation 4.3

$$4.3 \qquad \mathrm{EPOL} = \sum_{j=1}^{n} \sum_{i=1}^{p} \frac{(334)(Q_{ion})^2 \alpha_{i,j}}{2R^4_{i,j}}$$

Q_{ion} is the ionic charge, $\alpha_{i,j}$ is the polarizability of the i^{th} atom of the j^{th} molecule with p atoms per molecule and n molecules per cluster. The polarizability of oxygen and

hydrogen were taken as 0.60 and 0.44 $\mathring{A}^3$ respectively (63). $R_{i,j}$ is the ion-atom distance.

C. Ion-ligand and ligand-ligand interaction due to dispersion forces (EDIS)

The interaction energies due to dispersion forces between ion and water molecules and between water molecules themselves are calculated from London's equation 4.4

$$4.4 \qquad E = \frac{3}{2}\frac{h}{R^6}\left(\frac{\nu_1\nu_2}{\nu_1+\nu_2}\right)\alpha_1\alpha_2$$

where ν's are the frequencies of the ionization limit for the ion and the molecule (61), hν thus being equal to the ionization energy of the corresponding ion and the molecule. The α's are static polarizabilities. If we substitute hν by the ionization potential in the above equation, we obtain equation 4.5 used in the present calculation. This equation has been also used by Muirhead-Gould and Laidler (61) for similar evaluations.

$$4.5 \qquad \mathrm{EDIS} = \frac{3}{2}\,\frac{\alpha_i\alpha_j}{R_{i,j}^6}\,\frac{I_iI_j}{I_i+I_j}$$

α_i is the (point dipole) polarizability and I_i the ionization potential of molecule i. $R_{i,j}$ is the distance between the molecules. The distance between the ion and the water molecules was taken as equal to the distance from the ion nucleus

to the oxygen nucleus ($R_{1,3}$) plus 0.3 Å. The distances between the water molecules themselves were measured from centre to centre assuming that the centre of the molecules lies on the bisector of the OH_2 angle and 0.3 Å from the oxygen nucleus. The total dispersion energy was obtained by summing up the energies of all appropriate molecules. The ionization potential and polarizability of water were taken as 12.56 ev (61) and 1.48 $Å^3$ (61) respectively. The values of ionization potentials and polarizabilities of alkali ions are given in Table 4.1.

D. Dipole-dipole repulsion energies (RDIP)

The dipole-dipole repulsion energy can be divided into three components: permanent dipole - permanent dipole repulsion ($R_{P.P.}$), induced dipole-induced dipole repulsion ($R_{I.I.}$) and induced dipole-permanent dipole repulsion ($R_{I.P.}$)

$$RDIP = R_{P.P.} + R_{I.I.} + R_{I.P.}$$

For the calculation of the term due to permanent dipole-permanent dipole, $R_{P.P.}$ repulsion, the point charge model for the water molecule was used. However the point charge model becomes too cumbersome in the calculation of the permanent dipole-induced dipole ($R_{I.P.}$) and induced dipole-induced dipole ($R_{I.I.}$) interactions. Therefore these were calculated by using the point dipole and point polarizability of water.

TABLE 4.1

Ionization Potentials and Polarizabilities of Alkali Ions

Ion	Ionization Potential (eV)	Polarizability (Å^3)
Li^+	75.3	0.03
Na^+	47.1	0.24
K^+	31.7	0.89
Rb^+	27.4	1.81
Cs^+	23.4	2.79

Ionization potentials and Polarizabilities, ref (61).

The following equations, taken from references (62) (71) were used to calculate various contributions to the total dipole-dipole repulsion energy (RDIP)

$$4.6 \quad R_{P.P.} = \sum_{l=2}^{n} \sum_{j=1}^{l-1} \sum_{i=1}^{p} \sum_{k=1}^{p} \frac{(334)(Q_{i,j})(Q_{k,l})}{R_{i,j,k,l}}$$

$Q_{i,j}$ is the charge on the i^{th} atom of the j^{th} molecule with p atoms per molecule and n molecules per cluster. $R_{i,j,k,l}$ is the distance between the i^{th} atom of j^{th} molecule and k^{th} atom of the l^{th} molecule.

$$4.7 \quad R_{I.I.} = \sum_{j=1}^{n-1} \sum_{m=j+1}^{n} \frac{14.397\alpha_M^2 e^2}{R_{ion,j}^4 \; S_{j,m}^3} (1 + \cos^2\theta_{j,m})$$

$$4.8 \quad R_{I.P.} = \sum_{j=1}^{n-1} \sum_{m=j+1}^{n} \frac{28.794P\alpha_M e}{R_{ion,j}^2 \; S_{j,m}^3} (1 + \cos^2\theta_{j,m})$$

α_M is the polarizability of the water molecule and P is its permanent dipole moment. e is the electronic charge. $S_{j,m}$ is the distance of the j^{th} molecule from the m^{th} molecule in the cluster and $R_{ion,j}$ is the distance between the central ion and the j^{th} molecule. The numerical factors in the above equations are adjusted to give the energy factors in kcal/mole, for values of α in Å^3, permanent dipole P in Debye, the electronic charge e in e.s.u. and the distances R and S in Å, respectively.

E. Ion-ligand molecule repulsive energies (REL)

The ion-molecule repulsive forces may be treated in several ways. For some purposes a hard sphere model is adequate, but it is somewhat more satisfactory to interpret repulsive energies by using a term of the form AR^{-n}; A and n are constants and R is the internuclear separation. A value of 12 for n is assumed in the well known Lennard-Jones potential. A term of the form AR^{-12} has been used by Laidler (61) in electrostatic potential energy calculations. The same form is adopted in present calculations, represented by equation 4.9

$$4.9 \quad REL = \sum_{j=1}^{n} \sum_{i=1}^{p} A_{i,j} R^{-12}$$

The evaluation of the repulsion constant A is given in the next section.

For the clusters with more than one water molecule many different structures are possible. In the present calculations the most symmetrical ligand arrangement was assumed, where all M^+——OH_2 distances are equal. In all cases the water molecules were considered to be oriented with respect to the ion in such a way that the ion was on the bisector of the H—O—H angle. The orientation of the molecules with respect to one another was determined by minimizing the total potential energy with respect to rotations around the H—O—H bisector.

The clusters with two water molecules were assumed to be linear with the positive M^+ ion placed equidistant between two water molecules. For three water molecules, a trigonal planar structure was used. A tetrahedron, a trigonal bipyramid and an octahedron were used for four, five and six water molecules bonded to the ion M^+. The potential energies E_n, for the cluster $M^+(H_2O)_n$, were computed over the range of M^+——$(H_2O)_n$ distances by means of an IBM 360/67 computer. The program used was taken from the work of S. K. Searles (50) and adapted for the present calculations. The program used can be obtained from the author on request.

4.3 Evaluation of the Numerical Value for the Constant A in the Electronic Repulsion Term REL = AR^{-12}

The selection of the numerical value for the constant A in the term REL = AR^{-12} representing the electronic repulsions is probably the most critical step in electrostatic calculations of the type used here. Thus, the nature of the central ion Li^+ or Na^+, etc. finds expression in the calculation essentially only through the value of A. The dispersion terms also depend on the nature of the ion, but these terms are quite small. For determination of the values of the constant A the following procedure was adopted. The values of A for the repulsions between Ne...Ne, Ar...Ar etc., were calculated from the six-twelve

potential function of Lennard-Jones using the equation 4.10, $A = 4\varepsilon\sigma^{12}$, ε is the depth of the potential well and σ is the interatomic distance for zero potential energy. The values for ε and σ, taken from the literature (64), as well as values of A calculated from the equation 4.10 are presented in Table 4.2. It has been suggested (65) that the A values for the interactions between two non-identical noble gas atoms like Ne...Ar can be approximated quite well by taking the geometric mean of the A values for Ne...Ne and Ar...Ar. Thus $A_{Ne,Ar} \simeq A^{\frac{1}{2}}_{Ne,Ne} \times A^{\frac{1}{2}}_{Ar,Ar}$. This property was the basis of the selection of A values for the present calculation. The plot of Figure 4.2 shows the values of $A^{\frac{1}{2}}$ for the inert gases on a logarithmic scale versus the respective Van der Waals radii of these gases. The straight line obtained allows one to select an $A^{\frac{1}{2}}$ value for any species for which an appropriate radius is available. It is important to realize that the selected radius must be consistent with the Van der Waals radii used for the inert gases. Thus the radius for the isoelectronic positive alkali ion should be smaller than that of the corresponding inert gas atom.

One set of $A^{\frac{1}{2}}$ values for the alkali ion-water repulsions were obtained by using the Van der Waals radii for the alkali ions obtained by R. H. Stokes (66) who determined these radii by quantum mechanical scaling of the Van der Waals radii of the corresponding isoelectronic inert gas

TABLE 4.2

The Coefficient "A" for Repulsion Term (A/R^{12}) between Two Atoms of the Inert Gases from Equation $A = 4\varepsilon\sigma^{12}$.

	ε Electron-volt	σ A°	A kcal - $A°^{12}$
Helium-Helium	0.70×10^{-3}	2.59	0.5959×10^{4}
Neon-Neon	3.00×10^{-3}	2.77	5.5901×10^{4}
Argon-Argon	1.04×10^{-2}	3.40	3.5978×10^{5}
Krypton-Krypton	1.41×10^{-2}	3.60	6.1486×10^{6}
Xenon-Xenon	1.88×10^{-2}	4.03	3.2113×10^{7}

ε is the depth of the potential well

σ is the inter-atomic distance for zero potential energy.

FIGURE 4.2 Plot of $A^{\frac{1}{2}}$ on logarithmic scale versus the Van der Waals radius of the inert gas atoms. A is the constant in the repulsion energy term REL - AR^{-12}. Points shown on the graph represent $A^{\frac{1}{2}}$ values for repulsion between the inert gas atoms: He---He, Ne---Ne, etc.

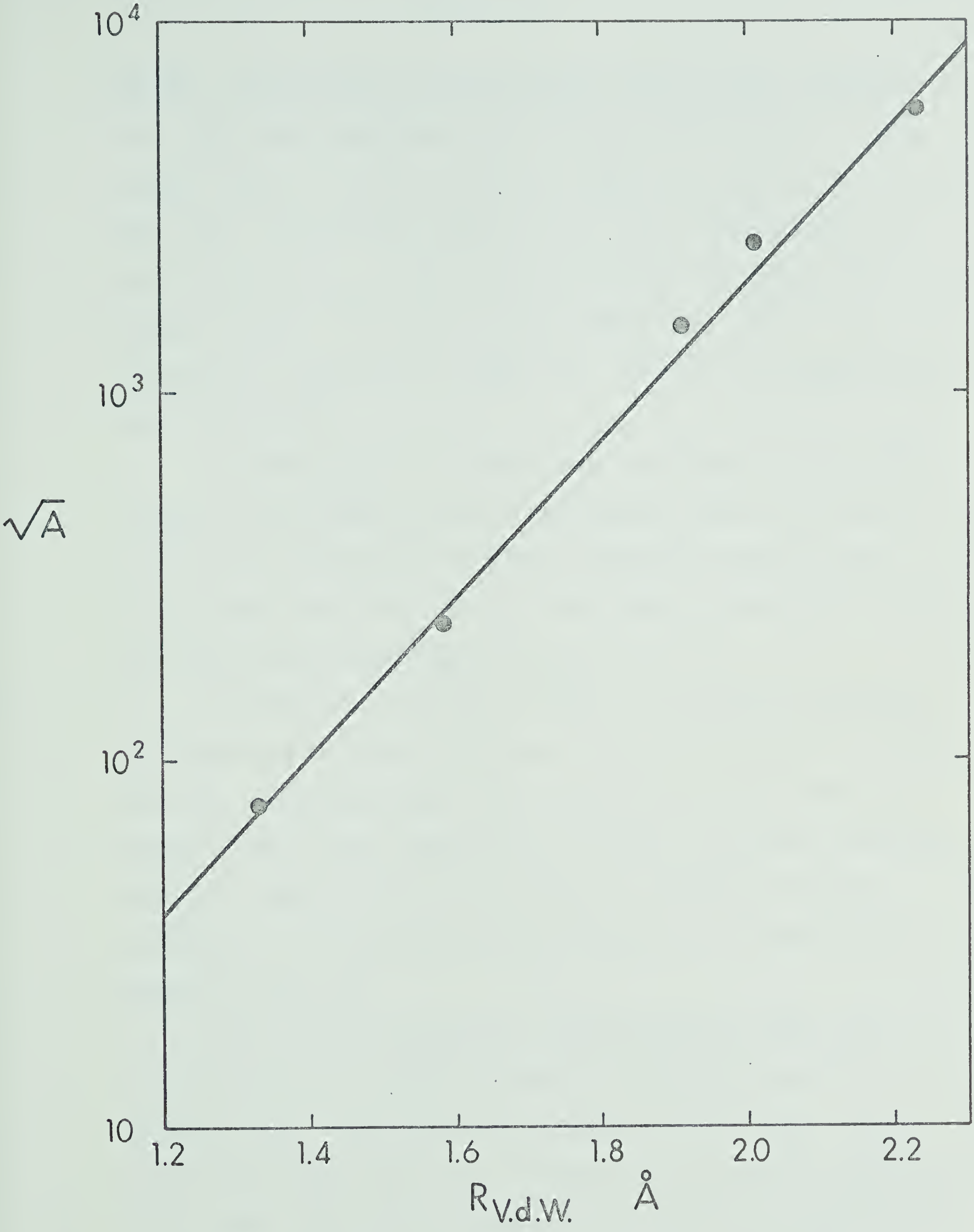

FIGURE 4.2

atoms. In one set of calculations the $A^{\frac{1}{2}}$ term representing the water molecules was taken as the $A^{\frac{1}{2}}$ term of the oxygen atom. The Van der Waals radius of oxygen, 1.4 Å, was used. The radius in the AR^{-12} term corresponded in this case to $R_{3,1}$, the distance between the alkali and oxygen nuclei. The resulting A values for the $M^{+}...O$ repulsions are given in Table 4.3. The $M^{+}...H$ repulsions were neglected.

A second set of A values was obtained with the $A^{\frac{1}{2}}$ values of the alkali ions as determined above and the $A^{\frac{1}{2}}$ value for water-water molecule repulsions given in the literature (p.214 ref (64)). The radius in the AR^{-12} term in this case corresponded to $R_{3,1}$ + 0.3 Å.

A third set of A values was evaluated for $Na^{+}(OH_2)_n$ in which the A value was taken to be the same as that for the Ne...Ne repulsions. The justification for this procedure lies in the observation that Na^{+} should be somewhat smaller than Ne while H_2O should be somewhat larger therefore an approximate cancellation of the two errors might be expected.

The potential energies, calculated by using the first set of A values are given in Table 4.3 for all alkali ions. The potential energies for $Na^{+}(H_2O)$ calculated from three sets of A values are plotted in Figure 4.3.

The above three choices of A values are consistent with the accepted set of Lennard-Jones parameters for

TABLE 4.3

Potential Energies of Clusters $M^+(H_2O)_n$ from Electrostatic Calculations Using Repulsion Term AR^{-12}.[a]

$-\Delta E_{o,n}$	Li^+	Na^+	K^+	Rb^+	Cs^+
0,1	53.3	42.9	31.2	28.1	23.1
$R_{3,1}$	1.56	1.74	2.04	2.16	2.38
0,2	95.9	79.1	58.8	53.6	44.4
$R_{3,1}$	1.60	1.76	2.06	2.18	2.38
0,3	119.6	102.7	79.8	73.7	62.0
$R_{3,1}$	1.66	1.80	2.08	2.20	2.42
0,4	129.7	116.5	94.9	89.1	76.3
$R_{3,1}$	1.72	1.86	2.12	2.24	2.44
0,5	123.8	117.4	101.6	97.5	85.4
$R_{3,1}$	1.84	1.94	2.18	2.28	2.48
0,6	118.4	116.0	105.9	103.6	92.6
$R_{3,1}$	1.96	2.04	2.24	2.34	2.52
$A \times 10^5$ kcal x $\mathring{A}^{12}$	0.0298	0.0861	0.4200	0.8400	2.100

(a) Repulsion term determined according to procedure described in this Chapter from noble gas A values, Van der Waals radii of noble gases and Stokes radii of M^+.

$\Delta E_{o,n}$ in kcal/mole

$R_{3,1}$ in Angstroms corresponds to distance from centre of ion to nucleus of oxygen atom of water molecule.

the inert gases. These parameters were determined from second virial coefficients which are due to weak intermolecular interactions. Assuming that these parameters are correct in the weak interaction range they will be applicable to stronger interactions (smaller intermolecular distances) only if the Lennard-Jones potential function is of the correct form. It would be desirable to obviate the use of the Lennard-Jones six, twelve potential by dropping both these terms (EDIS and EREP) from the potential energy expression and replacing them with experimentally determined potentials based on molecular beam scattering experiments. The scattering in relatively high kinetic energy beams is due to strong interactions occurring at close distances between the colliding partners. Unfortunately, experimental potential functions for the present pairs $Li^+ \ldots H_2O$, $Na^+ \ldots H_2O$ are not available. However, as shown previously the interaction for the pair Ne...Ne appears to be a good approximation for that between Na^+ and H_2O. Therefore, calculations were made for sodium using the potential term $7190/_r{}^{9.99}$ kcal/mole instead of EDIS and REL. This potential energy term was determined by Amdur from experimental studies of Ne...Ne atom collisions at high energies (67).

The numerical results calculated on the basis of the assumptions discussed above will be considered in the next section.

4.4. Discussion of Electrostatic Calculations

The potential energies E_n, where n represents the number of water molecules (n=1 to 6) bonded to the central ion, were calculated for all the alkali ions using an IBM 360/67 computer. The potential energy minima found are given in Table 4.3, where the notation $\Delta E_{o,n}$ is used in analogy with the notation for the experimental $\Delta H_{o,n}$ values. The electrostatic potential energies $\Delta E_{o,n}$ correspond best to the heats of hydration $\Delta H_{o,n}$ at 0°K, because of the neglect of all thermal motions in the calculations. The comparison at 298°K assumes the $\Delta C_p = 0$. This assumption does not involve considerable approximation, since ΔC_p for reaction 0,1 for example can be roughly estimated to be $-\frac{5}{2}R$. The value of ΔC_p is estimated

$$0,1 \qquad M^+ + H_2O \rightarrow M^+(H_2O)$$

by taking into account only the translational and rotational motions of molecules. It was also assumed that H_2O and $M^+(H_2O)$ have the same rotational contributions to the heat-capacity. Thus the value of $\Delta C_p = -\frac{5}{2}R$ would be mainly due to the loss of translational degrees of freedom by M^+. Vibrational contributions to the heat-capacities of H_2O and $M^+(H_2O)$ were not taken into account since they make a very small contribution. Vibrational motion can contribute any amount (between 0 and R) to the heat

capacity, the later value is approached only at high temperatures for most molecules (68). However, since the product $M^+(H_2O)$ in reaction 0.1 has more vibrational degrees of freedom than the reactant H_2O, the absolute value of ΔC_p will probably be even smaller than $-\frac{5}{2}R$ or -5 cal/degree mole. At 298°K $\Delta C_p \Delta T$ is approximately equal to ~ -1.5 kcal/mole^{-1}.

Thus if we assume $\Delta Cp \Delta T \approx -1.5$ kcal/mole^{-1}, then by use of equation 4.11 which expresses the temperature dependence of reaction heats,

$$\Delta H_{0,1} \approx \Delta E_{0,1} + \int_{0°K}^{298°K} \Delta C_p dt \qquad 4.11$$

we obtain the following relation:

$$\Delta H_{0,1} \approx \Delta E_{0,1} - 1.5 \text{ kcal}$$

The $\Delta H_{0,1}$ is negative value, therefore its absolute value should be larger by approximately 1.5 kcal/mole^{-1} than the $|\Delta E_{0,1}|$. The difference of 1.5 kcal between $\Delta H_{0,1}$ and $\Delta E_{0,1}$ is not significant. Therefore, it is felt that meaningful conclusions may be drawn by a comparison of the electrostatic calculations with experimental enthalpy values, without taking into consideration the above correction.

Given in Table 4.4 are the values of the individual energy terms: EDIP, EPOL etc., for the Na^+ ion in order to illustrate the relative magnitude of each contri-

TABLE 4.4

Individual Energy [a] Contributions to Potential Energy Calculations of Cluster $Na^+(OH_2)_n$

n	-EDIP	-EPOL	-EDIS	RDIP	REL
1	36.871	14.982	2.283	0	11.180
2	72.243	28.741	4.425	6.810	19.494
3	104.064	39.720	6.531	25.236	22.330
4	130.794	47.015	8.353	49.490	20.117
5	151.423	50.385	10.680	80.234	15.149
6	165.773	50.341	11.608	104.830	9.946

(a) All values in kcal/mole.

bution. Figures 4.3 and 4.4 give plots of $\Delta E_{o,n}$ and the experimentally measured $\Delta H_{o,n}$ for sodium and cesium. It can be seen from the Figures that for all these different choices of "A" value, the calculated values are considerably larger than the experimental values. In general, the calculated $\Delta E_{0,1}$ and $\Delta E_{0,2}$ are about 70% larger than the corresponding enthalpy values.

At present we cannot understand very well why all choices of A values lead to $\Delta E_{o,n}$ results which are too high. See Figure 4.3. Figure 4.3 also shows, that $\Delta E_{o,n}$ values, calculated from the Amdur empirical term $7190/_{r}{}^{9.99}$ kcal/mole, are approximately as high as the $\Delta E_{o,n}$, calculated from different choices of A values derived from the Lennard-Jones potential function. Thus the Amdur empirical term also represents a "soft" repulsion between the ion and molecule. The following consideration may be an explanation for the differences between calculated and experimental values. All choices of A depend on a certain assumed size parameter (radius) for the positive ion and the water molecule. However, since the electron cloud of the positive ion is compressed, because of the larger nuclear charge, the electronic repulsive forces in a strong collision between the positive ion and the neutral should be larger than those occurring in a collision of two neutrals of the same size. This stiffness of the electron cloud of the alkali ion is not taken into account in the present choices of A. An empirical way of correcting for

FIGURE 4.3

Comparison between experimental enthalpies $\Delta H_{o,n}$ and potential energies $\Delta E_{o,n}$ obtained on the basis of electrostatic type calculations for sodium hydrates $Na^+(H_2O)_n$. O experimental $\Delta H_{o,n}$, ● $\Delta E_{o,n}$ calculated by adjusting value of constant A in repulsion term AR^{-12} so as to make $\Delta H_{0,1} = \Delta E_{0,1}$ ▨ $\Delta E_{o,n}$ with A value for Na^+---O repulsion obtained from Stokes radius for Na^+ and Van der Waals radius of oxygen, □ calculated with A value for Na^+—H_2O repulsion set equal to A value for Ne-Ne repulsion (65) ▲ calculated with A value for Na^+—H_2O repulsion based on Stokes radius of Na^+ and A value for H_2O—H_2O repulsion (64), ◐ calculated with the potential term $7190/r^{9.99}$ kcal/mole instead of EDIS and REL (67) ◬ $E_{o,n}$ calculated by Garrick (71).

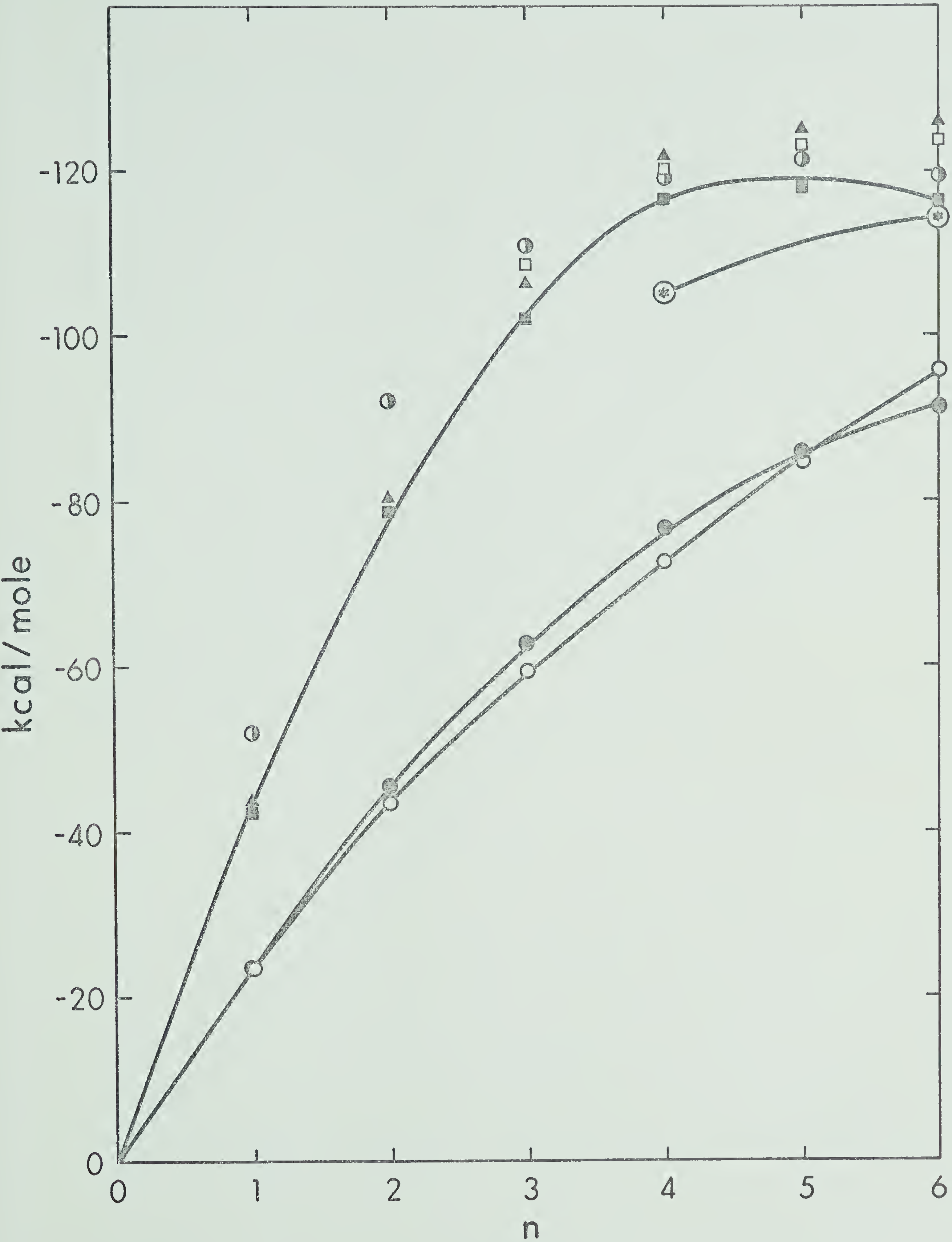

FIGURE 4.3

FIGURE 4.4

Comparison between experimental enthalpies $\Delta H_{o,n}$ and potential energies $\Delta E_{o,n}$ obtained on the basis of electrostatic type calculations for cesium hydrates $Cs^+(H_2O)_n$. O experimental $\Delta H_{o,n}$, ● $\Delta E_{o,n}$ calculated by adjusting the value of constant A in repulsion term AR^{-12} so as to make $\Delta H_{0,1} = \Delta E_{0,1}$, ◐ $\Delta E_{o,n}$ with A value for Cs^+---O repulsion obtained from Stokes radius for Cs^+ and Van der Waals radius of oxygen, □ calculated with A value for Cs^+-H_2O repulsion based on Stokes radius of Cs^+ and A value for H_2O-H_2O repulsion, ▲ calculated with A value for Cs^+-H_2O repulsion set equal to A value for Xe-Ne repulsion, ○ $E_{o,n}$ calculated by Garrick (71).

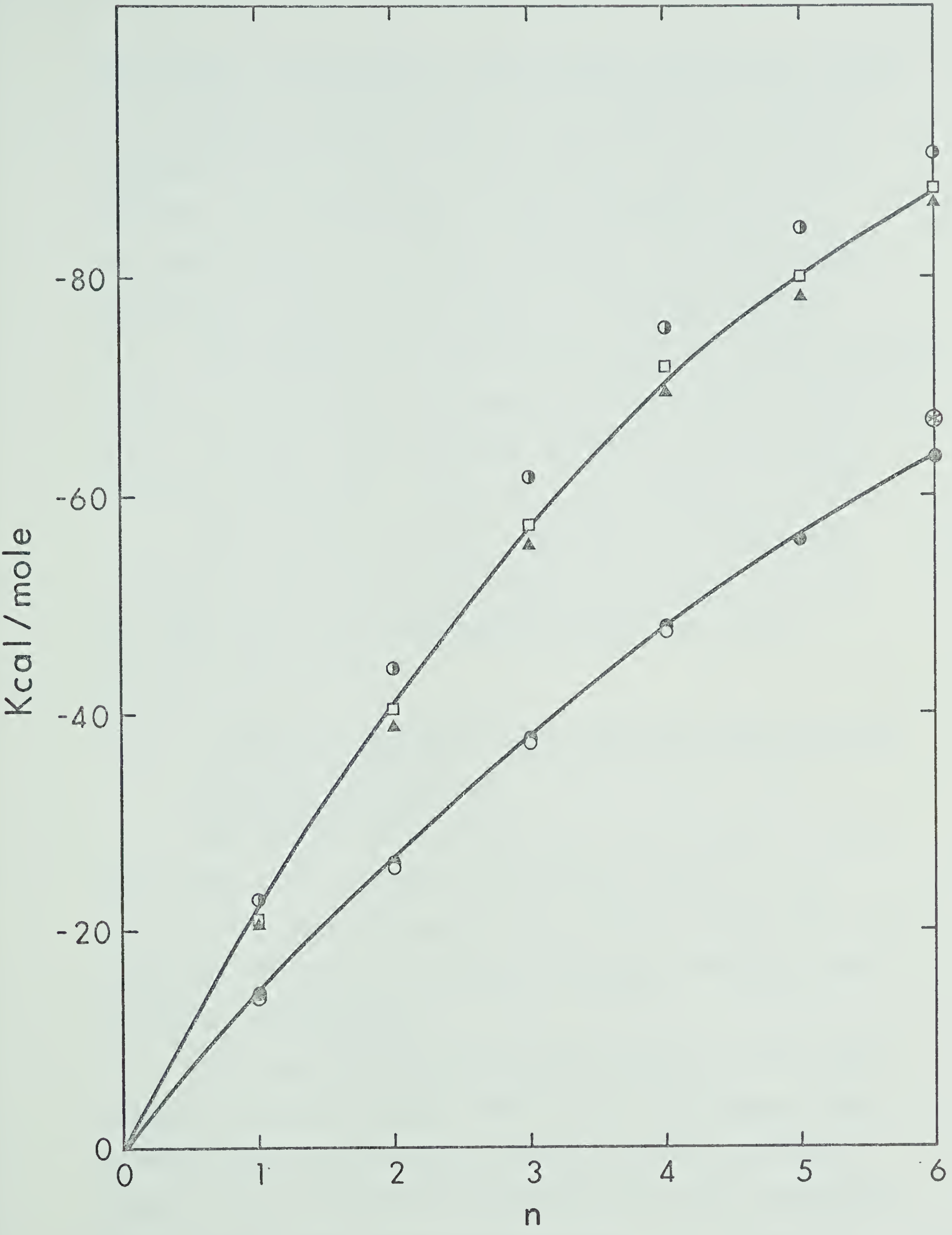

FIGURE 4.4

the greater "stiffness" of the positive ion electron cloud is to choose a bigger radius. For example the radii of Pauling (69) or Gourary and Adrian (70) might have been selected. The difficulty in such a procedure lies in the correlation of the ionic radii with the radii of the inert gases, which are the bases of the plot in Figure 4.2. This becomes more obvious when the Na^+ radius obtained by Gourary and Adrian is compared with the atomic radius of neon and it is found that the radius of Na^+ is bigger than that of Ne ($Na^+ = 1.17$, $r_{F^-} = 1.16$ and $Ne = 1.12$ Å).

This is not of course acceptable, and shows that the Gourary and Adrian ionic radii are probably too low for negative ions and too high for positive ions by approximately 10% (30).

4.5 Comparison of Electrostatic Potential Energies with Previous Calculations.

The present calculations are very similar to those of Garrick (71) who used a point dipole model to calculate the potential energies of a number of hydrated ions including $Na^+(H_2O)_4$, $Na^+(H_2O)_6$, $K^+(H_2O)_6$, $Rb^+(H_2O)_6$ and $Cs^+(H_2O)_6$ respectively.

For the ion-molecule repulsion ($REL = AR^{-12}$), the equation used by Garrick, ($REL = \lambda R^{-\nu}$) was adapted from Lennard-Jones calculations of inert gas ion-atom repulsions. The λ in Garrick's expression for REL corresponds to A value in the present calculations. The values of

force constant λ and force index ν for different ions were deduced by means of certain more or less plausible assumptions (71).

Garrick's *a priori* calculations for $M^+(H_2O)_6$ gave the equilibrium distance between the point ion and point molecule as 2.22 (2.04), 2.58 (2.24), 2.71 (2.34), 2.92 (2.52) Å, for M^+ = Na, K, Rb, Cs, respectively. In comparison, the values for the ion-oxygen atom ($R_{3,1}$) equilibrium distance, from this work are given in the brackets. The values for EDIP + EPOL + RDIP are 135 (115), 102 (108), 93 (101), 81 (92) kcal/mole and REL are 18 (10), 18 (16), 15 (18), 14 (19) kcal/mole for hexahydrate of Na, K, Rb and Cs respectively. The total potential energies in Garrick's calculations are 114 (116), 83 (105), 78 (103), 67 (92) kcal/mole, compared to present calculations in the brackets. The higher total potential energies obtained here are mainly due to dispersion forces which were not included in Garrick's calculations.

Besides Garrick, Laidler (72) has performed point dipole calculations for a number of hydrated alkali ions. Unfortunately most of the $M^+(H_2O)_n$ results were presented as the total of a cycle dealing with the heat of hydration of the ion. The electrostatic energy of formation for $Li^+(H_2O)_4$ and $Rb^+(H_2O)_4$ obtained by Laidler were 120 and 67 kcal/mole, compared to 129 and 89 kcal/mole in present calculations.

Both Laidler and this author used the same dependence of the ion-molecule repulsion (REL = AR^{-12}), but Laidler adopted a semi-empirical method to evaluate the constant A in a repulsion term. The value of A was adjusted so as to give a distance between the ion and the water molecule equal to the sum of the Goldsmith ionic radius and the radius for the water molecule. Laidler's value for $Rb^+(H_2O)_4$ is closer to our experimental value $\Delta H_{0,4}$ = 53.0 kcal/mole, than to our calculated one. The values of the constant A and the equilibrium distances between the ion and the water molecules for $Rb^+(H_2O)_4$ or $Li^+(H_2O)_4$ are not reported in Laidler's work, so that a more detailed quantitative comparison of the two calculations cannot be made.

4.6 The Comparison of Calculated $\Delta E^\circ_{n-1,n}$ with Experimental $\Delta H^\circ_{n-1,n}$ for $M^+(H_2O)_{n-1} + H_2O \rightarrow M^+(H_2O)_n$

One of the purposes of doing electrostatic calculations was to make a qualitative comparison between predicted and experimentally obtained enthalpy changes for $M^+(H_2O)_n$ complexes. Since the calculated $\Delta E_{o,n}$ obtained were found to be quite different from the experimental results we decided to utilize the calculations only for a comparison of the relative changes of $\Delta E^\circ_{n-1,n}$ predicted by calculation and experimentally determined $\Delta H^\circ_{n-1,n}$. To calculate such relative changes it appeared most meaningful

to determine an empirical value for the constant A in the term AR^{-12} by setting $E_{0,1} = H_{0,1}$. The evaluation of value A by this method is given in the following paragraph.

To calculate the M^+——H_2O repulsion energy from the term AR^{-12} it is necessary to assign values to A_O, a constant for the ion-oxygen atom repulsion and A_H, a constant for the ion-hydrogen atom repulsion. Minimization of the total potential energy equations for $M^+(H_2O)$ with respect to $R_{i,j}$ leads to equation 4.12 from which A_O can be calculated as a function or $R_{i,j}$ assuming each value of $R_{i,j}$

$$4.12 \qquad \frac{\partial E_{0,1}}{\partial R_{i,j}} = 0$$

corresponds to the equilibrium ion-ligand distance. The terms containing A_H may be expected to be negligible compared with the A_O terms. The A_O is expected to be larger than A_H since the repulsion depends on the number of electrons associated with the atom (75). Also, the ion-hydrogen distances are much greater than the ion-oxygen distance. Neglecting the A_H, one obtains a relation of the type:

$$4.13 \qquad A_O = f(R_{3,1})$$

which gives A_O as a function of ion-oxygen distance, $R_{3,1}$. The potential energy of the cluster $M^+(H_2O)$, which depends on the parameters $R_{3,1}$ and A_O is given by equation 4.14

$$4.14 \qquad \Delta E_{0,1} = F(A_0, R_{3,1}).$$

In order to obtain a value for A_0 and $R_{3,1}$ at equilibrium we equate $\Delta E_{o,1}$ with the experimental $\Delta H_{0,1}$ which leads to 4.15

$$4.15 \qquad \Delta H_{0,1} = F(A_0, R_{3,1})$$

Expressions 4.13 and 4.15 represent a system of two equations with two unknowns (A_0, $R_{3,1}$ eq.) which can be solved. The values of $R_{3,1}$ with the corresponding numbers for A_0 (obtained by 4.13) are substituted into equation 4.14. This procedure leads to the $\Delta E_{0,1}$ as a function of $R_{3,1}$. The value of $R_{3,1}$ corresponding to the $\Delta E_{0,1} = \Delta H_{0,1}$ is $R_{3,1}$ equilibrium distance between the centre of the ion M^+ and the centre of oxygen atom in the water molecule. The associated value for A_0 which corresponds to $R_{3,1}$ equilibrium distance was then used to calculate REL and $\Delta E_{o,n}$ for higher clusters.

The $\Delta E_{o,n}$ values obtained by this procedure were then used to evaluate $\Delta E_{n-1,n} = \Delta E_{o,n} - \Delta E_{o,n-1}$ for all ions, for the range of n=1 to 6. See Table 4.5. In Figure 4.5, $\Delta E_{0,1}$ is shown as a function of $R_{3,1}$ for $M^+ + H_2O \rightarrow M^+(H_2O)$. The energy minimum for each individual ion corresponds to the total calculated binding energy of the clusters relative to M^+ and H_2O molecules at infinite distance.

TABLE 4.5

Potential Energies of Clusters $M^+(H_2O)_n$ from Electrostatic Calculations Using Repulsion Term AR^{-12} [a]

$-\Delta E_{o,n}$	Li^+	Na^+	K^+	Rb^+	Cs^+
0,1	34.0	24.0	17.9	15.9	13.7
$R_{3,1}$	1.92	2.26	2.60	2.76	2.98
0,2	63.5	45.5	34.4	30.9	26.5
$R_{3,1}$	1.92	2.26	2.60	2.76	2.98
0,3	85.8	63.0	48.7	43.9	37.9
$R_{3,1}$	1.96	2.30	2.62	2.76	2.98
0,4	100.0	76.7	60.6	55.0	47.9
$R_{3,1}$	2.02	2.34	2.66	2.76	2.98
0,5	105.3	85.1	69.2	63.2	55.9
$R_{3,1}$	2.10	2.38	2.68	2.78	3.00
0,6	107.2	90.8	76.0	70.5	63.5
$R_{3,1}$	2.16	2.44	2.74	2.84	3.06
A x 10^5 kcal x $\mathring{A}^{12}$	0.19	0.95	3.9	7.37	15.87

(a) A values for term $AR_{3,1}^{-12}$ in electrostatic calculations obtained by setting $\Delta H_{0,1} = \Delta E_{0,1}$

$R_{3,1}$ in Å corresponds to distance from centre of ion to nucleus of oxygen atom of water molecule.

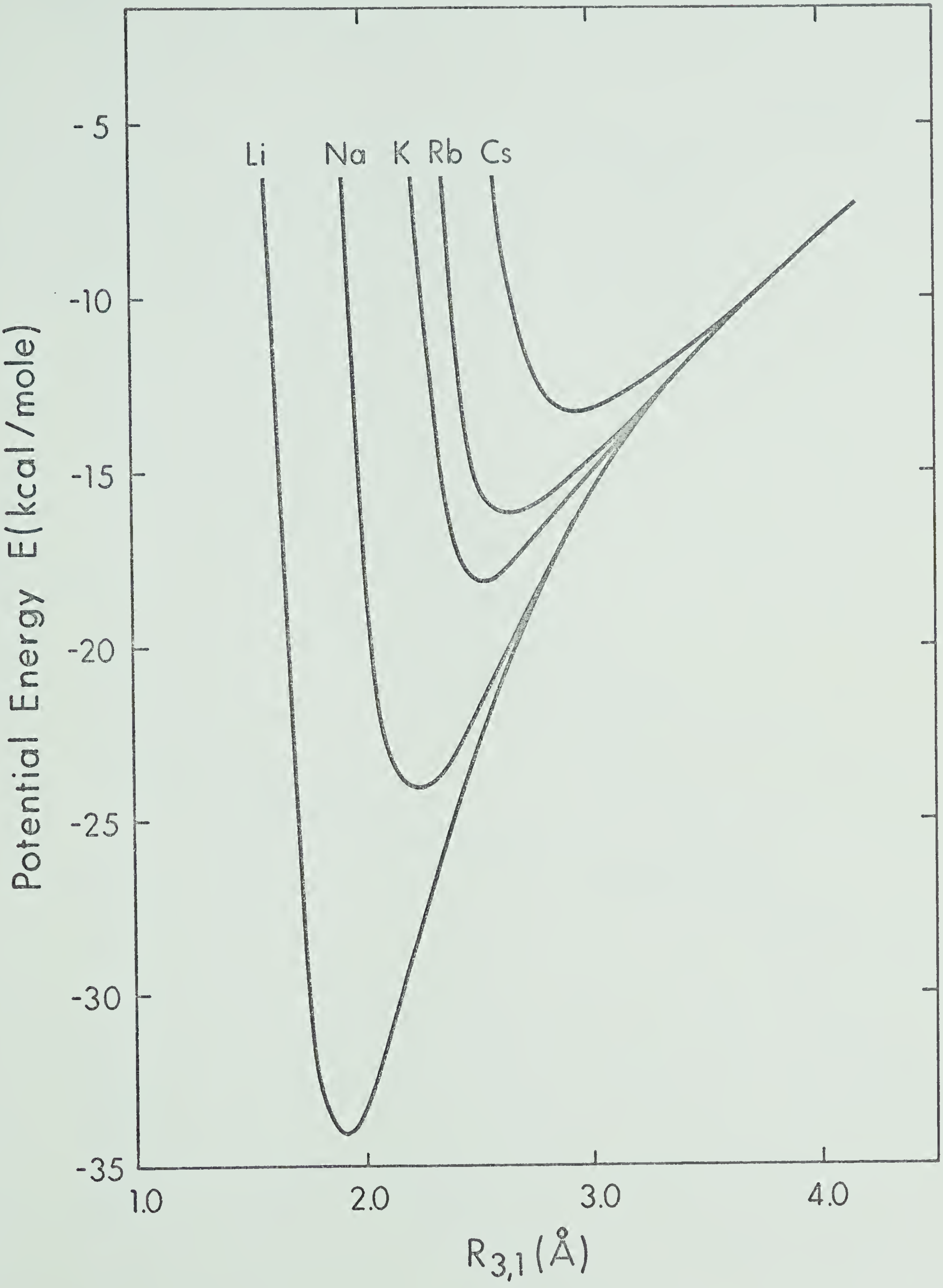

FIGURE 4.5 Plot of the potential energies evolved for the reaction $M^+ + H_2O \rightarrow M^+(H_2O)$

FIGURE 4.6

Comparison of experimental $\Delta H^{\circ}_{n-1,n}$ and calculated potential energy differences $\Delta E^{\circ}_{n-1,n}$, for alkali ion clusters $M^+(H_2O)_n$. ○ ΔH of Li$^+$, ● ΔE of Li$^+$, □ ΔH of Na$^+$, ▨ ΔE of Na$^+$, △ ΔH of Cs$^+$, ▲ ΔE of Cs$^+$.

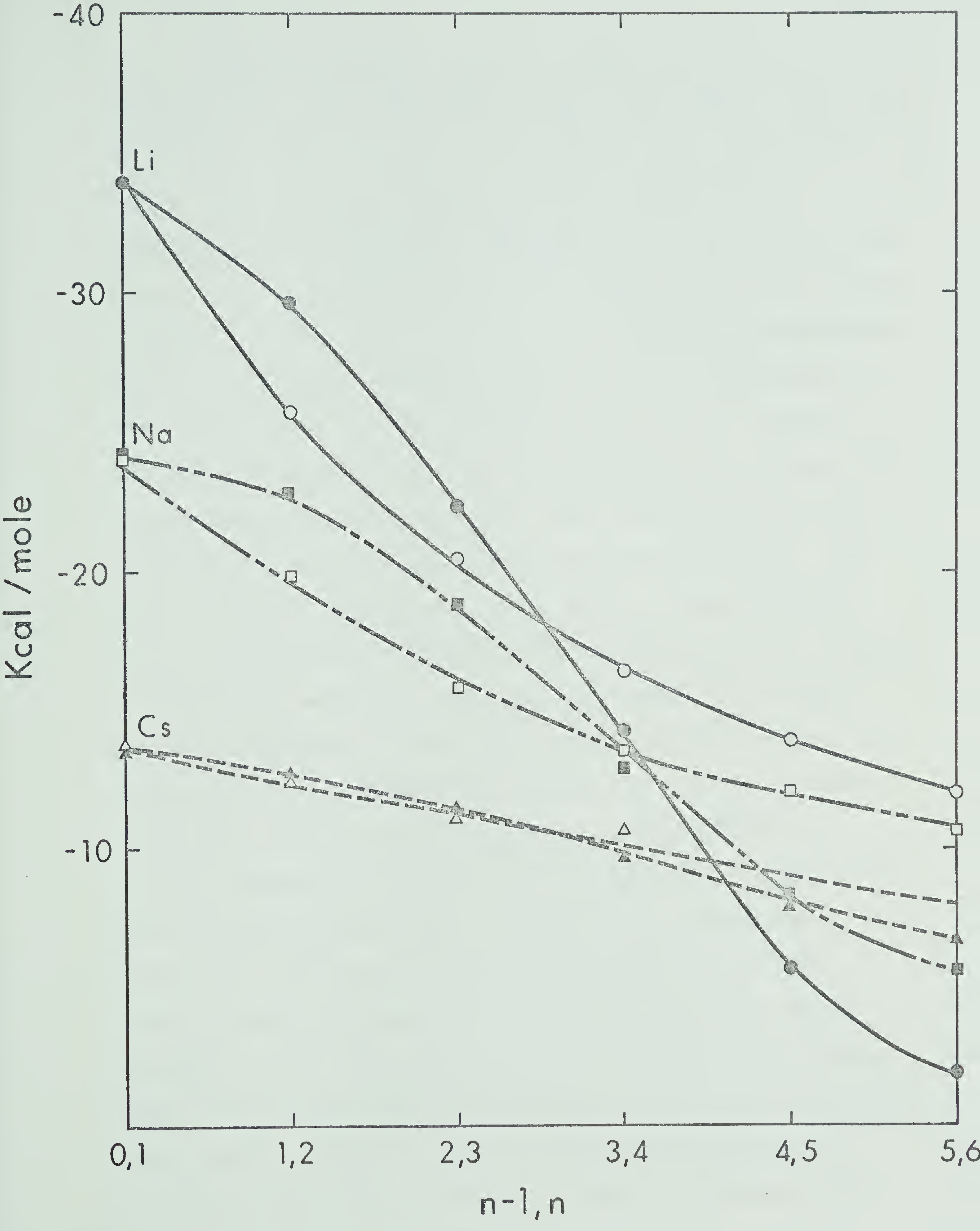

FIGURE 4.6

Figure 4.6 shows a plot of $\Delta H^{\circ}_{n-1,n}$ and $\Delta E^{\circ}_{n-1,n}$ as a function of n, for the small ion Li^+, the medium sized ion Na^+ and the large ion Cs^+. According to the theoretical model, the decrease of $\Delta E^{\circ}_{n-1,n}$ with n is due to an increase in dipole-dipole repulsions. As can be seen from Figure 4.6 the electrostatic calculations result in values of $\Delta E^{\circ}_{n-1,n}$ which qualitatively agree with the experimental $\Delta H^{\circ}_{n-1,n}$. Thus the changes in $\Delta H^{\circ}_{n-1,n}$ should be mostly due to increases in dipole-dipole repulsions. However, for small n (n=2 and 3) it is found that $\Delta E^{\circ}_{n-1,n}$ falls off less rapidly than the $\Delta H^{\circ}_{n-1,n}$. This effect is most pronounced for Li^+ and is almost unnoticeable for Cs^+. The more rapid initial drop of the $\Delta H^{\circ}_{n-1,n}$ terms could be due to the presence of chemical (non-electrostatic) bonding in the M^+OH_2 complex. This bonding should occur only for the attachment of the first water molecule and be completely or almost completely absent for the other water molecules. Such a state of affairs would exist if a certain amount of dative bonding between the oxygen lone pair and the lowest empty orbital of the alkali ion occurred. The oxygen lone pair electrons would then partly screen the positive charge from the other water molecule (73). The effect should be largest in lithium which has the most covalent character and should be weakest with cesium. This is what is observed in Figure 4.6. At higher n the $\Delta E^{\circ}_{n-1,n}$ curve is found to decrease more

rapidly and cross the $\Delta H^{\circ}_{n-1,n}$, n curve. For Li^+ and Na^+, $\Delta E_{4,5}$ and $\Delta E_{5,6}$ are very much smaller than the corresponding ΔH (Figure 4.6). As mentioned before the calculations are made under the assumption that all water molecules are equidistant from the ion. For Li^+ and Na^+ which are small ions this assumption is probably inadequate at n=5 and n=6. Thus the cross-over at n=4 should indicate that at this point a change to a new structure occurs in which all water molecules are not equivalent. The $\Delta E_{4,5}$ and $\Delta E_{5,6}$ for Cs are somewhat smaller than the corresponding ΔH values. However, the differences between the calculated and experimental values are very small so that one may conclude that the data do not indicate a change of structure at n=4 or 5 but a persistence of the equivalence of all water molecules to about n=6. This is, of course, consistent with the larger radius of Cs^+

Yu. A. Kruglyak (74) investigated the theory of the solvation of ions having external completed sp-shells. He suggests that the nature of bonds in ion-solvates interactions can be understood only on a quantum mechanical basis; purely electrostatic interpretations are not sufficient and many facts can only be explained by means of donor-acceptor bond representations. This supports our evidence of the presence of chemical (non-electrostatic) bonding in the M^+OH_2 complex, explained previously.

4.7 Calculation of the Entropy of $M^+(H_2O)$

The experimental entropy change for a reaction such as $M^+ + H_2O \rightarrow M^+(H_2O)$ can be compared to the theoretical value obtained by means of statistical mechanics. The change of the entropy for such a reaction can be represented as the sum of translational, rotational and vibrational entropy charges.

$$4.14 \qquad \Delta S = \Delta S_t + \Delta S_r + \Delta S_v$$

Each term of the right hand side of equation 4.14 is then evaluated separately.

The translational entropy change for the condensation reactions considered here is given by the Sackur-Tetrode equation 4.15 (75)

$$4.15 \qquad \Delta S_t = \frac{3}{2} R \text{ Ln } \frac{N_{M^+(H_2O)}}{N_{M+} \times N_{H_2O}} - \frac{5}{2} R \ln T + 2.311$$

where $N_{M^+(H_2O)}$, N_{M^+} and N_{H_2O} are molecular weights (g/mole) of $M^+{}_{(H_2O)}$, M^+ and H_2O respectively. T is the absolute temperature in degrees K; the gas constant R must be substituted in cal/mole-degree to obtain ΔS_t in cal/mole-deg.

The rotational entropy change can be calculated from the rotational entropy of H_2O and $M^+(H_2O)$. The appropriate equation (75) is 4.16

$$4.16 \qquad S^{\circ}_{rot} = R(\ln Q_{rot} + 1)$$

where Q_{rot}, the rotational partition function (75) is given by 4.17

$$4.17 \qquad Q_{rot} = \frac{(8)^{5/2}(KT)^{3/2}\,(I_x I_y I_z)^{1/2}}{\sigma h^3}$$

where I_x, I_y, I_z are the three moments of inertia about the three principal axes and "σ" is the symmetry number. When equation 4.16 is applied to calculate the change of entropy for the reaction of $M^+ + H_2O \rightarrow M^+(H_2O)$, the following equation will be obtained

$$4.18 \qquad S^{\circ}_{rot} = R \ln \frac{[Q_{rot}]M^+(H_2O)}{[Q_{rot}]H_2O}$$

When the proper values of the partition functions are substituted in equation 4.18 and appropriate simplification has been made, the S°_{rot} becomes

$$4.19 \qquad S^{\circ}_{rot} = \frac{R}{2} \ln \frac{[I_x I_y I_z]M^+(H_2O)}{[I_x I_y I_z]H_2O}$$

The moments of inertia of H_2O are (76) $I_x = 1.92$, $I_y = 1.02$ and $I_z = 2.95 \times 10^{-40}$ g cm^2. The moments of inertia for the cluster $M^+(H_2O)$ are based on the $M^+ \ldots OH_2$ equilibrium distances. As shown in section 4.7 reasonable distances between the centers of the M^+ ion and the oxygen atoms were obtained from electrostatic calculations. The M^+---OH_2 equilibrium distances as well as moments of inertia are given in Table 4.6. Substitution of the moment of inertia into 4.19 leads to rotational entropy change, given in Table 4.9.

TABLE 4.6

Moments of Inertia and M^+-OH_2 Equilibrium Distances

Cluster	M^+-OH_2 Distance Å	$I \times 10^{40}$ g - cm^2		
		I_x	I_y	I_z
$Li^+(H_2O)$	1.92	1.95	33.2	35.0
$Na^+(H_2O$	2.26	1.95	87.3	89.0
$K^+(H_2O)$	2.60	1.95	147.0	149.0
$Rb^+(H_2O)$	2.76	1.95	182.4	184.0
$Cs^+(H_2O)$	2.98	1.95	233.0	235.0

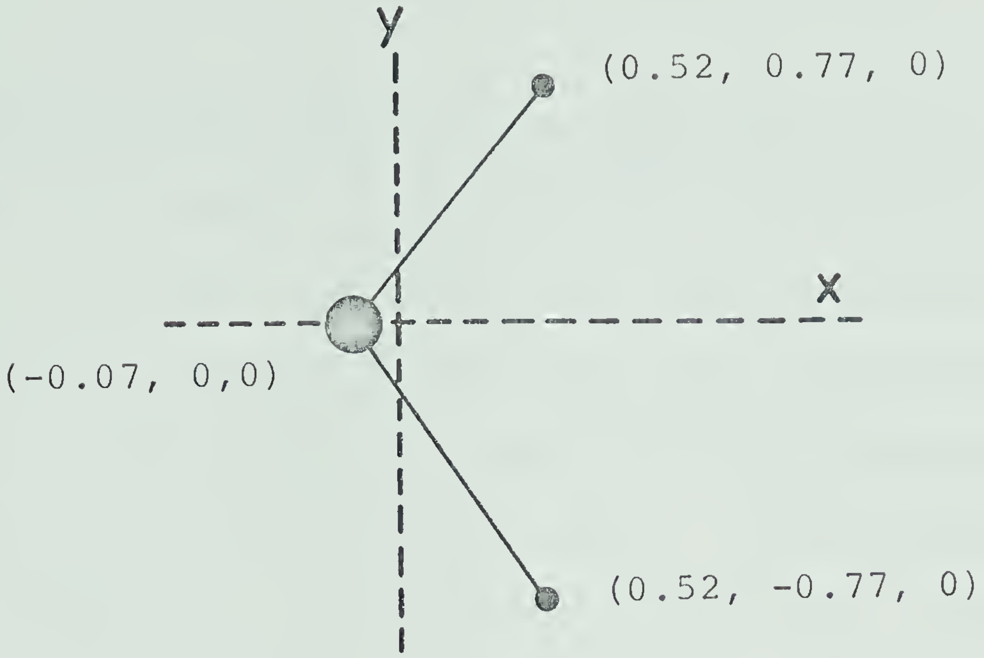
y
(0.52, 0.77, 0)
x
(-0.07, 0,0)
(0.52, -0.77, 0)

Principal axes of H_2O

The z axis is mutually perpendicular to the x and y axes and passes through the point (0.04, 0, 0)

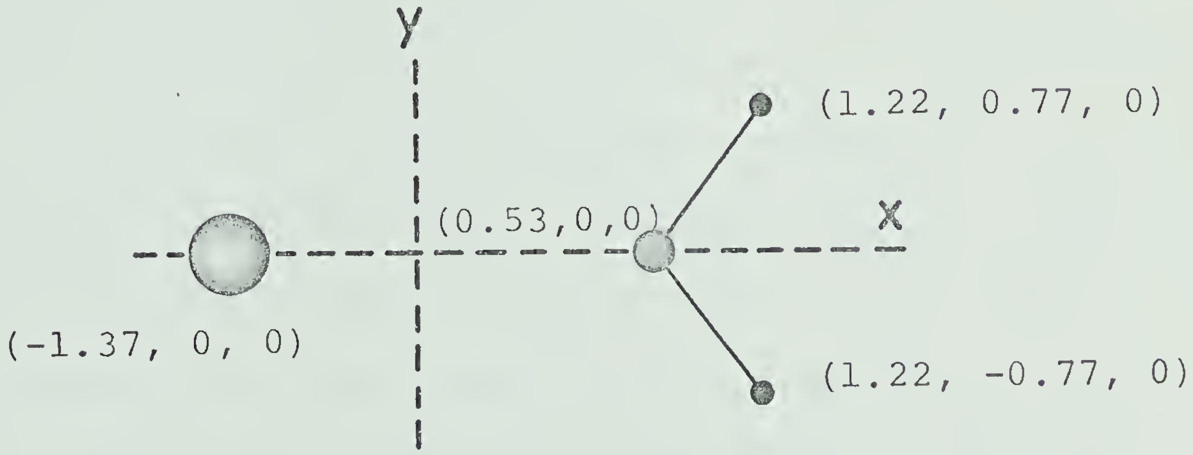
y
(1.22, 0.77, 0)
(0.53,0,0)
x
(-1.37, 0, 0)
(1.22, -0.77, 0)

Principal axes of $Li^+(H_2O)$

The z axis is mutually perpendicular to the x and y axes and passes through the point (0.02, 0,0)

FIGURE 4.7 Principal axes of H_2O and $Li^+(H_2O)$ used to calculate the moments of inertia.

The three principal axes for the H_2O and $Li^+(H_2O)$ used to calculate the moments of inertia are shown in Figure 4.7.

To calculate the vibrational contribution to the entropy change, it was assumed that the fundamental vibrations of water molecule remain the same before and after the formation of the cluster $M^+(H_2O)$. The coordinated H_2O is treated as a rigid molecule which has a stretching vibration along the M^+——oxygen axis and two rocking vibrations about its y and z axes.

In the calculation of the stretching vibrational frequency, the water molecule and the M^+ ion were treated as two mass points. The force constant for this vibration was estimated by fitting an equation of a parabola to the bottom portion of the potential energy curves of Figure 4.5 obtained in section 4.7. The frequency ν then can be calculated from the equation 4.20 $\nu = \frac{1}{2\pi}(\frac{k}{\mu})^{\frac{1}{2}}$ where μ is the reduced mass of water —M^+ ion system and k is the force constant. From $\varepsilon_o = h\nu$ and equation 4.21 (75) S°_{vib} were calculated. In Table 4.7 the force constants k, the vibrational frequencies ν and entropy contribution $S^\circ_{stretching}$ are tabulated.

$$4.21 \quad S^\circ_{vib} = \left(\frac{R}{\exp(\varepsilon_o/kT)^{-1}}\right)\left(\frac{\varepsilon_o}{kT}\right) - R\ln[1-\exp(-\varepsilon_o/RT)]$$

TABLE 4.7

Force Constants, Vibrational Frequencies and Entropy Contributions Due to Stretching Vibrations of M^+-OH_2

Cluster	Force Constant $k \times 10^{-4}$ dyne/cm	Frequency $\nu \times 10^{12}$ sec^{-1}	Entropy $\Delta S°$ (298°K) e.u.
$Li^+(H_2O)$	11.70	18.0	0.50
$Na^+(H_2O)$	8.10	11.05	0.60
$K^+(H_2O)$	5.80	8.47	1.60
$Rb^+(H_2O)$	4.35	6.68	2.00
$Cs^+(H_2O)$	3.50	5.80	2.27

The two rocking vibrational frequencies can be approximately evaluated from equation 4.22 (76) where n is the symmetry number, ΔP.E. is the potential energy barrier for rotation, and I is the moment of inertia.

$$4.22 \qquad \nu = \frac{n}{2}\left(\frac{\Delta P.E.}{2I}\right)^{\frac{1}{2}}$$

ΔP.E. can be calculated from the coordinates of the molecule in its minimum energy position and its maximum energy position (rotation by 180° about the y and z axes from the minimum position) by use of equations 4.2, 4.3, 4.5 and 4.9. From $\varepsilon_{o(y,z)} = h\nu_{(y,z)}$ and equation 4.21, S°_{y} and S°_{z} were calculated. In Table 4.8 $\Delta P.E_{y}$ and $\Delta P.E_{z}$, the vibrational frequencies ν_{y} and ν_{z} and entropy contribution S°_{y} and S°_{z} are tabulated.

The total entropy change can now be calculated by summing the individual entropy contributions. As can be seen from Table 4.9 relatively good agreement is obtained between the calculated and observed entropy changes. Entropy values calculated at 298°K and entropy values calculated at the temperatures corresponding to the middle of the Van't Hoff plot temperature range from which the experimental ΔS values were obtained are shown in Table 4.9. The entropy changes for the formation of the larger clusters [$M^{+}(H_2O)_n$ for n greater than one] can also be calculated but the above procedure would involve an increasing number of assumptions. Therefore, such calculations were

TABLE 4.8

Potential Energy Barriers for Rotation (ΔP.E.), Vibrational Frequencies and Entropy Contributions Due to Two Rocking Vibrations of M^+-OH_2

Cluster	$\Delta P.E_y$ kcal/mole	$\Delta P.E_z$ kcal/mole	$\nu_y \times 10^{13}$ sec^{-1}	$\nu_z \times 10^{13}$ sec^{-1}	$\Delta S°_y$(298°K) e.u.	$\Delta S°_z$(298°K) e.u.
$Li^+(H_2O)$	26.0	30.7	1.49	1.35	0.72	0.82
$Na^+(H_2O)$	29.0	33.0	1.59	1.41	0.68	0.80
$K^+(H_2O)$	29.4	33.0	1.59	1.33	0.50	0.70
$Rb^+(H_2O)$	28.0	34.0	2.20	1.43	0.30	0.76
$Cs^+(H_2O)$	29.5	27.7	2.20	1.33	0.27	0.85

TABLE 4.9

Translational, Rotational and Vibrational Contributions to Experimentally Determined $\Delta S°_{298°K}$ for Reaction $M^+ + H_2O \rightarrow M^+(H_2O)$

Cluster	Components of $\Delta S°$ theoretical at 298°K			$-\Delta S°_{298°K}$ Theoretical	Components of $\Delta S°$ theoretical at t°K			$-\Delta S°_{t°K}$[a] Theoretical
	$\Delta S°_t$	$\Delta S°_r$	$\Delta S°_v$		$\Delta S°_t$	$\Delta S°_r$	$\Delta S°_v$	
$Li^+(H_2O)$	-30.93	5.96	2.04	23.0	-35.90	5.96	7.00	23.0 (835°K)
$Na^+(H_2O)$	-33.00	7.86	2.50	22.7	-37.14	7.86	6.37	22.9 (667°K)
$K^+(H_2O)$	-33.30	8.90	2.80	21.6	-36.8	8.90	5.90	22.0 (570°K)
$Rb^+(H_2O)$	-34.40	9.32	3.06	22.0	-36.24	9.32	5.00	22.0 (455°K)
$Cs^+(H_2O)$	-34.40	9.80	3.40	21.2	-36.37	9.80	5.21	21.3 (445°K)

Entropy values $\Delta S°$ in e.u.

(a) Entropy values calculated at the temperatures shown in brackets corresponding to the middle of Van't Hoff plot temperature range from which experimental ΔS values were obtained.

not performed.

It is interesting to note that the experimental $-\Delta S^{\circ}_{n-1,n}$ increases with increase of n. The same result is obtained for the halide ions by M. R. Arshadi, Ph.D. thesis. The increase of the ΔS values occurs even though the bonding forces (represented for instance by $\Delta H_{n-1,n}$) decrease. It is reasonable to assume that the increase of the ΔS terms reflect the gradual loss of freedom due to crowding of the molecules around the central ion. The study of the $H^+(H_2O)_n$ clusters (24) showed that the $\Delta S^{\circ}_{n-1,n}$ values decrease somewhat with increase of n. This difference of behaviour between the clusters around the centrally located (large) ions and water clusters containing an extra proton, may be considered as evidence for the mobility or non-localization of the charge in the hydrates $H^+(H_2O)_n$.

5. APPLICATION OF EXPERIMENTAL RESULTS TO PROCESSES IN AQUEOUS SOLUTIONS

5.1 Comparison Between the Hydration Energies of the Alkali and Halide Ions.

5.1a In Solution.

The heats of hydration ΔH_h for the reaction 5.1 are obtained from the heats of solution at infinite dilution,

$$5.1 \qquad M^+_{(g)} + X^-_{(g)} \rightarrow M^+_{(aq)} + X^-_{(aq)}$$

the entropies of hydration ΔS°_h from S° and the Sackur-Tetrode equation and the free energies ΔG°_h from ΔH°_h and ΔS°_h. An excellent review on the methods of assigning heats, free energies and entropies to single-ion ($M^+_{(aq)}$ or $X^-_{(aq)}$) is given by Rosseinsky (31). The review indicates that most methods are based on either dividing by 2 the thermodynamic functions of selected anion-cation pair or using some extrapolation procedure involving the ionic radii. Since water is not a dimensionless and structurless liquid, the hydration of equal size cations and anions is not necessarily the same (6). Latimer, Pitzer and Slansky (32) have attempted to account for the specificity in ionic hydration by adding different increments to the crystal radii of anions and cations. Verwey (33) has considered the different orientations of water molecules

around ions and Buckingham (34) has approached the problem by taking into account the quadrupole moment of the water molecule. The agreement between these different methods is often surprisingly good, especially in the case of ΔH°_{h}. Still, none of these absolute values seem entirely reliable since they are all based on the assumption that the true ionic radii are known. The only set of absolute hydration energies of single ions $M^{+}_{(aq)}$ and $X^{-}_{(aq)}$ without any assumption about the dimensions of the ions is the one by Randles (35) based on the measurement of the Volta potential between an electrolyte solution and another surface separated from the solution by vacuum or an inert gas.

The two sets of hydration energies which have found wide acceptance are those of Latimer, Pitzer and Slansky and Randles. These two sets were used in the previous discussion 3.2 for a correlation of the relative heats of hydration of alkali ions. The same sets of data will be used in the latter part of this discussion for the correlation of the present results with the total single ion hydration energies.

5.1b In the Gas Phase

The gas phase hydration enthalpies $\Delta H^{\circ}_{n-1,n}$ for the alkali (M^{+}) and the halide (X^{-}) ions are shown together in Figure 5.1. The data for halide ions are taken from

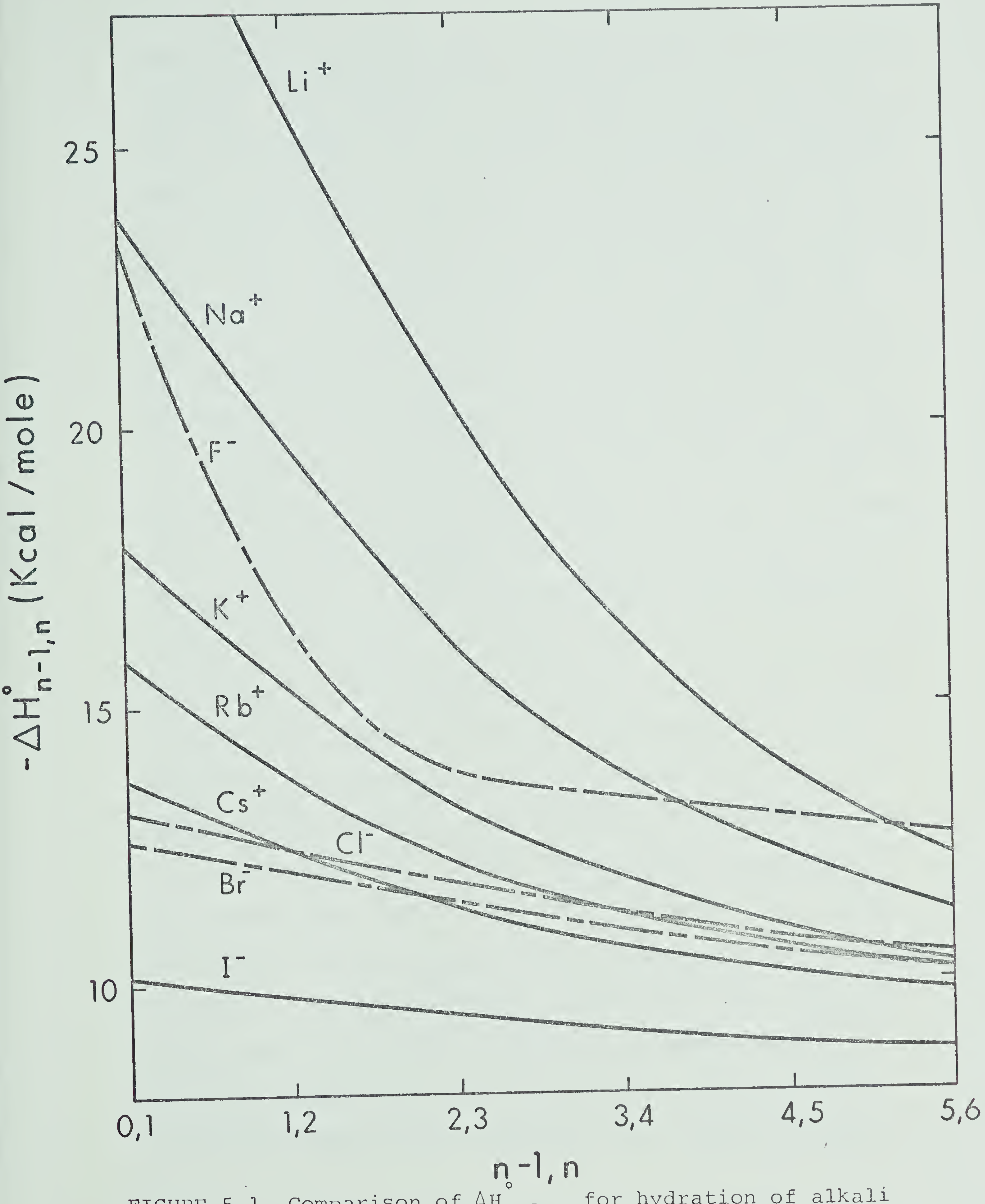

FIGURE 5.1 Comparison of $\Delta H^\circ_{n-1,n}$ for hydration of alkali positive and halide negative ions.

the studies of Arshadi (30) which were made in this laboratory. The hydration interactions of these spherical ions are probably best examined if one compares the hydration energies of isoelectronic pairs like K^+ and Cl^-, Rb^+ and Br^- etc. Since the nuclear charge of the negative ion in the isoelectronic pair is two units lower, the size of the electron cloud of the isolated negative ion will be definitely larger than that of the positive ion. Therefore, if one considers only the effect of ionic size (in vacuum) one would definitely predict that the positive isoelectronic ion should have higher $-\Delta H^\circ_{n-1,n}$. In Chapter 4.7 we have also suggested that the initial steps of hydration of positive ions are assisted by the formation of a dative bond between the oxygen atom of the water molecule and the ion. The existence of such a dative bond between isoelectronic negative ions and water molecules is not possible. As explained in a previous Chapter (4.7) the effect of the dative bond decreases with increasing size of the positive ion. If one examines the enthalpies of the larger ions like Rb^+ and Br^-, Cs^+ and I^-, for which the effect of any covalent dative bonding to water should be small, one still notices (Figure 5.1) that isoelectronic positive ions have considerably higher $-\Delta H^\circ_{n-1,n}$. Thus the present results of hydration energies of isoelectronic positive and negative ions, support at least

qualitatively the prediction based only on the size of the ions. It is interesting to note that the difference between the $\Delta H^{o}_{n-1,n}$ of the isoelectronic pairs decreases as n becomes larger and that in the cases of Na^+ and F^-, K^+ and Cl^-, Rb^+ and Br^- a crossover is observed within the range of the figure in which the $-\Delta H^{o}_{n-1,n}$ of the negative ion becomes higher. Furthermore the smaller the size of the ions, the sooner the crossover occurs. For Na^+, F^- crossover occurs at about $n = 4$, for K^+, Cl^- at $n \approx 5.5$ and for Rb^+, Br^- at $n \approx 6$. These observations can be explained on the basis of electrostatic calculations which indicated (30) that the slower decrease of $-\Delta H_{n-1,n}$ of the negative ions is due to the ability of the water molecules to assume nonsymmetric positions in which only one of the hydrogen atoms "touches" the negative ion. It has been shown (30) that these nonsymmetric arrangements result in lower water-water repulsions for ligands in the same shell and become of importance when the shell becomes crowded. Of course, crowding occurs soon in the smaller ions.

It is of interest to examine at this point the correlation of the present results with the total single ion hydration enthalpies. Values for the total enthalpies of hydration have been obtained by several authors discussed previously (31). We used two sets of data for total enthalpies of hydration, those of Latimer, Pitzer

and Slansky (32) and Randles (35). The same sets were used earlier in Chapter (3) for correlation of the relative heats of hydration of alkali ions.

Examining the values that the Latimer set gives for the alkali and halide ions one finds that the $-\Delta H_h$ for the negative ion is substantially larger than that for the positive ions. Thus $-\Delta H_h(Br^-) = 81.4$ kcal/mole while $-\Delta H_h(Rb^+) = 69.2$ kcal/mole. Therefore, Latimer's heats of hydration are exactly of opposite magnitudes to those expected from the standpoint of electron cloud size of the gaseous alkali and halide ions. Two basically different reasons have been put forward to explain the Latimer data. The first explanation which exists in several variations (32) proposes that the arrangement of water molecules around the negative ion and/or in the transition from the hydrated ion to the bulk liquid is more favorable. The second suggestion has been that water molecules have an electrical quadrupole moment which is of such a size that it leads to an attraction with negative ions and repulsion with positive ions (34). On the basis of the present results which give higher energies of interactions for the positive ions, it is possible to eliminate the quadrupole theory since the effect of the quadrupole should be particularly large at close range i.e. exactly the condition present in the gaseous

clusters. It should be pointed out that the present results do not prove that a quadrupole moment is completely absent. They only show that a water quadrupole moment of the magnitude required to explain the Latimer data cannot be present. In any event, as is shown in the subsequent discussion, the present results cannot be reconciled with the very strong hydration interactions for negative ions predicted by the Latimer data.

The Randles total hydration energy set assigns a slightly higher $-\Delta H_h$ for F^- than for Na^+ but for the larger ions the $-\Delta H_h$ of the positive isoelectronic ions are somewhat larger than those of the negative ions. The Randles data are thus closer to expectations based on the present results. A correlation of the present data and the single ion hydration energies of Latimer and Randles is given in the composite Figure 5.2a,b which shows plots of $[-\Delta H_{o,n}(M^+)] - [-\Delta H_{o,n}(X^-)]$ for isoelectronic pairs. The plots are based on the experimental $\Delta H^o_{n-1,n}$ whenever these were available (low n). For higher n the values from Figure 5.1 were used. Also indicated in Figure 5.2 (as two horizontal lines) are the differences of the total single ion hydration energies for the isoelectronic pairs based on the data of Latimer and Randles. It can be seen that the $\Delta H_{o,n}$ differences are in all cases much closer to the Randles differences,

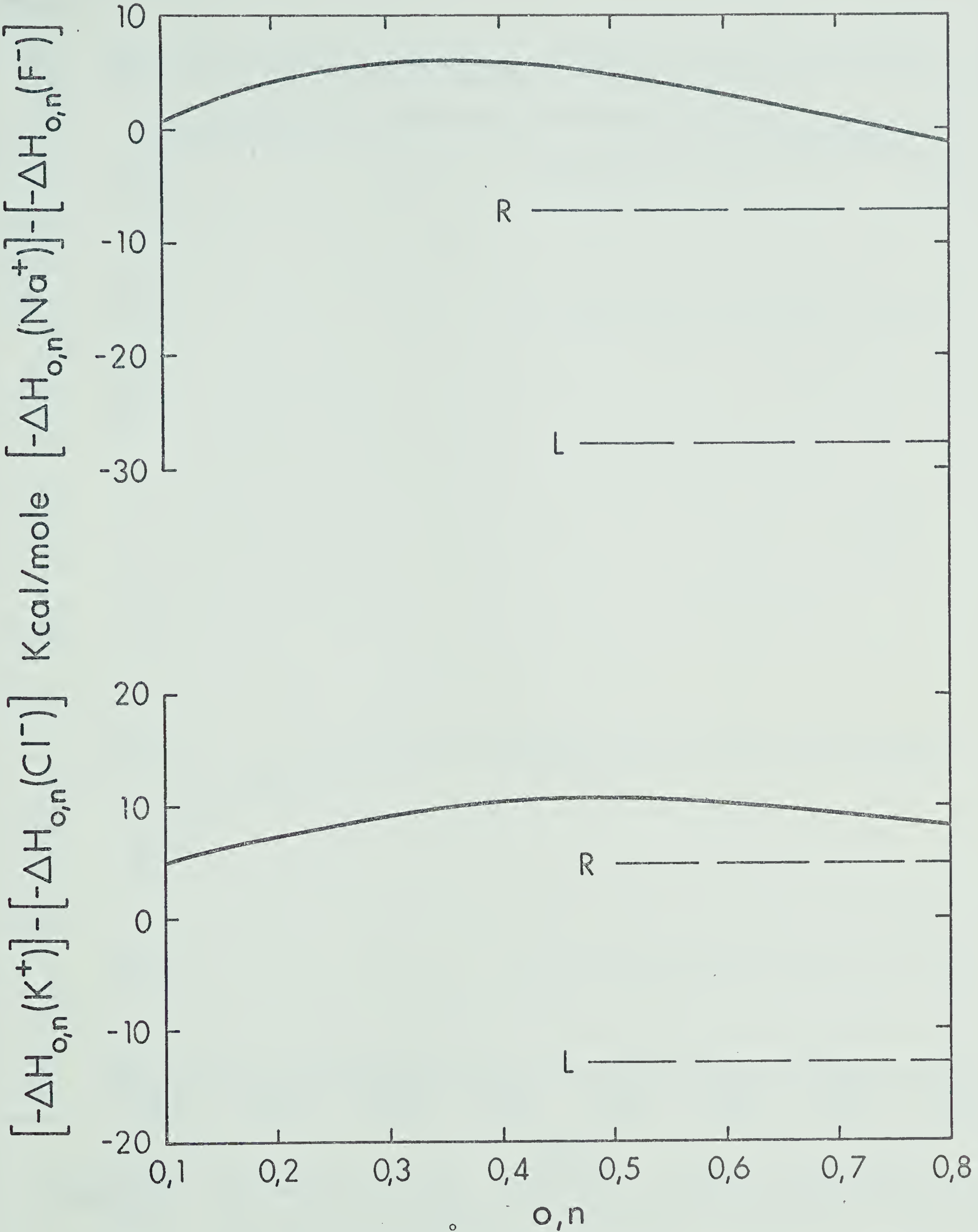

FIGURE 5a Comparison of $\Delta H^{\circ}_{o,n}$ hydration of alkali and halide ions with total enthalpies of hydration of Latimer, Pitzer and Slansky (L) and Randles (R).

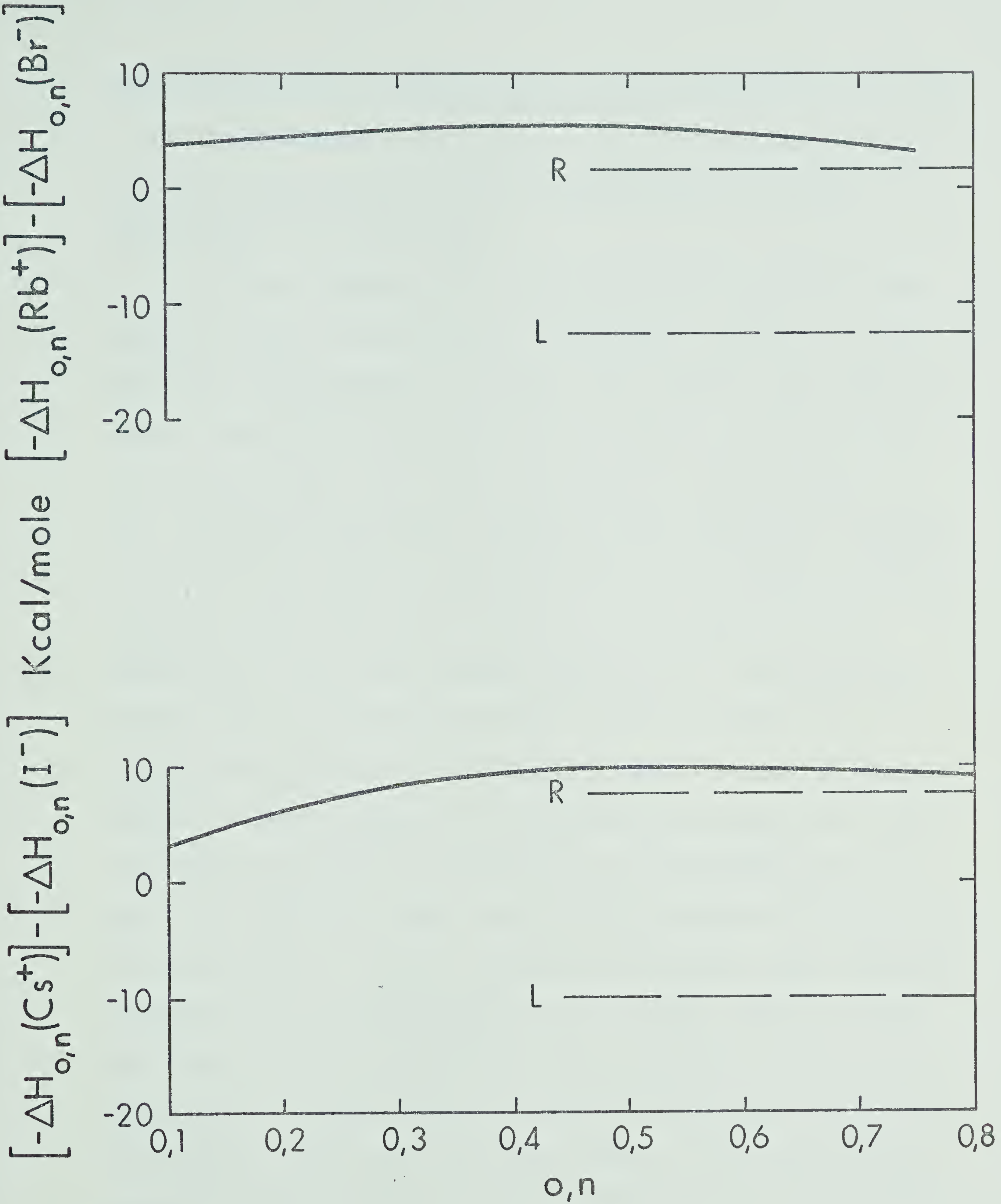

FIGURE 5b Comparison of $\Delta H^{\circ}_{o,n}$ hydration of alkali and halide ions with total enthalpies of hydration of Latimer, Pitzer and Slansky (L) and Randles (R).

moreover the $\Delta H_{o,n}$ differences seem to extrapolate for high n into the Randles differences. Of course by definition the $\Delta H_{o,n}$ differences should become equal to the ΔH_h differences for very high n.

We can summarize the observations on positive and negative isoelectronic pairs as follows. In the initial hydration interactions (n small) the positive ion gives higher energies of interaction as would be expected from its smaller size. As the cluster grows interactions in the negative ion become gradually more favourable (Figure 5.1 and 5.2). This is probably due to the ability of the negative ion to pack the water molecules more closely without too large water-water repulsions. Extrapolation of the data to moderately high n seems to lead to an asymptotic approach to the Randles data. Thus the present results are in support of the Randles data and also indicate that the decisive interactions determining the total heats of hydration occur during the attachment of the first 8-12 molecules. One may consider the further path towards formation of a liquid solution as a single step in which the large clusters are fitted into the bulk of the liquid. The present results indicate that the hydration energy for this final "step" will be quite similar for a positive or negative cluster containing the corresponding isoeletronic ion.

5b. Ion-Ligand Bond Energies and Hydration Numbers in Solution.

According to Bockris (5) the term *hydration number* when applied to simple ions in solution corresponds to the coordination number of the ion in solution. Since the water molecules coordinated to the ion are in rapid exchange with the bulk of the solution it is only on a time average that we may speak of some molecules being immobilized by the ionic field. The hydration number is therefore an empirical parameter which gives the *effective* number of water molecules that have undergone some constant critical change in property related to a suitable definition of hydration (6). It has been suggested (6) that whenever possible, properties at infinite dilution should be used for the determination of hydration numbers in order to avoid any overlap with other types of interactions in the solutions. Since the hydration in the gas phase may be compared to the properties of hydration at "infinite dilution" in solution, one way of evaluating the hydration numbers of alkali ions would be the use of present data. One way in which the present $\Delta H^{o}_{n-1,n}$ values can be related to the liquid phase is through the theoretical arguments of Bernal and Fowler (77). They have proposed the following relating to the ionic solvations in liquid water. The hydration of an ion will occur when the

potential energy of a water molecule coordinated to an ion is less than that of a free water molecule. The free water molecule has four neighbors while a single water molecule bonded to an ion has three, namely the ion and two water molecules. The condition for an ion having at least one coordinated water molecule is, therefore, that the potential energy $\Delta E^\circ_{n-1,n(l)}$ for a water molecule due to coordination to an ion be less than that due to two other water molecules. The electrostatic potential energy due to two water molecules is calculated by Bernal and Fowler to be -15 kcal/mole. This fact gives rise to equation 5.2 which expresses the ion-water molecule bond energy B.E.

$$5.2 \qquad \text{B.E.} = \Delta E^\circ_{n-1,n(l)} + 15$$

$\Delta E^\circ_{n-1,n(l)}$ can be set equal to $\Delta E^\circ_{n-1,n(g)}$, the potential energy for a water molecule due to coordination to an ion in the gas phase. This is not unreasonable since Bernal and Fowler appear to have taken the dielectric constant as unity in their calculation of the electrostatic potential energy due to two water molecules.

Since in section 4.7 it was found that $\Delta H^\circ_{n-1,n} \approx \Delta E^\circ_{n-1,n(g)}$, $H^\circ_{n-1,n} \approx \Delta E^\circ_{n-1,n(l)}$ Equation 5.2 can be rewritten as equation 5.3

$$5.3 \qquad \text{B.E.} = \Delta H^\circ_{n-1,n} + 15$$

The bond energies calculated for $M^+(H_2O)_n - H_2O$ with the $\Delta H^\circ_{n-1,n}$ values from Tables 3.1 to 3.4 are listed in Table 5.1. The bond energies for $M^+(H_2O)_n - H_2O$ show that the Li^+ in solution may have up to 4 coordinated water molecules (hydration number ~4), Na^+ ion up to 3, K^+ ion up to 2, Rb^+ ion may have one and Cs^+ ion no coordinated water molecules, (hydration number ~0). The hydration numbers obtained show a regular decrease with increasing size of the ion. For Li^+ to Cs^+ the hydration number varies from 4 to 0. It has been pointed out (6) that ions of low charge and large radius (Cs^+ for example) cannot form ion-ligand bonds in solution (hydration number ~0), since there will be a critical radius above which the charge density falls below the value required to reorient water molecules. At larger values of the radius of the ion there is no preferred orientation of the water molecules. Thermal agitation is then able to break up the water structure in the vicinity of the ion. The original calculations of Bernal and Fowler (77) indicated that for univalent ions this critical radius would be about 1.6A. According to Pauling (69), Goldschmidt (61) and Gourary and Adrian (70) the ionic radii of Cs^+ are 1.69, 1.65 and 1.83 respectively. Thus if the original calculations of Bernal and Fowler are correct one would expect a zero

TABLE 5.1

Ion-water Molecule Bond Energies in the Liquid Phase

Bond	Bond energy (kcal/mole)
$Li^+ — H_2O$	-19.0
$Li^+(H_2O) — H_2O$	-10.8
$Li^+(H_2O)_2 — H_2O$	- 5.7
$Li^+(H_2O)_3 — H_2O$	- 1.4
$Li^+(H_2O)_4 — H_2O$	+ 1.1
$Na^+ — H_2O$	- 9.0
$Na^+(H_2O) — H_2O$	- 4.8
$Na^+(H_2O)_2 — H_2O$	- 0.8
$Na^+(H_2O)_3 — H_2O$	+ 1.2
$K^+ — H_2O$	- 2.9
$K^+(H_2O) — H_2O$	- 1.1
$K^+(H_2O)_2 — H_2O$	+ 1.8
$Rb^+ — H_2O$	- 0.9
$Rb^+(H_2O) — H_2O$	+ 1.4
$Cs^+ — H_2O$	+ 1.3

TABLE 5.2

Hydration Numbers h for Alkali Ions

Ion	Hydration numbers h a	 b	 c	 d
Li^+	4	4.2-4.7	4	4
Na^+	3	2.7-3.3	3	3.1
K^+	2	1.7-1.8	2	2.1
Rb^+	1	1.5	1	1.6
Cs^+	0	1.4	0	1.0

(a) Present calculation

(b) Modified activity coefficient equations, ref. (78).

(c) Mean values from methods, mobility, entropy, compressibility, density, ref. (5).

(d) N.M.R. effects in aqueous solutions of electrolytes, ref. (79).

hydration number for the Cs^+ ion.

The values of hydration numbers calculated here are very close to those obtained from other types of measurements, described in references (78) (5) (79). See Table 5.2.

6. OTHER APPLICATIONS OF THE GAS PHASE HYDRATION MEASUREMENTS

6.1 Clustering Equilibria and the Catalysis of Water Condensation by Ionic Charges.

It can be seen from Figure 3.27 where $-\Delta G^{\circ}_{n-1,n}$ is plotted versus n, that with increasing n (n >> 6) the $-\Delta G^{\circ}_{n-1,n}$ values will approach the free energy of evaporation $-\Delta G_{evap(298°K)} = 2.03$ kcal/mole for reaction

$$H_2O_{(g)} \rightarrow H_2O_{(\ell)}$$

In other words as the ionic charge in the cluster $M^{+}(H_2O)_n$ becomes more and more shielded by water molecules (large increase of n) the cluster $M^{+}(H_2O)_n$ will approach a liquid droplet.

In Figure 6.1 the $-\Delta G^{\circ}_{n-1,n}$ values at 298°K were plotted versus n, using a logarithmic scale for n in order to be able to accomodate a large increase of n. The dashed line is calculated by equation 6.1

$$6.1 \qquad \Delta G^{\circ}_{evap} = \Delta G^{\circ}_{(1)} - \Delta G^{\circ}_{(2)}$$

where the free energy change $\Delta G_{(1)}$ is equivalent to the transfer (of one mole of water) from pressure P = 23.7 torr (water vapour pressure at 298°K) to P = 1 atm, given by equation 6.2

$$6.2 \qquad \Delta G^{\circ}_{(1)} = -RT \ln \frac{760}{23.7}$$

FIGURE 6.1

Comparison of free energy of hydration $\Delta G^{\circ}_{n-1,n}$ with free energy of evaporation of 1 mole of water molecules from 1 mole of water droplets carrying a single ionic charge. Number of molecules contained per droplet given in the abscissa. Free energy of evaporation calculated from J. J. Thomson formula.

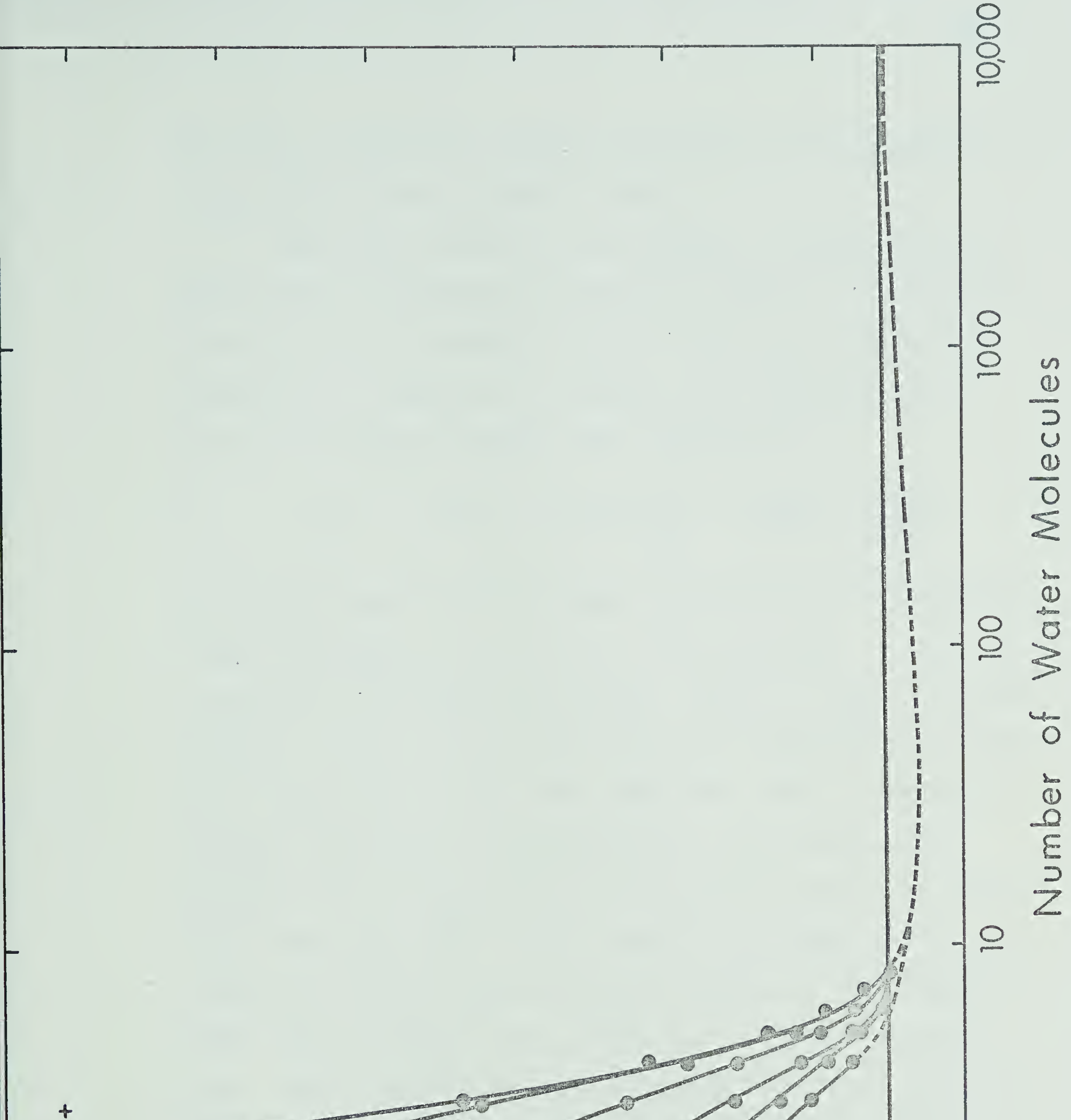
$-\Delta G_{n-1,n}$ (Kcal/mole)
24.0
20.0
16.0
12.0
8.0
4.0
0
10
100
1000
10,000
Number of Water Molecules
H^+
Li
Na
K
Rb
Cs

FIGURE 6.1

The $\Delta G^{\circ}_{(1)}$ represents normal free energy of evaporation from a flat water surface at 298°K.

The $\Delta G_{(2)}$ gives the free energy of evaporation of water from the spherical droplet of radius r, carrying a single centrally located charge. The $\Delta G_{(2)}$ values as a function of radius of the droplet are represented by the J. J. Thomson formula (80) equation 6.3

$$6.3 \qquad \Delta G^{\circ}_{(2)} = RT \ln \frac{P_{\infty}}{P_r} = - \frac{M}{\rho}\left(\frac{2\theta}{r} - \frac{e^2}{8\pi\varepsilon r^4}\right)$$

P_r is the vapour pressure over the droplet while P_{∞} is the vapour pressure of water with a flat surface. ρ and M are the density and molecular weight, while θ, e and ε are the surface tension, electronic charge and dielectric constant. The equation 6.3 gives the condition, when a droplet of radius r will be in equilibrium with the surrounding medium, that is the droplet will neither shrink nor grow. The first term $(\frac{2\theta}{r})$ in the equation represents the lowering of the $\Delta G^{\circ}_{(2)}$ with decreasing radius of the droplet. This effect is due to the operation of surface tension. The vapour pressure of the spherical droplet is greater than that of the flat surface, the pressure increasing as the radius of the droplets decreases. The higher vapour pressure of small droplets accounts for their tendency to disappear by "distillation" to larger droplets. Large droplets thus tend to grow at the expense of the smaller

ones. The second term $(\frac{e^2}{8\pi\varepsilon r^4})$ in the equation 6.3 expresses the increase of $\Delta G_{(2)}$ (becomes less negative) with the decreasing radius of the droplet. This effect is due to the increased attraction between the charge and the water dipoles. As the radius decreases the distinction between charged water droplets and water clusters $M^+(H_2O)_n$ becomes less pronounced. The P_∞/P_r and consequently the $\Delta G_{(2)}$ approach zero values, due to the increased attraction between the charge and water dipoles (second term in equation 6.3). Thus the ΔG°_{evap} by equation 6.1 begins to approach $\Delta G^\circ_{n-1,n}$.

In Figure 6.2, taken from reference (80), the variation of P_r/P_∞ as a function of droplet radius is plotted as a broken line for the case of water vapour and as a solid line for a singly charged water vapour droplet at 298°K. Table 6.1 gives the values of $\Delta G^\circ_{(1)}$, $\Delta G^\circ_{(2)}$ and ΔG°_{evap} as a function of the radius of the charged droplet. The $\Delta G^\circ_{(2)}$ values were obtained with macroscopic values for ρ, θ and ε.

The calculated values for $\frac{P_r}{P_\infty}$ as a function of the radius of the droplet, given in Table 6.1, are compared with the values from Figure 6.2. For the $r \gtrsim 7 \times 10^{-8}$ cm, the calculated P_r/P_∞ values are consistent with those from Figure 6.2. However for $r < 7 \times 10^{-8}$, the P_r/P_∞ ratios were taken from Figure 6.2 (solid line), since the P_r/P_∞ values for very small droplets cannot be calculated with macro-

TABLE 6.1

Free Energy Changes $\Delta G^{\circ}_{(1)}$, $\Delta G^{\circ}_{(2)}$ and ΔG°_{evap} as a function of radius of charged droplet

N (number of water molecules in a charged droplet)	r (radius of a charged droplet in cm)	P_r/P_∞	$\Delta G^{\circ}_{(1)}$ (kcal/mole)	$\Delta G^{\circ}_{(2)}$ (kcal/mole)	ΔG°_{evap} (kcal/mole)
48	7×10^{-8}	4.45	2.063	0.387	1.676
140	10×10^{-8}	2.85	2.063	0.271	1.792
470	15×10^{-8}	2.01	2.063	0.180	1.883
1116	20×10^{-8}	1.69	2.063	0.135	1.928
3766	30×10^{-8}	1.43	2.063	0.089	1.973
17437	50×10^{-8}	1.23	2.063	0.054	2.009

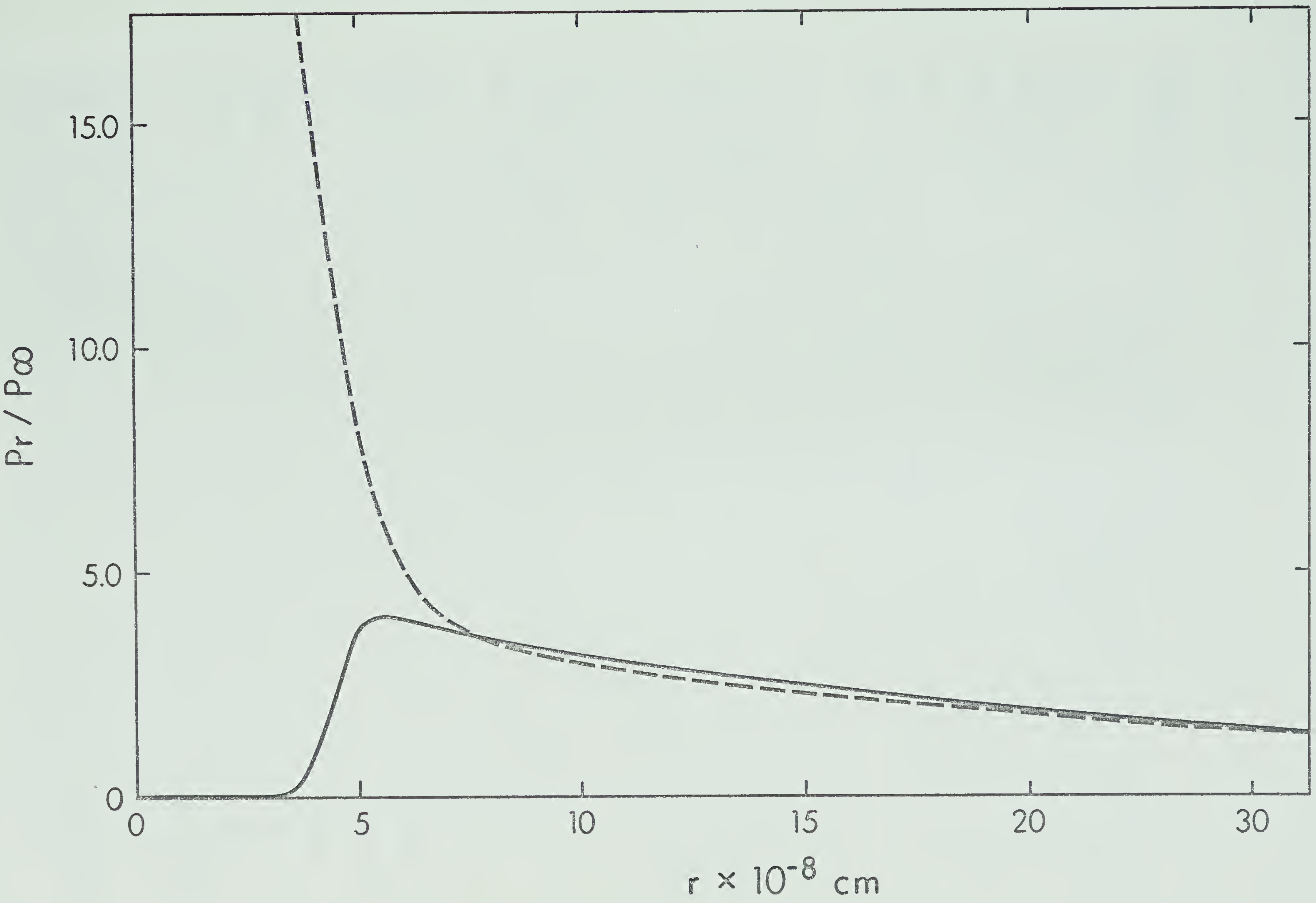

FIGURE 6.2 The variation of P_r/P_∞ as a function of droplet radius is plotted as a broken line for the case of water vapour and as a solid line for a singly charged water vapour droplet at 298°K (80).

scopic values for ρ, θ and ε (81).

Figure 6.1 shows that the experimentally determined $\Delta G^{\circ}_{n-1,n}$ values for all ions are consistent with the predictions of equation 6.3 since the $\Delta G^{\circ}_{n-1,n}$ for all ions extrapolate smoothly for high n into the calculated curve. The $\Delta G^{\circ}_{n-1,n}$ values for $H^+(H_2O)_n$ clusters, presented in this figure were taken from reference (24).

Figure 6.1 also illustrates the fact that there is a theoretical limit for n beyond which clustering equilibria cannot be measured. Thus when $\Delta G^{\circ}_{n-1,n}$ becomes smaller than ΔG°_{evap} = 2.063 kcal/mole at 298°K (normal free energy of evaporation from flat water surface indicated by a black horizontal line in Figure 6.1) the condensation to bulk liquid water becomes theoretically possible. However, in the absence of other nucleation catalysts, condensation will not occur and ion clustering equilibria will exist (at water pressure above saturation pressure) until n becomes about equal to 20. Beyond this point the $\Delta G^{\circ}_{n-1,n}$ (dashed curve) begins to increase which means that clusters with higher n become thermodynamically more stable and growth of the clusters becomes spontaneous ending in bulk water.

In experiments done up to the present we found that clustering equilibria could not be measured beyond $n \approx 7$ due to condensation of water in the ion source. According to the above discussion the condensation must have been

catalyzed by some other nucleating agents (i.e. active points on the metal surfaces of the walls etc.). Thus application of special techniques, for instance those used in cloud chamber experiments coupled with rapid mass scanning might allow equilibria to be measured for n up to about 20, but not higher.

6.2 Proton Affinities (Basicities) of the Alkali Hydroxides in the Gas Phase.

One interesting result from the present work is that enthalpy changes $\Delta H_{0,1}$, for the reaction $M^+ + H_2O \rightarrow (MOH_2)^+$ (0,1) when combined with available thermochemical data allow the determination of the proton affinities of the (gaseous) alkali hydroxides. These proton affinities are of considerable chemical interest especially when compared to those of other related compounds.

The proton affinity (P.A.) of the hydroxides, MOH is defined as the negative of the enthalpy change for the gas phase reaction 6.1

$$6.1 \qquad MOH + H^+ \rightarrow (MOH_2)^+ \qquad P.A.(MOH) = -\Delta H$$

The enthalpy change for reaction 6.1 can be evaluated from the enthalpy of formation of the reactants and the product. The enthalpies of formation of MOH and H^+ are available. The enthalpy of formation of $(MOH_2)^+$ can be evaluated from reaction (0,1) since $\Delta H_{0,1}$ was determined and $\Delta H_f(M^+)$ and $\Delta H_f(H_2O)$ are available. Thus the equation 6.4

$$6.4 \quad \Delta H_{0,1} = \Delta H_f(MOH_2)^+ - \Delta H_f H_2O - \Delta H_f M^+$$

when combined with the equation 6.5 representing the enthalpy change for reaction 6.1.

$$6.5 \qquad \Delta H = \Delta H_f(MOH_2)^+ - \Delta H_f MOH - \Delta H_f H^+$$

would give the proton affinity of MOH represented by equation 6.6

$$6.6 \quad P.A.(MOH) = \Delta H_f(MOH) - \Delta H_{0,1} - \Delta H_f(M^+) + \Delta H_f(H^+) - \Delta H_f(H_2O)$$

The results and the data used for their calculation are given in Table 6.2. The values $\Delta H_f(H^+) = 367$ and $\Delta H_f(H_2O) = -57.8$ kcal/mole were also used. The proton affinities of the hydroxides which are in the range 240 - 270 kcal/mole are considerably larger than those of water, methanol and ammonia which are approximately 160, 185 and 206 kcal/mole respectively (82). It has been pointed out (83) that in the series R-OH the proton affinity should increase with the electron donating ability of the substituent R (84). The very high proton affinity of the alkali hydroxides can be thus understood in terms of the very high electron donating ability of the substituent M. This ability is so extreme that in the protonated species essentially all the charge resides in M i.e. the resulting structure is that of the hydrated alkali ion as indicated by the conventional formula M^+OH_2.

TABLE 6.2

Proton Affinities of Alkali Hydroxides MOH and Thermochemical Data Used for Their Evaluation.[a]

	$\Delta H_f(M)$	$I_p(M)$[b]	$\Delta H_f(M^+)$	$-\Delta H_{0,1}$	$\Delta H_f(M^+H_2O)$	$\Delta H_f(MOH)$	P.A.(MOH)
Li	38.0	124.3	162.3	34	71.3	55	240.7
Na	25.9	118.5	144.4	24.0	63.4	56	247.6
K	21.6	100.1	121.7	17.9	46.8	57.6	262.6
Cs	18.7	89.8	108.5	13.7	37.8	60.0[c]	269.2

(a) All values in kcal/mole, refer to gas phase species at 300°K. All data except $\Delta H_{0,1}$ taken from ref. (82).

(b) $I_p(M)$ = ionization potential of M.

(c) Estimated from heat of formation of other alkali hydroxides.

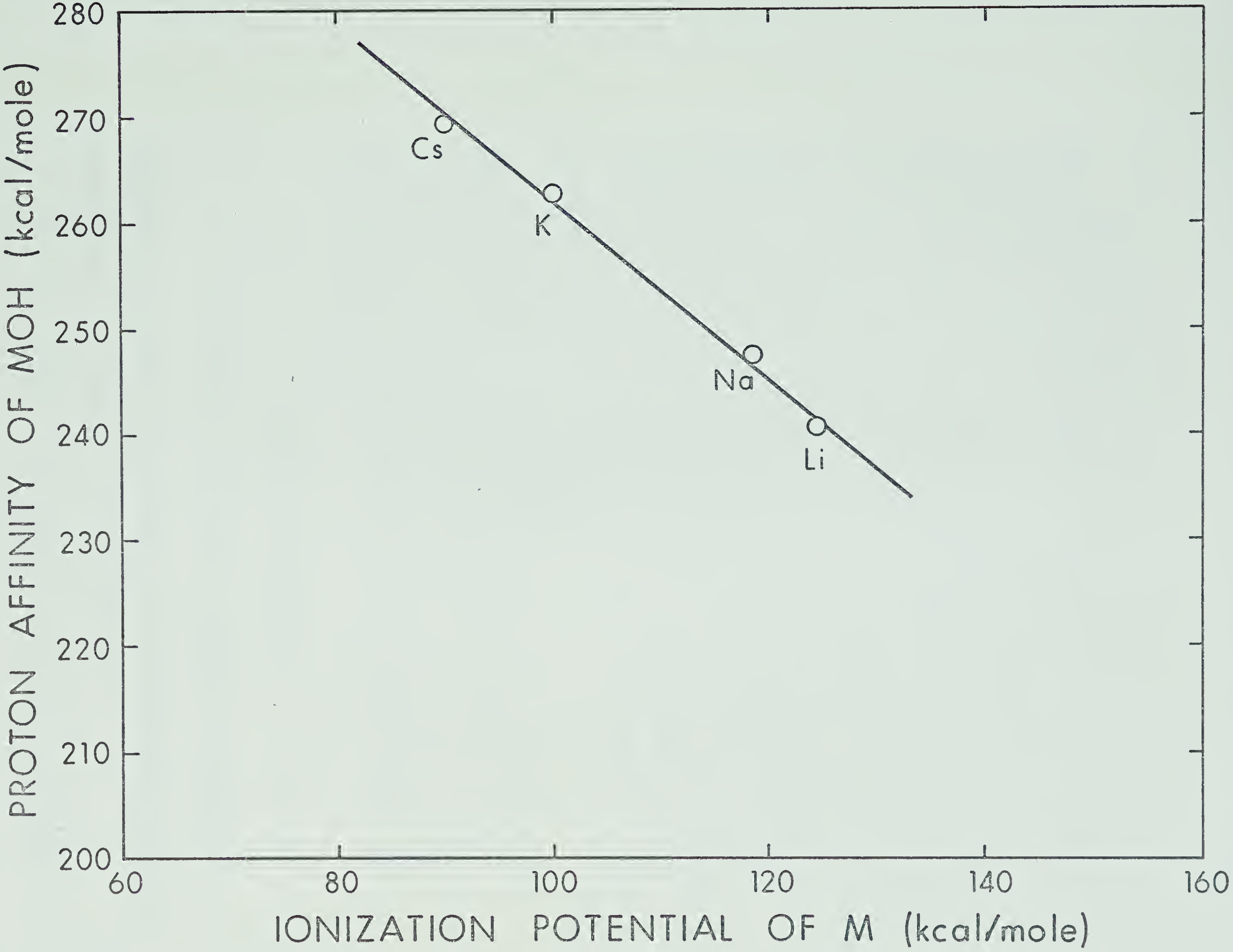

FIGURE 6.3 Proton affinities of MOH versus ionization potential of M.

The variation of the proton affinity in the MOH series with the electron releasing ability of M is illustrated in Figure 6.3, where the proton affinities are plotted as a function of the ionization potential of the alkali atoms. The rationale of the plot being that the electron releasing ability decreases as the ionization potential of the alkali ion increases. It can be seen that an almost linear relationship is obtained. Considering the proton affinity as a measure of the base strength of a (gas phase) Brönsted base we find that the base strength of hydroxides increases from LiOH to CsOH. This order of base strength need not be observed in solutions since there the process is complicated by solvation effects.

Since the proton affinity (P.A.) of a hydroxide is defined as the negative of the enthalpy change for the reaction 6.1, the hydrogen affinity (H.A.) can be similarly defined as the negative of the enthalpy change for the reaction 6.2.

6.2 $$MOH^{+} + H \rightarrow (MOH_2)^{+}$$

6.7 $$H.A.(MOH^{+}) = \Delta H_f(MOH^{+}) + \Delta H_f(H) - \Delta H_f(MOH_2)^{+}$$

Relating P.A.(MOH) to H.A.(MOH^{+}), the following expression represented by equation 6.8 is obtained

6.8 $$P.A.(MOH) - H.A.(MOH^{+}) = I.P.(H) - I.P.(MOH)$$

where I.P.(H) and I.P.(MOH) are the ionization potentials of H and MOH respectively. Thus the proton and hydrogen affinities of hydroxides and their corresponding ions are interrelated by ionization potentials as shown in the above equation 6.8. The hydrogen affinity H.A.(MOH^+) is simply the MOH^+- H bond strength D(MOH^+- H). From equation 6.7 D($NaOH^+$- H) = 140 kcal/mole was calculated. The values I.P.(H) = 313 and I.P.(NaOH) = 207 kcal/mole (85) were used. Unfortunately the ionization potentials for other alkali hydroxides are not available in the literature therefore the hydrogen affinities for other alkali hydroxides were not calculated.

The hydrogen affinity H.A. ($NaOH^+$) = 140 kcal/mole, can be compared to that of water, H.A. (H_2O^+) = 141 kcal/mole (86). Assuming that the values of P.A. (NaOH = 247.6 and P.A.(H_2O) = 164 kcal/mole are of right order of magnitude, the difference in proton affinities ΔP.A. = 83.6 kcal/mole would be compensated by ΔI.P. = 83 kcal/mole, since I.P.(H_2O) = 290.6 and I.P.(NaOH) = 207 kcal/mole. Thus according to equation 6.7 D(HOH^+-H) ≈ D($NaOH^+$-H) ≈ 140 kcal/mole.

7. SUGGESTION FOR FURTHER RESEARCH

7.1 Solvation of Alkali and Halide Ions by Polar Aprotic Solvents.

Since the gas phase solvation of alkali ions plays an important role in gas phase chemistry generally and has particular relevance to the solvation in solutions, it is proposed that further work be carried out in this area.

The energetics of ion solvation in nonaqueous solutions have recently become the subject of many investigations, for example (87,88). Considerable evidence indicates (89) that in polar aprotic solvents, such as acetonitrile (CH_3CN), acetone (CH_3COCH_3), nitromethane (CH_2NO_2) etc., negative ions are solvated more weakly than positive ions. It was also observed that all negative ions are solvated more weakly in aprotic solvents than in water (89).

Although the dipole moments of aprotic solvents are much higher, acetonitrile for example has a dipole moment of 3.37D, compared to 1.85D for water, water is still a better solvating agent for negative ions than acetonitrile. It has been suggested that this effect is due to steric inhibition (89). Because of the vicinity of the electron cloud of the $C{\equiv}N$ bond, an anion probably will be forced to take up the specific position indicated in structure I, resulting in loss of freedom of rotation. Furthermore, solvation of a (small) anion by more than one acetonitrile

molecule then becomes improbable. The same is not true for the cylindrically symmetrical solvation of a positive ion indicated in structure II.

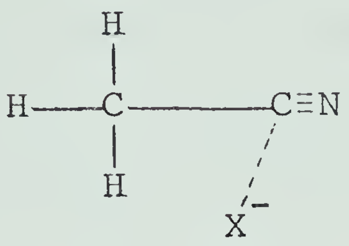

I

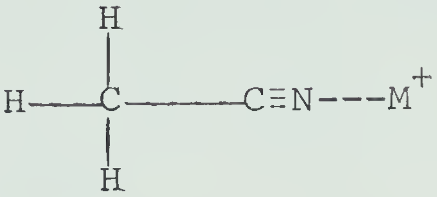

II

Therefore it would be very desirable to measure the gas phase solvation of positive alkali and negative halide ions by acetonitrile. The data obtained would indicate how many molecules of acetonitrile are attached to each particular ion in the first and second shell. Furthermore, the enthalpies for the positive and negative ions will show directly whether the solvation by negative ions is much weaker.

REFERENCES

1. S. K. Searles and P. Kebarle, Can. J. Chem., 47, 2619 (1969).
2. G. H. Nancollas, Interactions in electrolyte solutions, Elsevier Publishing Company, New York, (1966).
3. Discussions Faraday Soc., 2 (1910).
4. J. P. Hunt and H. Taube, J. Chem. Phys., 18, 757 (1950).
5. J. O'M. Bockris, Quart. Rev. (London) 3, 173, (1949).
6. J. E. Desnoyers and C. Jolicoeur, Modern Aspects of Electrochemistry No. 5, Plenum Press, New York, 1969, Chapter 1. Edited by J. O'M. Bockris and B. E. Conway.
7. A. M. Hogg and P. Kebarle, J. Chem. Phys., 43, 449 (1965).
8. L. B. Loeb, Phys. Rev., 32, 81 (1928).
9. L. B. Loeb, Basic Processes of Gaseous Electronics, Second Edition, University of California Press, Berkeley (1955), p.46-7.
10. R. J. Munson, A. M. Tyndall, and K. Hoselitz, Proc. Roy. Soc., A172, 28, (1939).
11. R. J. Munson and K. Hoselitz, Proc. Roy. Soc. A172, 43 (1939).
12. J. J. Thomson, Phil. Mag., 24, 241 (1912).
13. V. L. Talroze and A. K. Lyobimova, Dokl. Akad. Nauk. SSSR, 86, 909 (1952).

14. D. P. Stevenson and D. O. Schissler, J. Chem. Phys., 23, 1353 (1955).

15. G. G. Meisels, W. H. Hamill and R. R. Williams, J. Chem. Phys., 25, 790 (1956).

16. F. H. Field, J. Franklin and F. Lampe, J. Am. Chem. Soc., 79, 2419 (1957).

17. H. D. Beckey, Z. Naturforsch, 15a, 822 (1960).

18. P. F. Knewstubb and T. M. Sugden, Proc. Roy. Soc., A255, 520 (1960).

19. L. W. Sieck, F. P. Abramson and J. H. Futrell, J. Chem. Phys., 45, 2859 (1966).

20. (a) M. S. B. Munson, J. Am. Chem. Soc., 87, 5313 (1965).
    (b) M. S. B. Munson, J. Phys. Chem., 70, 2039 (1966).

21. (a) J. Yang and D. C. Conway, J. Chem. Phys., 40, 1729 (1964).
    (b) D. C. Conway and J. Yang, J. Chem. Phys., 43, 2900 (1965).

22. W. A. Chupka, J. Chem. Phys., 30, 458 (1959).

23. (a) A. N. Hayhurst and T. M. Sugden, IUPAC Meeting on Plasmas, Moscow, (1965).
    (b) A. N. Hayhurst and T. M. Sugden, Proc. Roy. Soc., A293, 36 (1966).

24. P. Kebarle, S. K. Searles, A. Zolla, J. Scarborough and M. Arshadi, J. Am. Chem. Soc., 89, 6393 (1967).

25. F. H. Field, J. Am. Chem. Soc., 91, 2827 (1969).

26. A. Good, D. Durden and P. Kebarle, J. Chem. Phys., 52, 212 (1970); 52, 222 (1970).

27. P. Kebarle, R. N. Haynes and J. G. Collins, J. Am. Chem. Soc., 89, 5753 (1967).

28. A. M. Hogg and P. Kebarle, J. Chem. Phys., 43, 449 (1965).

29. S. K. Searles and P. Kebarle, J. Phys. Chem., 72, 742 (1968).

30. M. R. Arshadi, Ph.D. Thesis, University of Alberta, (1969).

31. D. R. Rosseinsky, Chem. Rev., 65, 467 (1965).

32. W. M. Latimer, S. K. Pitzer and C. M. Slansky, J. Chem. Phys., 7, 108 (1939).

33. E. J. W. Verwey, Rec. Trav. Chim. 61, 127 (1942).

34. A. D. Buckingham, Discussions Faraday Soc., 24, 151 (1957).

35. J. E. B. Randles, Trans. Faraday Soc., 52, 1573 (1956).

36. S. C. Lind, Radiation Chemistry of Gases, Reinhold Publishing Corp. New York, 1961, p.8

37. H. Eyring, J. O. Hirschfelder and H. S. Taylor, J. Chem. Phys., 4, 479, 570 (1936).

38. D. P. Stevenson and D. O. Schissler, J. Chem. Phys., 29, 282 (1958).

39. K. M. Bansal and G. R. Freeman, J. Am. Chem. Soc., 90, 71, 83 (1968).

40. R. S. Narcisi and D. Bailey, J. Geophys. Res., 71, No. 15, 3687 (1965).

41. E. E. Ferguson and F. C. Fehsenfeld, J. Geophys. Res. 74, No. 24. 5743 (1969).

42. R. E. Lenier and L. M. Branscomb, J. Geophys. Res., 73, 27 (1968).

43. D. R. Bates and A. Dalgarno, Atomic and Molecular Processes, Academic Press, (1962).

44. W. Swider, Nature, 217, 438 (1968).

45. Symposium on Physics and Chemistry of the Upper Atmosphere, Stanford Research Institute, June 1969.

46. F. C. Fehsenfeld, E. E. Ferguson and D. K. Bohme, Planet Space Sci., Vol. 17 1759 (1969).

47. R. S. Narcisi, The Formation of Cluster Ions in Laboratory Sources and in the Ionosphere, to be published.

48. J. Payzant and P. Kebarle, to be published.

49. G. Collins, Ph.D. Thesis, University of Alberta, (1966).

50. S. K. Searles, Ph.D. Thesis, University of Alberta, (1968).

51. See for example Mass Spectrometry edited by C. A. McDowell, McGraw Hill Book Co. Inc., New York, (1968).

52. R. O. Jenkins and W. G. Trodden, Electron and Ion Emission from Solids, Routledge and Kegan Paul Ltd., London (1965) Chapter 7.

53. W. J. Moore, Physical Chemistry, Prentice-Hall Inc., Englewood Cliffs, New Jersey (1962) p.225.

54. A. Guthrie, Vacuum Technology, John Wiley and Sons, Inc., New York (1963), -.509.

55. J. P. Blewett and E. J. Jones, Phys. Rev., 50, 464 (1936).

56. E. W. McDaniell, Collision Phenomena in Ionized Gases, John Wiley & Sons, Inc., New York (1964) p.490.

57. J. Payzant and P. Kebarle, to be published.

58. W. C. Lineberger and L. J. Puckett, Bull. Am. Phys. Soc., 14, 261 (1969).

59. H. E. Stanton, W. A. Chupka and M. G. Inghram, Rev. Sci. Inst. 27, 109 (1956).

60. J. M. Beynon, Mass Spectrometry and its Applications to Organic Chemistry, Elsevier Publishing Co., New York, 1960, p.212.

61. J. S. Muirhead-Gould and K. J. Laidler, Chemical Physics of Ionic Solutions, John Wiley & Sons Inc., New York, 1966, Chapter 6, Edited by B. E. Conway and R. G. Barradas.

62. G. J. Doyle and R. G. Caldwell, Report AD635552, Stanford Research Institute, South Pasadena, California (1966).

63. American Chemical Society, Adv. Chem. Ser. 15, 9 (1955).

64. J. O. Hirschfelder, C. F. Curtis, R. B. Bird, Molecular Theory of Gases and Liquids, John Wiley and Sons (1954) p.1110.

65. E. A. Mason and J. I. Vanderslice, High Energy Elastic Scattering of Atoms, Molecules and Ions, Chapter 17 in Atomic and Molecular Processes, Edited by D. R.

Bates, Academic Press, New York (1967).

66. R. H. Stokes, J. Am. Chem. Soc., 86, 979 (1964).

67. Amdur I. and Mason E. A., J. Chem. Phys., 23, 415 (1955).

68. Mahan B. H. , College Chemistry, Addison-Wesley Publishing Company Inc., Reading, Mass., (1966) p.66.

69. L. Pauling, The Nature of the .Chemical Bond, Cornell University Press, Ithaca, New York (1948).

70. B. S. Gourary and F. J. Adrian, Solid State Phys., 10, 127 (1960).

71. F. J. Garrick, Phil. Mag., 9, 131 (1930), 10, 76 (1930).

72. J. S. Muirhead-Gould and K. J. Laidler, Trans. Faraday Soc., 63, 944 (1967).

73. L. B. Magnusson, J. Chem. Phys., 39, 1953 (1963).

74. Yu. A. Kruglyak, Tr. Khim. Fak. i Nauchn-Issled Inst. Khim. No. 19, 172-8 (1963).

75. S. Glasstone, Textbook of Physical Chemistry, D. Van Nostrand Co. Inc., New York (1964), Chapter 11.

76. N. Davidson, Statistical Mechanics, McGraw-Hill Book Co. Inc., New York (1962) Chapter 11.

77. J. D. Bernal and R. H. Fowler, J. Chem. Phys., 1, 515 (1933).

78. E. Glueckhauf, The Structure of Electrolytic Solutions (J. Wiley & Sons, Inc., New York 1959) Chapter 7.

79. J. C. Hindman, J. Chem. Phys. 36, 1000 (1962).

80. J. J. Thomson, Applications of Dynamics to Physics and Chemistry, Vol. I, p.165, London McMillan & Co., (1888) C. M. York, "Cloud Chambers" Sect. 3 Vol. XLV,

Handbuck der Physik, Springer Verlag Berlin (1958).

81. W. H. Rodebush, Ind. Eng. Chem. Vol. 44, No. 6 (1952).

82. V. I. Vedeneyev, L. V. Gurvich, V. N. Kondrat'yev, V. A. Medvedev and Ye. L. Frankevich, Bond Energies Ionization Potentials and Electron Affinities (English Translation) Edward Arnold Publishers Ltd., London 1966.

83. E. W. Godbole and P. Kebarle, Trans. Faraday Soc., 58, 1897 (1962).

84. M. S. B. Munson, J. Am. Chem. Soc., 87, 2332 (1965).

85. R. W. Kiser, Introduction to Mass Spectrometry, Prentice-Hall Inc., Englewood Cliffs, New Jersey (1965) p.317.

86. J. L. Beauchamp and S. E. Buttrill Jr., J. Chem. Phys., 48, 1783 (1968).

87. M. K. Chantooni Jr., and I. M. Kolthoff, J. Am. Chem. Soc., 89, 1582 (1967).

88. J. F. Coetzee and J. J. Campion, J. Am. Chem. Soc., 89, 2513 (1967).

89. J. F. Coetzee and J. J. Campion, J. Am. Chem. Soc., 89, 2518 (1967).

B29965